2001

Fatigue crack propagation in steel components at resonance.

Sameh. Guirgis
University of Windsor

INFORMATION TO USERS

This manuscript has been reproduced from the microfilm master. UMI films the text directly from the original or copy submitted. Thus, some thesis and dissertation copies are in typewriter face, while others may be from any type of computer printer.

The quality of this reproduction is dependent upon the quality of the copy submitted. Broken or indistinct print, colored or poor quality illustrations and photographs, print bleedthrough, substandard margins, and improper alignment can adversely affect reproduction.

In the unlikely event that the author did not send UMI a complete manuscript and there are missing pages, these will be noted. Also, if unauthorized copyright material had to be removed, a note will indicate the deletion.

Oversize materials (e.g., maps, drawings, charts) are reproduced by sectioning the original, beginning at the upper left-hand corner and continuing from left to right in equal sections with small overlaps.

Photographs included in the original manuscript have been reproduced xerographically in this copy. Higher quality 6" x 9" black and white photographic prints are available for any photographs or illustrations appearing in this copy for an additional charge. Contact UMI directly to order.

ProQuest Information and Learning
300 North Zeeb Road, Ann Arbor, MI 48106-1346 USA
800-521-0600

FATIGUE CRACK PROPAGATION IN STEEL COMPONENTS AT RESONANCE

by

Sameh Guirgis

A Thesis

Submitted to the Faculty of Graduate Studies and Research

through the Department of Civil and Environmental Engineering

in Partial Fulfillment of the Requirements for

the Degree of Master of Applied Science at the

University of Windsor

Windsor, Ontario, Canada

2000

938341

ABSTRACT

Fatigue crack propagation rate in carbon steel at resonance is investigated. The model under consideration is a diametrically loaded circular steel ring. The compliance method was simulated using the finite element analysis to determine the stress intensity factors for the ring with two diametrical cracks emanating from the inside surface, for two different boundary conditions.

A procedure to predict the fatigue crack propagation rate in resonant structures is presented. Tests were carried out on circular rings made of medium carbon steel SAE 1045, to investigate the sensitivity of the stress intensity factor to the crack length for short cracks.

Paris' law was considered valid in this investigation. However, it is recommended to verify experimentally the applicability of Paris' law to describe fatigue crack propagation rate at resonance in further investigations.

Dedicated to the Memory of my Father

HAKIM ANDRAWES GUIRGIS

ACKNOWLEDGEMENTS

I would like to express my sincere gratitude to my advisor Dr. Sudip S. Bhattacharjee, for his guidance, encouragement, and patience throughout the period of this research.

I would also like to thank the staff and graduate students of the Department of Civil and Environmental Engineering, as well as the staff of the Leddy Library, especially, the Interlibrary Loan Department, for their assistance during the period of this research.

Thanks are also due to Miss JoAnn Grondin, Mr. Richard Clark, and Mr. Patrick Seguin for their assistance and cooperation.

TABLE OF CONTENTS

LIST OF TABLES

LIST OF FIGURES

NOMENCLATURE

All symbols in this work are defined were they first appear. However, some symbols denote more than one quantity, but the meaning should be clear when read in context.

A	the area of the cross-section.
∂A	the corresponding increase in cracked area due to the change in strain energy.
a	the crack length.
Δa	the value of the crack extension.
b	the width of the cross-section.
C	the compliance of a structural system (the inverse of its stiffness).
C_n	the generalized damping for mode "n".
C_o	the compliance of the uncracked section.
C_s	the additional compliance introduced by a crack.
$\overline{C}$	shifted compliance due to crack initiation or crack extension.
c	the viscous damping coefficient for an SDOF system, or the damping matrix for an MDOF system.
$\tilde{c}$	the generalized damping for an MDOF system.
C, m	Paris' Law material constants.
D	material constant, or a deflection.
E	the modulus of elasticity.
F (s)	dimensionless shape function for the additional compliance introduced by a crack.
f (s)	dimensionless shape function for the stress intensity factor
f_i	the natural frequency of mode "i".
G	the strain energy release rate.
g	the acceleration due to gravity.
h	the height of the cross-section.
I	the inertia of the cross-section about an axis that is perpendicular to the plane of geometry.

ID	the inner diameter of the ring.
i + 1	the natural mode of vibration number.
K	the stress intensity factor.
K_I	the stress intensity factor for opening loading mode.
K_c	the critical stress intensity factor.
K_{Ic}	the plane strain fracture toughness.
K_{max}	the maximum stress intensity factor.
K_{min}	the minimum stress intensity factor.
K_{op}	the opening stress intensity factor.
(K_I) st.	the stress intensity factor where the load rate has no effect on the system response, (K_I) st. = K_I, $R_d = 1$.
(K_I) dyn.	the stress intensity factor where the load rate has a considerable effect on the system response, (K_I) dyn.= (Rd) x K_I, $R_d >> 1$.
ΔK	the stress intensity factor range.
ΔK_{eff}	the effective stress intensity factor range.
k	the stiffness matrix for an MDOF system.
K	the stiffness of an SDOF system or the generalized stiffness matrix of an MDOF system.
K_n	the generalized stiffness for mode "n".
k_o	the stiffness of the uncracked section.
k_s	the inverse of the compliance introduced by a crack.
$\bar{k}$	the reduced stiffness due to crack.
Λk	the change of stiffness due to crack.
$\tilde{k}$	the generalized stiffness of an MDOF system.
L	span of a simply supported beam.
M	the generalized mass matrix, or a moment.
M_n	the generalized mass for mode "n".
M_{nr}	the generalized mass for the resonant mode "n".
m	the mass matrix, or the mass per unit length.
$\tilde{m}$	the generalized mass for an MDOF system.
N, n	material constant.

N	the number of cycles of the constant amplitude fatigue load.
Nst.	the number of cycles of the constant amplitude fatigue load that is required for a certain crack growth, where $\Delta K_I = (K_I)$ st.
Ndyn	the number of cycles of the constant amplitude fatigue load that is required for a certain crack growth, where $\Delta K_I = (K_I)$ dyn.
OD	the outer diameter of the ring.
P	the excitation vector, or a concentrated static load.
P_o	the amplitude of the harmonic excitation load.
P_n	the generalized excitation load for mode "n".
P_{no}	the amplitude of the harmonic excitation load for mode "n".
P_{nro}	the amplitude of the harmonic excitation load for the resonant mode "n".
$\widetilde{P}$	the generalized excitation load for an MDOF system.
P_i	the constant loads that act in direction "i".
p (t)	the time variation of the excitation load vector P.
q	the modal coordinate.
q_n	the modal coordinates for mode "n".
q_{nr}	the modal coordinates for the resonant mode "n".
$\dot{q}$	the first derivative of the modal coordinate in respect of time.
$\ddot{q}$	the second derivative of the modal coordinate in respect of time.
R, r	ring mean radius.
R	the stress Ratio.
R_x	the rotational degree of freedom about the X-axis.
R_y	the rotational degree of freedom about the Y-axis.
R_z	the rotational degree of freedom about the Z –axis.
r_y	the radius of the plastically deformed zone at the crack tip.
R_d	the deformation response factor.
R_{dn}	the deformation response factor for mode "n".
R_{dnr}	the deformation response factor for the resonant mode "n".
$\widetilde{R}$	the deformation response factor for a generalized MDOF.
S	the spatial distribution of load vector P, independent of time.

s	a/h.
U	the strain energy.
u	the displacement vector.
$\dot{u}$	the velocity vector.
$\ddot{u}$	the acceleration vector.
u_{nr}	the displacement for the resonant mode "n".
u_{nro}	the amplitude of the displacement for the resonant mode "n".
$(u_{st})_{no}$	the displacement under the static forces P_{no}.
$(u_{st})_{nro}$	the displacement under the static forces P_{nro}.
X	the transitional degree of freedom in direction of the X-axis.
Y	the transitional degree of freedom in direction of the Y-axis.
Z	the transitional degree of freedom in direction of the Z-axis.
z	the displacement of a generalized MDOF system.
$\dot{z}$	the velocity of a generalized MDOF system.
$\ddot{z}$	the acceleration of a generalized MDOF system.
α_n , β_n	the constants of the solution for the equation of motion for a harmonic excitation for mode "n".
Γ_n	the modal participation factor for mode "n".
γ	the weight per unit volume, or a dimensionless factor.
δ	the maximum deflection of the structural system.
Δ_i	the components of displacements in direction of P_i.
ζ_n	the damping ratio for mode "n".
ζ_{nr}	the damping ratio for the resonant mode "n".
ζ	the generalized damping ratio for an MDOF system.
λ, μ, ρ	dimensionless factors.
ν	the Poisson's ratio.
ξ	the loss factor.
θ_n	the phase angle for mode "n".
$\tilde{\theta}$	the phase angle for a generalized MDOF system.

σ_{ys}	the yield stress.
σ_{max}	the maximum normal stress.
σ_y	the stress component in direction of the Y-axis.
ϕ	the modal matrix.
ϕ_n	the mode shape vector for mode "n".
Φ	the mass normalized modal matrix.
Φ_n	the mass normalized mode shape vector for mode "n".
Φ_{nr}	the mass normalized mode shape vector for the resonant mode "n".
Ψ	the shape function.
Ω	the spectral matrix.
ω	the excitation frequency, or the spectral matrix.
ω_n	the natural frequency of mode "n".
ω_{nr}	the resonant frequency for mode "n".
$\widetilde{\omega}$	the generalized natural frequency of an MDOF system
$\overline{\omega}_n$	the shifted natural frequency for mode "n", due to crack initiation or crack extension.
$\overline{\omega}_{nr}$	the shifted natural frequency for the resonant mode "n", due to crack initiation or crack extension.
$\Delta\omega_{nr}$	the shift in the resonant frequency for mode "n", due to crack.

Abbreviations

LEFM	Linear Elastic Fracture Mechanics.
EPFM	Elastic Plastic Fracture Mechanics.
DOF	Degrees of freedom.
SDOF	Single degree of freedom.
MDOF	Multi degree of freedom.
FCGR	Fatigue Crack Growth Rate.
COD	Crack Opening Displacement.

CHAPTER 1
INTRODUCTION

1.1 FRACTURE MECHANICS

Resonance of cracked structures is not a rare situation, and in many cases, is a direct reason for structural failure. However, the subject of fatigue crack propagation at resonance is an interdisciplinary one. While it falls within the realm of Fracture Mechanics, it also involves the subjects of Structural Dynamics and Material Sciences. In the following, a review of the early developments of fracture mechanics is presented.

Strength failures of structures can be either of the yielding-dominant (ductile) or fracture-dominant (brittle) types. Fracture mechanics is concerned almost entirely with fracture-dominant failure where fracture happens before general yielding of the net section. The stress-strain curve for a material is obtained by subjecting a bar to pure tension. When the stress in the bar goes beyond the elastic limit, the material will begin to acquire inelastic, or permanent, deformation. If the tension is sustained, the stress increases till failure occurs. However, in case of a cracked specimen, it may fail due to reaching the plastic collapse or fracture conditions. Collapse and fracture are competing conditions, and the one satisfied first will prevail. If failure occurs due to reaching the plastic collapse conditions, the maximum tensile stress reached before failure is called the *collapse strength*. However, fracture may occur already before the collapse conditions are attained and this is the concern of fracture mechanics.

The fracture of any stressed structural component demands the creation of a new surface. The energy required to create this surface is the fracture energy. In absence of any external force, the fracture energy can be defined as the increase of the elastic surface energy of the structural component due to the creation of the new crack surfaces, or as the decrease in the elastic strain energy stored in the structural component.

Griffith (1921) originated the above-mentioned concept and applied it only to brittle materials. In this instance the plastic flow was negligible and the fracture energy was the surface energy of the substance.

In the 1940s, catastrophic failure of many built-up structures occurred and that led to extensive investigations. They revealed that the failures occurred due to brittle fracture,

and that flaws and stress concentrations were responsible. That brought the subject of fracture-dominated failure of structures to the spotlight.

However, the formalization of *Linear Elastic Fracture Mechanics* (LEFM) as an independent discipline was largely the result of Irwin's work (1957a, 1960). In the middle 1950s, Irwin introduced the concept of *Stress Intensity Factor* (K); a parameter that represents the crack tip stress field. Shortly afterward, the use of the stress intensity factor as the characterization parameter for the crack extension had become the fundamental principle of Linear Elastic Fracture Mechanics.

Irwin modified Griffith's concept by accounting for the energy dissipated at the crack tip, where a plastically deformed zone does exist. In many engineering materials, this energy is substantially greater than the surface energy, but as the volume of material deformed plastically is essentially small and uniform as the crack deepens, the concept of fracture energy still holds.

Under conditions of limited crack plasticity, the parameter governing tensile fracture can be stated as a *Critical Stress Intensity*, either K_c (plane stress) or K_{Ic} (plane strain). The value of K_c at a particular temperature depends on the specimen thickness and constraint. The critical value of the stress intensity factor under plane strain conditions, called the *Plane Strain Fracture Toughness* (K_{Ic}), can be considered as a material property characterizing the crack resistance. Thus, the same value of K_{Ic} should be obtained for a given material while testing specimens of different geometric shapes and sizes.

In general, lower temperature and faster strain rate decrease the plane strain fracture toughness for a specific material, while increasing the length of a pre-existing crack or decreasing the fracturing area will increase the stress intensity factor, if all other factors remain unchanged. Figure 1.1 shows the effect of temperature on the fracture energy, Figure 1.2; the effect of the strain rate on K_{Ic}; and Figure 1.3, the variation of K_c with the specimen thickness.

In the 1960s and 70s, extensive research efforts were made to extend the basic principles of LEFM to mixed-mode situations, anisotropic and composite materials as well as cracked bodies subjected to dynamic loading. Moreover, research efforts were

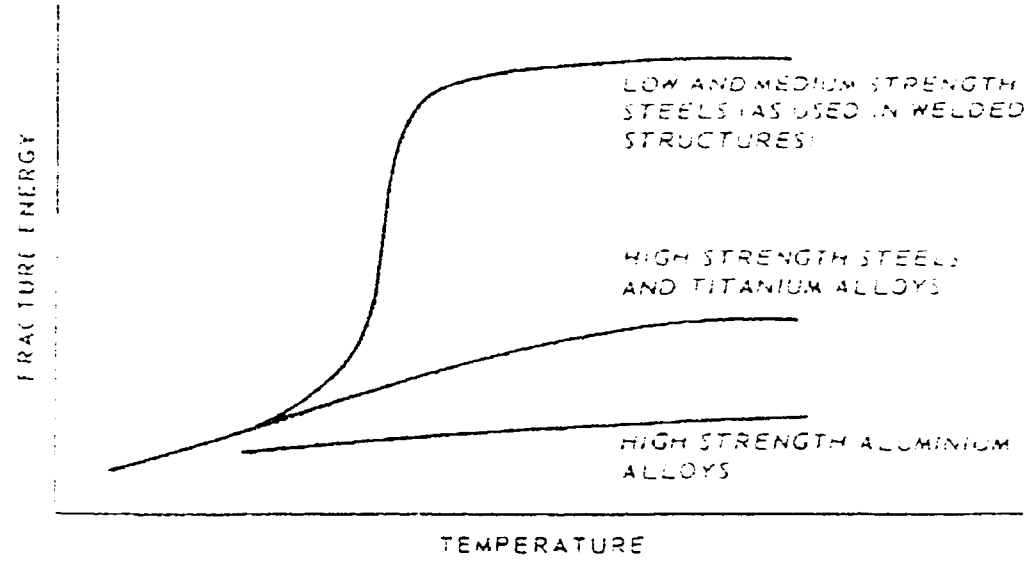

Figure 1.1

Schematic of the general effect of temperature on the fracture energy (Ewalds 1985)

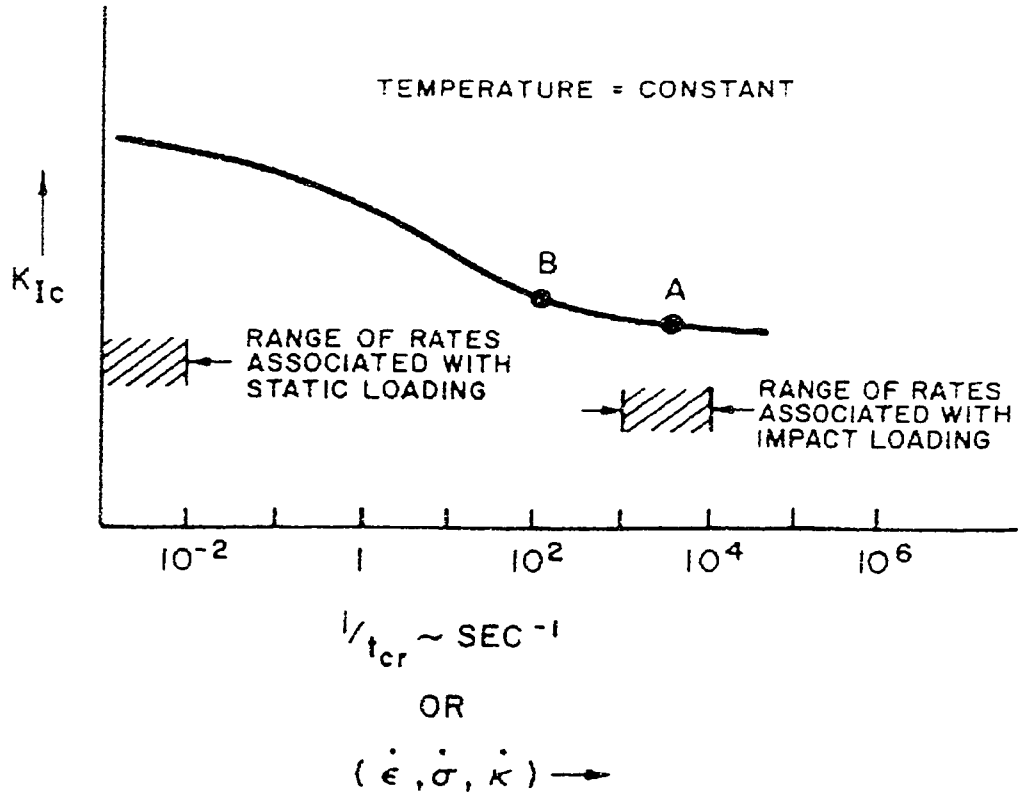

Figure 1.2

The effect of the strain rate on the fracture toughness (Paris 1974)

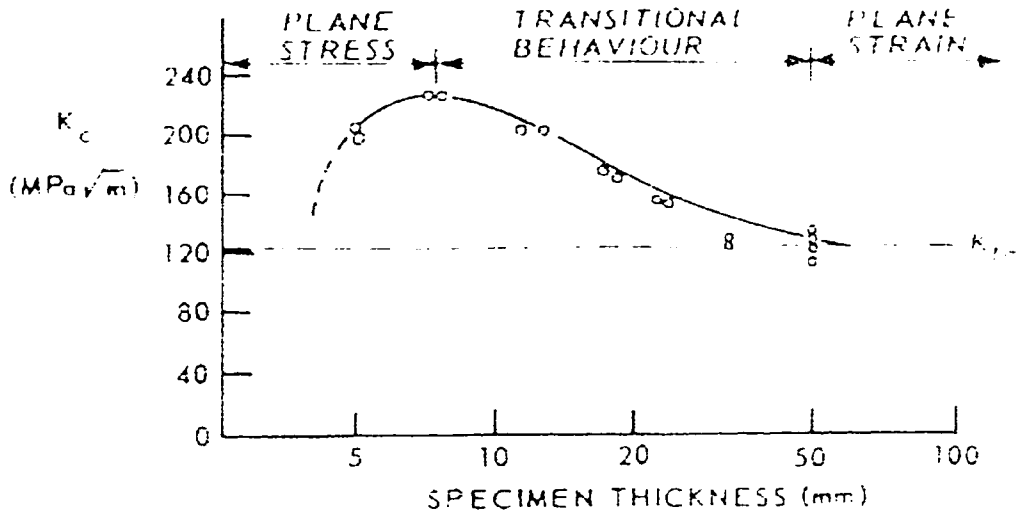

Figure 1.3

The variation of the stress intensity factor with specimen thickness (Ewalds 1985)

extended to study sub-critical crack growth such as fatigue crack growth and crack corrosion.

Up to the beginning of the 1960s, laws of *Fatigue Crack Growth Rate* (FCGR) used the stress amplitude to characterize the loading conditions. In 1961, Paris proposed the S*tress Intensity Factor Range* (ΔK) for characterization of the loading conditions (Paris 1961); it is one of the most widely used since then.

The beginnings of *Elastic-Plastic Fracture Mechanics* (EPFM) can be traced to a fairly early stage in the development of LEFM, notably Well's work (1962) on *Crack Opening Displacement* (COD). The *J-integral method* of analysis was proposed by Rice (1968), and was viewed by many (Paris 1977) as a direct extension of LEFM into the elastic-plastic regime. However, while the LEFM is a well-developed discipline, EPFM is still an evolving discipline.

In the early 1970s, Elber (1971) discovered the phenomenon of crack closure, the principle of the *Effective Stress Intensity Factor Range* (ΔK_{eff}), and also the important concept of *Crack Opening Stress* and the corresponding stress intensity factor (K_{op}). Elber's work helped to explain the effect of the *Stress Ratio* (R) on crack growth rate.

In the last three decades, a significant progress has been achieved in the field of fracture mechanics and fatigue crack propagation. Enormous numbers of related publications were prepared, and a wealth of experimental and analytical information was made available in the literature (Chona 1993; Jerina and Paris 2000).

1.2 PROBLEM STATEMENT

This work concerns itself with investigating *"fatigue crack propagation in steel components at resonance"*.

Most of the laws available in the literature to describe FCGR are based on wholly or partially empirical approach. Partially empirical formulae are based on theories and were derived analytically; however, constants contained in these formulae were obtained experimentally.

In this work, due to the complexity of the problem, theoretical analysis as well as finite element analysis were used to investigate the subject. However, experimental verification of the results in further investigations is recommended.

1.3 RESEARCH OBJECTIVES

The objectives of this investigation can be stated as the following:

a) to present formulae for estimating K_I in circular rings with the relative dimensions, boundary conditions, and external load system as shown in Figure 1.4; and
b) to develop a procedure for predicting the FCGR in a *Multi Degree of Freedom* structural system (MDOF) at resonance.

However, the scope of these objectives is very broad, and it is important to give attention to the assumptions and limitations of the proposed results and conclusions, before consideration is given to their application.

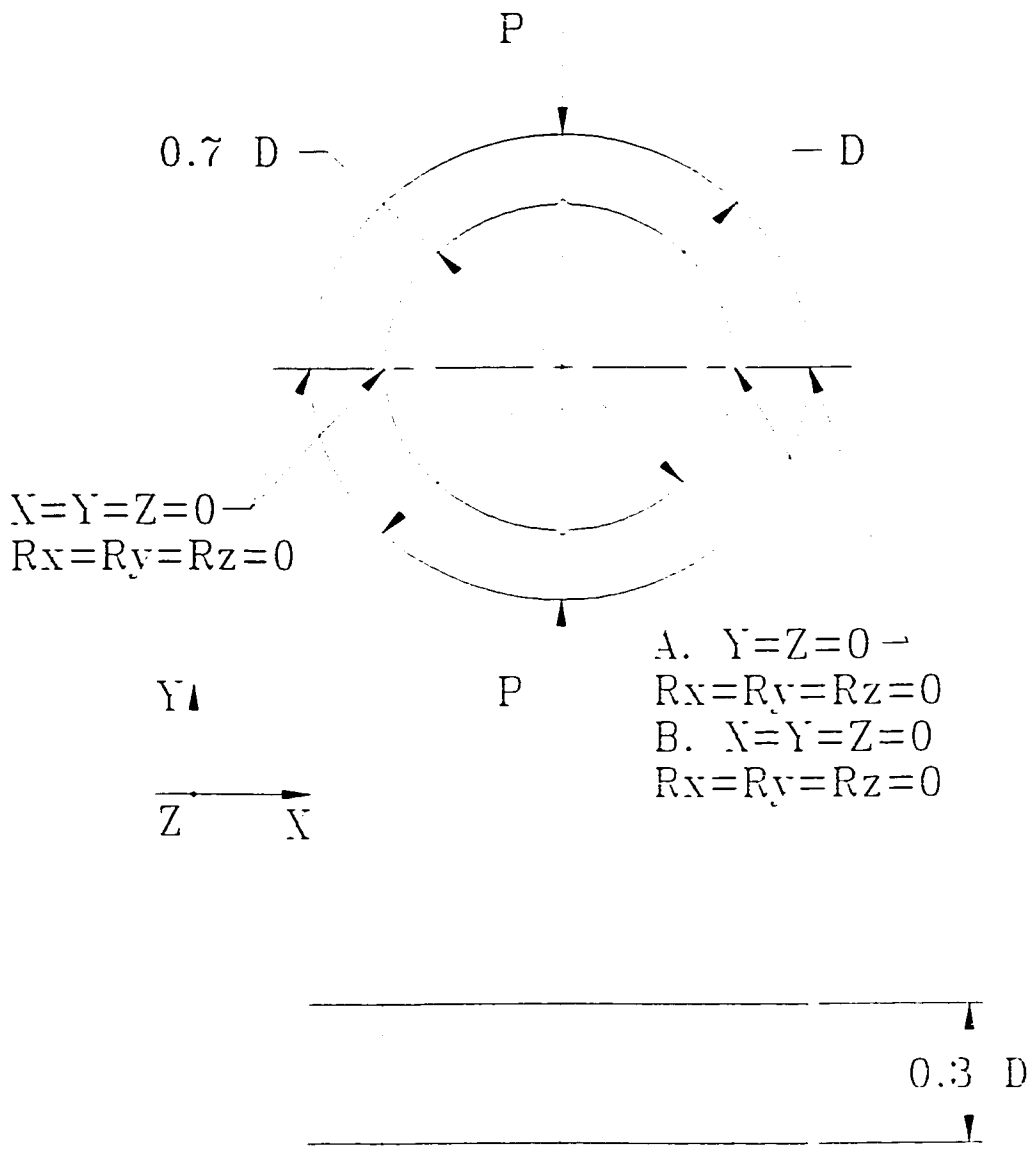

Figure 1.4

The ring model considered in this investigation

CHAPTER 2
LITERATURE REVIEW

2.1 INTRODUCTION

A brief review of the subjects relevant to this investigation is presented in the following sections of this chapter. Mainly, there are two areas of interest: fatigue crack propagation and the dynamic behavior of MDOF systems.

Extensive research work was performed to investigate the FCGR under sustained and dynamic loading conditions with constant as well as variable amplitudes. In section 2.2, theories describing the fatigue crack growth are reviewed. General formulae describing the FCGR are reviewed in section 2.3, with some specific formulae for carbon steels with different microstructures. Since ΔK is considered to be the characterizing parameter for crack extension, methods of determining the stress intensity factor are reviewed in section 2.4.

In section 2.5, the subject of the vibration of MDOF is reviewed, with some details about damping; the most influential factor in determining the system response at resonance, and vibration of circular rings. The effect of cracks on the response of MDOF systems is reviewed in section 2.6. Finally the fatigue crack propagation at resonance is reviewed in section 2.7.

2.2 CRACK GROWTH THEORIES

All the theories discussed in this section assume that the crack growth is in mode I (see different loading modes in Figure 2.1) and that a central transverse crack of length 2a, in an infinite sheet is subjected to a remote nominal stress of σ (Provan 1989).

2.2.1 The Theory of Head

Head (1953, 1956) developed this theory prior to the availability of treatments of plastic crack tips. Using the concept that a cracked body considered of composite array of independent bars having the constitutive properties:

a. of rigid-plastic bars, to describe the material directly ahead of the crack,
b. of elastic elements, to describe the material above and below the crack, and
c. of shear elements, to interconnect these two types of elements.

He showed that:

$$\frac{da}{dN} \quad \alpha \quad K_I^3 \tag{2.1}$$

2.2.2 The Geometrical Similarity Hypothesis

Frost and Dugdale (1958) based their geometrical similarity hypothesis upon consideration of a small idealized transverse slit in an elastic sheet of infinite extent subjected to plane stress uniaxial tension. If a unit diagram is prepared in which all dimensions are scaled to the size of the slit, i.e., the length of the slit is always considered to be unity, elasticity shows that at any point defined by a vector drawn from the origin, the stress or displacement is the same regardless of the actual slit length. A dimensional analysis of all the parameters that have a bearing on the problem always gives the same result. The same argument has been applied to finite sheets and to ductile materials where no change in their properties occurs as the crack grows, i.e., the size of the plastic zone ahead of the crack is directly proportional to the crack length. The geometrical similarity hypothesis thus leads to the growth law

$$\frac{da}{dN} \quad = \quad D\,a \tag{2.2}$$

where D is a coefficient depending on both the mean and alternating stresses and on the material and cannot be predicted but must be obtained from experimental data.

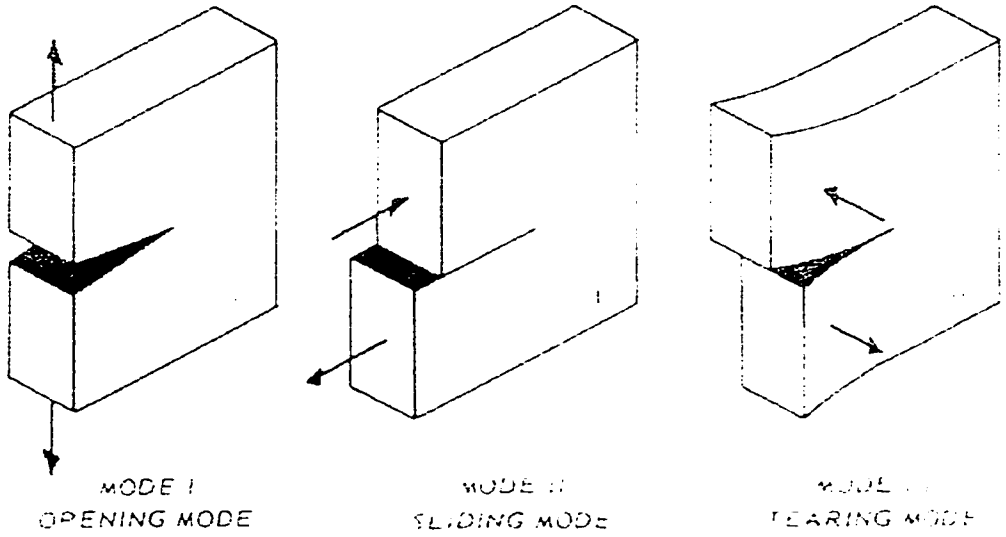

Figure 2.1

Different loading modes (Ewalds 1985)

2.2.3 Net Area Stress Theories

Weibull (1961) argued that as the crack length to sheet width ratio increased, the effective stress at the crack tip would also increase so that the rate of growth at a given crack length to sheet width ratio would depend only on the instantaneous value of the effective stress. He was able to show that:

$$\frac{d(2a)}{dN} = CW\sigma_N^n \tag{2.3}$$

where W is the finite width of the sheet and C and n are material constants.

2.2.4 The Accumulated Strain Hypothesis

Various hypotheses based on an element of material ahead of the crack tip fracturing when it has accumulated some critical amount of plastic deformation have been put forward. As an example, Isibasi (1958) assumed that an elementary length of material ahead of the crack fractures as an entity when the average tensile strain accumulated by the element reaches some critical value. By doing so he arrived at the expression:

$$\frac{da}{dN} = K^n \tag{2.4}$$

where n is an empirical constant.

2.2.5 Dislocation Theories

In general, such theories predict that the rate of crack growth is proportional to K_I^4. For example, Weertman (1965) took as a starting point a freely slipping crack subjected to applied shear. A crack of length 2a having plastic zones at either end is considered and dislocation theory used to calculate the displacement in the tip vicinity due to shear stress. Under cyclic loading it is assumed that the crack grows when the sum of the absolute values of cyclic displacement at the crack tip exceeds some critical value, D. Consideration of the rate at which the crack grows per stress cycle in terms of D leads to:

$$da = \frac{a^2\,\sigma_{max}^4}{D\,E\,\sigma_{ys}^3} \;;\; \frac{da}{dN} \;\alpha\; K^4 \tag{2.5}$$

2.2.6 Energy Theories

The energy associated with plastic zone at a crack tip is proportional to K_I^4, so that theories based on the energy required to operate the fracture mechanism, in general, will predict that the rate of the crack growth is also proportional to K_I^4, in agreement with dislocation theories. For example, Rice (1967) based a theory on a rigid-plastic strip model where the cracked body becomes two half-planes joined along a strip of rigid-plastic material, with a void in the strip to simulate the crack. Tracing the deformation history of a particular point ahead of the crack, from when the plastic zone first reaches it to the time it is reached by the crack tip, a K_I to the forth power dependency was deduced.

2.2.7 The Frost and Dixion Theory

Frost and Dixion (1967) argued that the crack grows because its tip profile is successfully blunted and resharpened during each stress cycle. The unloading part of the cycle is essential to the growth process since, unless the crack is resharpened each cycle, fresh surfaces cannot be created during the process of crack tip blunting when the load is reapplied. As noted by Pelloux (1970), the environment may also influence the amount of crack growth in each cycle since in any environment other than that of a vacuum the crack may not be able to close properly, thereby leaving striations. The result of deliberations of Frost and Dixon is best written as:

$$\frac{da}{dN} = \frac{8}{\pi}\left(\frac{\Delta K}{E}\right)^2 \tag{2.6}$$

2.2.8 A Fracture Mechanics Crack Growth Theory

Pook and Frost (1973) re-expressed Frost and Dixon's theory in fracture mechanics terms with Equation (2.6) being derived directly from the stress and displacement fields around the cracks and sharp notches.

For typical values of the plastic constraint factor, $(\sigma_{ys}/E)^2$, they derived:

$$\frac{da}{dN} = \frac{9}{\pi}\left(\frac{\Delta K}{E}\right)^2 \text{; plane stress} \tag{2.7}$$

$$\frac{da}{dN} = \frac{7}{\pi}\left(\frac{\Delta K}{E}\right)^2 \text{; plane strain} \tag{2.8}$$

2.3 FATIGUE CRACK GROWTH RATES

2.3.1 Introduction

For different types of carbon steels, proposed relationships are based on the microstructure of the steel, which depends mainly on its carbon content and the method of heat-treatment it was subjected to. A review of relevant heat-treatment terms and different types of carbon steel microstructure is presented in the following two sub-sections.

The problem of Mode I fatigue crack propagation has been the subject of extensive study. Consequently, numerous relationships describing the FCGR under constant amplitude loading have been made available in the literature (Toth 1997).

In 1961 Paris, Gomez and Anderson (Paris 1961), suggested the following correlation between the FCGR and the range of applied stress intensity factor:

$$\frac{da}{dN} = C(\Delta K)^m \tag{2.9}$$

This equation describes only the linear log-log part of the crack growth curve (region II), as indicated in Figure 2.2

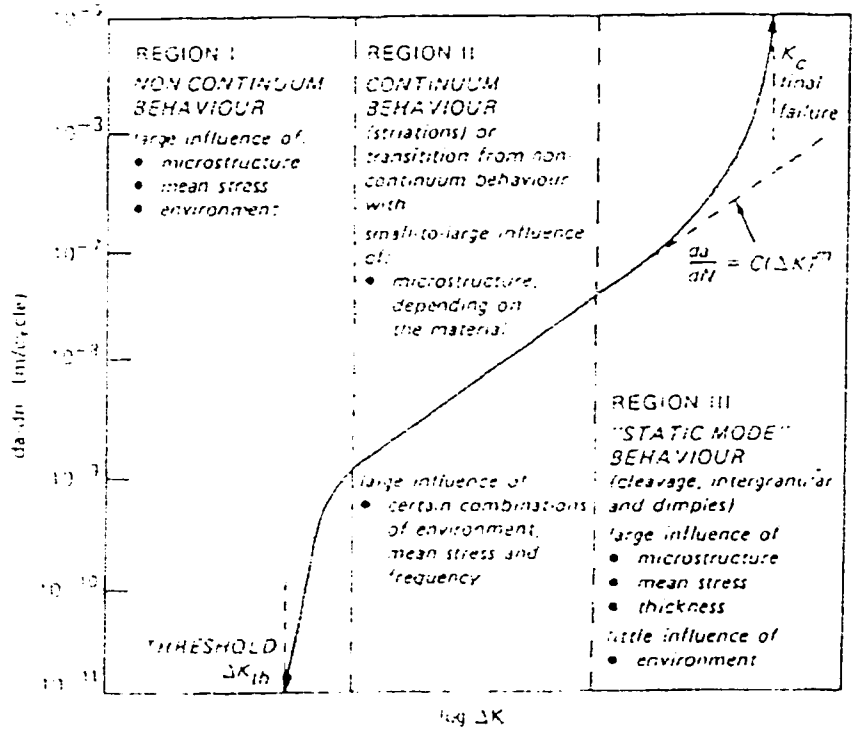

Figure 2.2

The crack growth curve (Ewalds 1985)

2.3.2 Heat Treatment of Standard Steels

The following definitions of heat-treating terms have been adopted by the American Foundrymen's Association, the American Society for Materials, the American Society for Testing and Materials, and the Society of Automotive Engineers (Oberg 1996).

Austenitizing: Forming austenite by heating into the transformation range (partial austenitizing) or above the transformation range (complete austenitizing). When used without qualification, the term implies complete austenitizing.

Annealing: A term denoting a treatment, consisting of heating to and holding at a suitable temperature followed by cooling at a suitable rate, used primarily to soften but also to simultaneously produce desired changes in other properties or in micro-structure.

Full Annealing: Austenitizing and then cooling at a rate such that the hardness of the product approaches a minimum.

Quenching: rapid cooling.

Transformation ranges or temperature transformation ranges: Those ranges of temperature within which austenite forms during heating and transforms during cooling. The two ranges are distinct, some times overlapping but never coinciding. The limiting temperatures of the ranges depend on the composition of the alloy and on the rate of change in temperature, particularly during cooling.

2.3.3 Microstructure of Carbon Steel

2.3.3.1 Structure of Fully Annealed Carbon Steel (Oberg 1996):

In carbon steel that has been fully annealed, there are normally present, apart from such impurities and phosphorous and sulfur, two constituents: the element iron in a form metallurgically known as *ferrite* and the chemical compound iron carbide metallurgically known as *cementite*. This latter constituent consists of 6.67 per cent carbon and 93.33 per cent iron. A certain proportion of these two constituents will be present as a mechanical mixture. This mechanical mixture, the amount of which depends upon the carbon content of the steel, consists of alternate bands or layers of ferrite and cementite. Under the microscope the matrix frequently has the appearance of mother-of-pearl and hence has been named *pearlite*.

Pearlite contains about 0.85 per cent carbon and 99.15 per cent iron, neglecting impurities. A fully annealed steel containing 0.85 per cent carbon would consist entirely of pearlite. Such a steel is known as *eutectoid* steel and has a laminated structure characteristic of a eutectic alloy. Steel which has less than 0.85 per cent carbon (*hypoeutectoid* steel) has an excess of ferrite above that required to mix with the cementite present to form pearlite, hence both ferrite and pearlite are present in the fully annealed state. Steel having a carbon content greater than 0.85 per cent (*hypereutectoid* steel) has an excess of cementite over that required to mix with the ferrite to form pearlite, hence both cementite and pearlite are present in the fully annealed state.

2.3.3.2 Effect of Heating Fully Annealed Carbon Steel

When carbon steel in the fully annealed state is heated above the lower critical point, which is some temperature in the range of 723.9 to 735.0 degrees C (depending upon the carbon content), the alternate bands or layers of ferrite and cementite which make up the pearlite begin to merge into each other. This process continues until the pearlite is thoroughly "dissolved," forming what is known as *austenite*. If the temperature of the steel continues to rise and there is present, in addition to the pearlite, any excess ferrite or cementite, this also will begin to dissolve into the austenite until finally only the austenite will be present.

2.3.3.3 Effect of Slow Cooling on Carbon Steel

If carbon steel which has been heated to the point where it consists entirely of austenite is slowly cooled, the process of transformation which took place during the heating will be reversed but the upper and lower critical points will occur at somewhat lower temperatures than they do on heating. Assuming that the steel was originally fully annealed, its structure upon returning to atmospheric temperature after slow cooling will be the same as before in terms of the proportions of ferrite or cementite and pearlite present. The austenite will have entirely disappeared.

2.3.3.4 Effect of Rapid Cooling or Quenching on Carbon Steel

Observations have shown that as the rate at which carbon steel is cooled from austenitic state is increased, the temperature at which the austenite begins to change into pearlite drops more and more below the slow cooling transformation temperature of about 704.4 degrees C. For example, a 0.80 per cent carbon steel that is cooled at such a

rate that the temperature drops 260.0 degrees C in one second will show transformation of austenite beginning at 498.9 degrees C. As the cooling rate is increased, the laminations of the pearlite formed by the transformation of austenite become finer and finer up to the point where they cannot be detected under high power microscope, while the steel itself increases in hardness and tensile strength. As the rate of cooling is still further increased, this transformation temperature suddenly drops to around 260 degrees C or lower, depending upon the carbon content of the steel. The cooling rate at which this sudden drop in transformation temperature takes place is called the critical cooling rate. When a piece of carbon steel is quenched at this rate or faster, a new structure is formed. The austenite is transformed to *martensite* which is characterized by an angular needlelike structure and a very high hardness.

2.3.4 Experimental Fatigue Crack Growth Rates

Extensive FCGR data for some steels show that the primary parameter affecting growth rate in region II is the stress intensity factor range and that the mechanical and metallurgical properties of these steels have negligible effect on the FCGR in air environments at room temperatures.

For a number of commonly used structural alloys, da/dN-ΔK data have been compiled (Frost *et al.*1971; Rolfe and Barsom 1977; NPFC 1981; UOD 1986). For other materials, such data may have to be generated; guidelines for performing crack growth rate experiments are given in reference (ASTM 1983). For a wide variety of structural steels, it has been found that upper bounds on crack growth rate can be described by the following relations over the linear region:

a) for Ferritic-Pearlitic Steels (Rolfe and Barsom 1977):

$$\frac{da}{dN} = 6.9\ X\ 10^{-12}\ (\Delta K)^{3.00} \tag{2.10}$$

b) for Martensitic Steels (Rolfe and Barsom 1977):

$$\frac{da}{dN} = 1.4\ X\ 10^{-10}\ (\Delta K)^{2.3} \tag{2.11}$$

c) for Austenitic Stainless Steels (Provan 1989)

$$\frac{da}{dN} = 5.61\ X\ 10^{-12}\ (\Delta K)^{3.25} \tag{2.12}$$

In these relations, da/dN has units of m/cycle and ΔK is in MPa-$m^{1/2}$.

Figure 2.3 shows the FCGR in different steels.

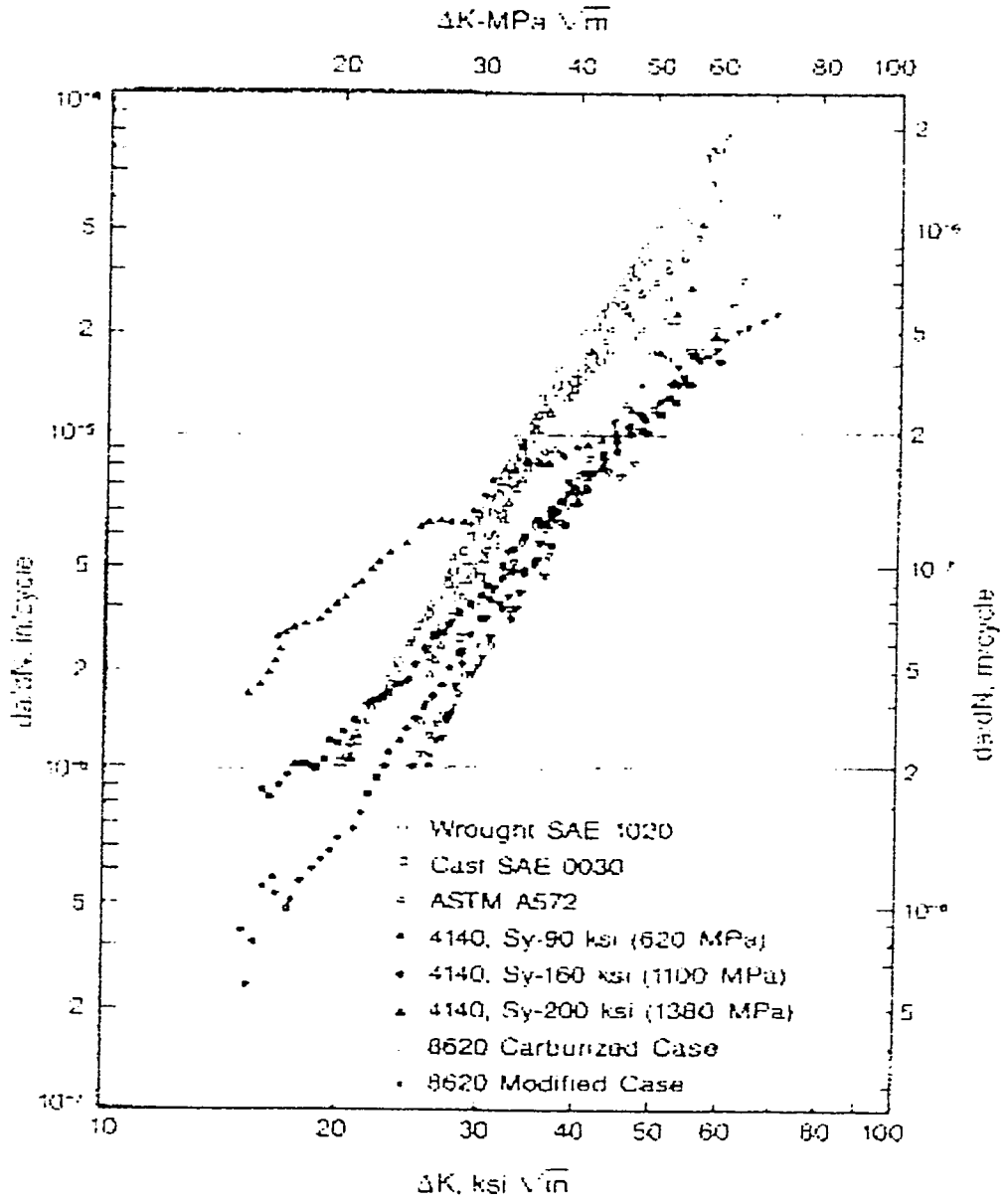

Figure 2.3

Fatigue crack growth rates in different steels (SAE 1997)

2.3.5 The Effect of Various Factors on Fatigue Crack Growth

The following factors influence the fatigue crack growth (Provan 1989):

2.3.5.1 The Mean Stress Effect

The effect of mean stress on the fatigue crack initiation and propagation can best be studied in terms of the stress ratio R (R = min. load/max. load). Several investigations have been conducted to study this effect on the crack growth rate and, generally, the results indicate that the stress ratio has a second order effect on the region II crack propagation rate. However, this is not the case for fatigue crack propagation threshold. Moreover, the value of ΔK at the transition rate region III also depends on the stress ratio R.

2.3.5.2 The Effect of Frequency

Since the loading rate has an effect on the fracture toughness and since a change in frequency corresponds to a change in the rate of loading, the influence of the cycle frequency was initially expected to have considerable influence on fatigue crack growth material characteristics. In the specific case of steel, however, it has been observed that at room temperature this effect is minimal for frequencies less than 60 Hz, provided the environment is inert. These observations are valid only for excitation frequencies away from the resonating frequencies.

2.3.5.3 The Effect of Wave Form

The primary parameter, ΔK, which governs the rate of crack growth, is itself related to the stress fluctuation and crack size, a. This parameter does not account for possible differences in growth rate that may exist between various cyclic wave forms. Barsom (1973) has shown that in the case of steel the rate of fatigue crack growth in an air environment at room temperature is not influenced by the waveform.

2.3.5.4 Other Influences

There are a number of factors that are known to affect the crack propagation characteristics of materials. They include environmental effects, the effects of stress concentrations and the effect of inherent material inhomogeneities. No general guidelines can be given except that these are very important considerations that should be investigated during the design stage of an engineering component.

2.4 STRESS INTENSITY FACTORS FOR A RING

2.4.1 Stress Intensity Factor Determination Methods

Determining the stress intensity factor for a particular crack shape and structural component geometry is a task of varying complexity. Since they are available for a wide variety of geometrical configurations, the first step should be a literature search (Sih 1973; Rooke and Cartwright 1976; Tada *et al.* 1985; Murakami 1987). If no applicable solution is directly available, one of the following methods could be used:

1. The weight function method (Bueckner and Giaever 1966; Paris *et al.* 1976).
2. The mapping collocation technique (Bowie and Freese 1970; Tracy 1975).
3. Boundary integral equations (Tracy 1979).
4. The compounding method (Carwright and Rooke 1974).
5. Finite element calculations (Jones 1973a, b; Buchalet and Bamford 1976).
6. Experimental determination methods (ASTM 1984).
7. The Compliance method (Ewalds and Wanhill 1985).

In the following a detailed presentation is given for simulating the compliance calibration method using finite element analysis, since it is used in this investigation to determine the stress intensity factor for the ring.

2.4.2 The Finite Element Method

Finite element analysis can be used in several ways to determine the stress intensity factors:

a. The compliance method: this method simply models the experimental compliance calibration in terms of finite element analysis. In this method, the stress state is assumed to be due to a constant external load system; displacements are computed for a series of crack sizes. The stress intensity factor can be calculated from the relation:

$$G = \frac{K^2}{E} = \frac{\partial U}{\partial A} = \frac{1}{2} \sum P_i \left(\frac{\partial \Delta_i}{\partial A} \right) \tag{2.13}$$

where G is the strain energy of the stress field, dU is the change in the strain energy due to incremental crack extension, dA is the corresponding increase in cracked area, P_i are the constant loads, and Δ_i are the corresponding components of displacements in direction of P.

The advantage of this procedure is that the refinement of the finite element mesh toward very small element sizes, near the crack tip, has little influence on the displacement differences, Δ_i, remote from the crack and therefore not required. In compensation, the computations must include a range of crack sizes and reliable results require careful study of accuracy of the load displacement differences (Tada *et al.* 1985).

b. The direct method (Broek 1988): In the direct use of finite element analysis, solutions must be obtained for models with cracks. The model can provide stresses, strains, and energy, from which the stress intensity factor can be obtained by a variety of methods. One of these methods is to consider the universal crack tip stress field solution which provides the crack tip stress σ_Y for $\theta = 0$ as:

$$\sigma_y = \frac{K}{\sqrt{2\pi x}} \tag{2.14}$$

The finite element solution provides σ_y at various locations (x). By substituting in equation (2.14), the stress intensity factor can be obtained. As equation (2.14) is valid only at very small x, the stress intensity obtained from this equation is in error unless x is extremely small. On the other hand, the calculated value σ_y contains a larger error for the smaller x (unless singular elements are used). In order to circumvent this problem, the equation can be solved a number of times using the values of σ_y at distances x_1, x_2, x_3, etc. For each combination (σ_y, x) an apparent value of K is obtained. None of these is the correct one. By plotting these apparent values against x distances, the correct value can be extrapolated at $x = 0$.

c. The indirect method (Broek 1988): In this method the finite element solution is obtained for uncracked structure only, and the stress distribution in the section of the future crack is calculated. Subsequently, the stress intensity factor is calculated through the use of Green's functions or weight functions.

It is worthwhile pointing out that stress distributions obtained with finite elements are of limited accuracy. Provided the elements are sufficiently small, especially in areas of large stress gradients, very good solutions can be obtained. However, in many practical solutions for complicated structures accuracies are seldom better than 10% (Tada *et al.* 1985; Broek 1988).

2.4.3 Stress Intensity Factors of a Ring

Because of the importance of the ring geometry as a basic structural element, the problem of a ring or a hollow cylinder containing an arbitrarily oriented crack or set of cracks, was the subject of several investigations.

Tracy (1975) studied the problem of curved beam or a circular ring segment containing a radial crack, emanating from the surface with the smaller radius. He considered two cases of loading; pure bending and three point loading. Jones (1973a, b) has considered a similar problem using the finite element approach.

Tracy (1979) also considered the problem of multiple cracks (one to four) emanating either from the inner or outer surface of a circular ring. For cracks emanating from the outer surface, he considered a loading case of internal pressure, while for cracks emanating from the inner surface, uniform external tension was considered.

Bowie *et al.* (1970) have studied the problem of a circular ring with one crack emanating from the inner boundary with internal pressure. Several investigators have studied the problem of one crack emanating from the outer surface of a cylinder under internal pressure (Kobayashi *et al.* 1969; Emery and Segedin 1972; Kapp 1977). Labbens *et al.* (1976) have used the weight functions for the ring problem with an inner edge crack. Delale and Erdogan (1982) have presented an exact solution of the plane elasticity problem for a hollow cylinder or a disk containing a radial crack. The crack may be an external edge crack, an internal edge crack, or an embedded crack. It was assumed that the external loads are symmetric with respect to the plane of the crack, and the basic ring problem without the crack has been solved. Thus the main problem of interest is the Mode I crack problem in which a self-equilibrating arbitrary normal crack surface traction is the only external load.

2.4.4 Stresses and Displacements on the Boundaries of Diametrically Loaded Circular Rings

The model considered in this investigation is a circular ring with a rectangular cross section, with pair of concentrated harmonic loads, applied diametrically. For verification purposes, the displacements and stresses for pair of static loads are needed.

because it represents one of the basic structural elements, and it has numerous applications in machine fabrications.

One of the most thorough treatments of the subject has been conducted by Nelson (1939); and based on his work, Durelli and Lin (1986) presented the stress and displacement values for all points at the inside and outside boundaries of rings for which the ratio of diameters ID/OD varies from 0 to close to 1.

2.5 VIBRATION OF MULTI DEGREE OF FREEDOM SYSTEMS

2.5.1 Discretization of MDOF Systems

Structures maybe discretized either as lumped-mass systems or distributed mass systems. Lumped mass systems can effectively idealize many classes of structures, especially multi-story buildings. However, a lumped mass idealization although applicable, is not a natural approach for certain types of structures, such as a ring, an arch dam, or a nuclear containment structure.

Distributed mass systems have infinite *number of degrees of freedom* (DOF). However, infinite DOF approach is not feasible for practical systems; distributed mass systems could be discretized as systems with finite number of DOF using different methods such as, Rayliegh-Ritz method and finite element method.

2.5.2 Modal and Harmonic Analyses

Modal analysis for a structure is performed to determine its vibration characteristic, i.e., its natural frequencies and mode shapes. For any structural system, subjected to dynamic loading conditions, the modal analysis is required as a first step in the dynamic analysis of that structure.

In case of dynamic harmonic loading conditions, i.e., where loads vary sinusoidally with time, the harmonic response analysis will be required to determine the steady-state response of the structure. The analysis is performed by calculating the structure's response at several frequencies and obtaining the peak responses and the corresponding frequencies at critical DOF, stresses to be reviewed at these peak frequencies.

The harmonic analysis can be performed by using the mode superposition method. In this technique, some response quantities (usually displacements) are expressed as the sum of corresponding factored modal quantities (obtained from modal analysis).

2.5.3 Damping and Loss Factor

Damping is the process by which vibration steadily diminishes in amplitude due to dissipation of vibration energy; it is the most important factor that affects the response of the system at resonance.

Various mechanisms contribute to the energy dissipation. In a vibrating building that includes: thermal effect of repeated elastic straining of the material, internal friction when a solid is deformed, friction at steel connections, opening and closing of microcracks in concrete, and friction between the structure itself and nonstructural elements such as partition walls (Chopra 1995).

Under static cyclic loading conditions, a perfectly elastic material has a single straight line as a force-deformation curve for both loading and unloading. However, under dynamic cyclic excitations, associated with viscous damping, the force-deformation curve becomes a hysteresis loop. This phenomenon is related to the dynamic nature of loading; therefore, it is known as *dynamic hysteresis*. The loop area due to dynamic hysteresis is proportional to the excitation frequency and equals the energy dissipated by viscous damping in one cycle.

Moreover, a hysteresis loop develops under static cyclic loading conditions, if the material undergo inelastic deformations. This phenomenon is known as *static hysteresis* because the force-deformation curve is insensitive to deformation rate.

More often damping is idealized by a linear viscous damping, where the damping coefficient is selected so that the vibrational energy it dissipates is equivalent to the energy dissipated in all the damping mechanisms, combined, in the actual structure. This idealization is therefore called *equivalent viscous damping*; it is dependent on the dynamic loading rate.

The *loss factor* ξ is a measure of the energy dissipated by viscous damping. If the energy could be removed at a uniform rate during a cycle of simple harmonic motion, ξ could be interpreted as the energy loss per radian divided by the total energy of the system.

For a *single degree of freedom* (SDOF) system:

$$\xi = \frac{c\,\omega}{K} \tag{2.15}$$

where K denotes the *stiffness* of the structure; ω, the *excitation frequency*; and c, the *viscous damping coefficient.*

It is worth mentioning that, the loss factor, as a measure of damping, is not often used in structural vibration analysis since it is most useful for very light damping, e.g., it is useful in comparing the damping capacity of materials.

Experiments on structural metals indicate that the energy dissipated internally in cyclic straining of the material is essentially independent of the cyclic frequency. Similarly, forced vibration tests on structures indicate that the equivalent viscous damping ratio is roughly the same for all natural modes and frequencies (Chopra 1995). This type of damping is refereed to as *rate independent linear damping.*

2.5.4 Vibration of a Ring

A circular ring of a constant cross-section, where each cross section has an axis of symmetry situated in the plane of the ring may vibrate in several different modes (Timoshenko 1955):

Pure Radial Vibration: In this case the center line of the ring forms a circle of periodically varying radius and all the cross sections move radially without rotation.

Torsional vibration: the simplest mode of torsional vibration is that in which the center line of the ring remains undeformed and all the cross sections of the ring rotate during vibration through the same angle

Flexural Vibrations: flexural vibrations of circular rings fall into two classes, i.e., flexural vibrations in the plane of the ring and flexural vibrations involving both displacements at right angles to the plane of the ring and twist.

The problem of vibration of a circular ring has been treated in the literature (Love 1927; Zacek 1938). Under the assumption that the cross-sectional dimensions of the ring are small in comparison with the radius of its centerline, Timoshenko (1955), presented an equation for calculating the natural frequencies f_i, for any mode of vibration:

$$f_i = \frac{1}{2\pi}\sqrt{\frac{E\,g}{\gamma}\,\frac{I}{Ar^4}\,\frac{i^2\,(1-i^2)^2}{1+i^2}} \tag{2.16}$$

where, E denotes the modulus of elasticity; g, the acceleration due to gravity; γ, the weight of the material of the ring per unit volume; A, the cross-sectional area; r, the radius of the circular ring; and I, the moment of inertia of the cross section with respect to a principal axis at right angles to the plane of the ring.

When $i = 1$, we obtain $f_i = 0$. In this case the ring moves as a rigid body. When $i = 2$, the ring performs fundamental mode of flexural vibration.

2.6 VIBRATION OF CRACKED STRUCTURES

2.6.1 INTRODUCTION

The presence of a crack in a structural member introduces an additional flexibility that affects its vibration response. In the literature, three basic methods of dealing with the problem have been reported:

a) simulating the crack effect by a local bending moment or by using an equivalent reduced section (Kirmsher 1944), with magnitudes which were estimated by experimentation,

b) simulating the crack effect by a local flexibility calculated from fracture mechanics (Westmann and Yang 1967; Dimargonas 1976), and

c) formulating and applying a theory to describe the response of a cracked continuous bar or beam (Christides and Barr 1984, 1986).

Hundreds of papers were published in the last decade on the dynamic response of cracked structures. Several reviews on the subject were reported in literature (Wauer 1990; Entwistle and Stone 1990; Dimargonas 1996).

2.6.2 The Additional Flexibility Introduced by a Crack

The analysis of the additional flexibility of a cracked region of structural member was quantified in the 1950s by Irwin (1957a, b) and Bueckner (1958) by relating local flexibility to the crack stress intensity factor. Based on this principle, a method was developed for the computation of stress intensity factor based on the local bending stiffness (inverse of the local flexibility) of a cracked prismatic beam, determined experimentally (Liebowitz *et al.* 1967, 1968; Okamura *et al.* 1969).

Since 1957, several investigators computed the stress intensity factor and the additional flexibility for a variety of geometries of cracked structural members, using the

fracture mechanics relations between the strain energy release rate and stress intensity factor and Castigliano theorem.

2.6.3 Cracks and Notches

Realizing the confusion in the literature in distinguishing the difference between a crack and a notch, Dimargonas (1996) emphasizes the difference: no matter how thin a saw cut is, it will not behave as a fatigue crack. In his experience, a thin cut results in an additional flexibility substantially less than the additional flexibility associated with a fatigue crack.

Silva and Gomez (1990a, b, 1991) performed an extensive experimental dynamic analysis of beams and investigated the difference in behavior of slots and cracks. According to this work, cracks of small depth result in about twice the change in natural frequency observed with slots of the same depth.

2.6.4 The Closing Crack

A crack that opens and closes during vibration is called a breathing crack. A structural system with loading condition that leads to crack closing or crack breathing is nonlinear. In stress analyses, cracks are frequently modeled as linear springs, because for a given crack depth, the equivalent spring constant remains the same for both directions of loading. In the case of the breathing cracks, the spring constant appears to be different for open and closed cracks. In most cases, fatigue cracks develop in areas of varying stresses superposed on static stresses; the latter are usually the result of static loads. In this case, if the stresses are sufficiently high, the crack remains always open and the linear analysis is valid. In the absence of a static force which keeps the crack open, the crack will close during the part of the cycle when the stresses are compressive and it will behave as a bilinear spring (Dimargonas 1996).

2.6.5 Change of Natural Frequencies Due to Crack

In a cracked system, natural frequencies change due to crack extension. The depth of the crack determines the additional flexibility introduced by the crack, which in turn influences the system natural frequencies and its dynamic response.

Gudmundson (1982), presented a first order perturbation method that predicts the changes in natural frequencies of a structure resulting from a crack. He has shown that the eigenfrequency changes due to a crack are dependent on the strain energy of a static

solution, which is easily obtainable for small cracks and cutouts. The results compared well with values obtained by experiments and finite element method for small cracks.

The change in natural frequencies of structure, caused by crack nucleation or crack propagation, is the most popular identification method in detecting crack location and magnitude in machinery, rotors, and other structures (Chondros 1980, 1981).

Moreover, a crack changes the natural mode shapes of a structure. Several methods have been presented for crack detection in structures based on changes in mode shapes (Pandey *et al.* 1991; Fox 1992).

2.6.6 Damping Due to Cracks

A crack in a structural member leads to changes in damping because a plastic zone appears along the crack edge. The change of damping caused by the crack is a relatively small part of the damping of the structure.

2.6.7 Vibration Coupling Due to Surface Cracks

A crack introduces new harmonics to the vibration spectrum of the structural system. The flexibility matrix of the cracked region has off-diagonal terms, which indicates a coupling between the longitudinal, lateral and torsional vibrations.

A full 6 x 6 flexibility matrix for a general loading of a Timoshenko beam was obtained by Ostachowicz and Krawczuk (1992), for a beam of rectangular or circular cross-section. Similar results for a Bernoulli-Euler beam were obtained by Gudmundson (1982, 1983), by way of a 2 x 2 flexibility matrix for a rectangular cross-section subjected to longitudinal and lateral motion, the same result for the local flexibility as the one by Rice and Levy (1972).

2.6.8 Vibration of Cracked Circular Rings

Vibration of circular rings, with a transverse crack, was investigated by Yao and Dimargonas (1988). Their analysis was based on the assumption that the ring thickness is small relative to its radius.

In their work, the local flexibility introduced by the crack was approximated by three stiffness factors representing the local flexibility of a cracked strip, the governing differential equations for the cracked ring were solved, and a general solution for the dynamic response of the system was presented.

They concluded the following:

"1. Higher modes and thicker rings have higher natural frequency reduction with increasing crack depth,
2. this measurable frequency drop provides a methodology to identify cracks in a system,
3. the stiffer a structure or a system is, the higher the frequency drop will be,
4. the frequency change can give information for the magnitude of the crack".

"Location of the crack can be found only with vibration mode measurements. However, in rotating machinery, vibration spectrum analysis can be performed as a service monitoring procedure to detect frequency reduction in operation and relate it to a possible crack development. During an outage, a local procedure can be used, such as ultrasonics, to locate the crack".

2.7 FATIGUE CRACK GROWTH AT RESONANCE

2.7.1 Introduction

While the subjects of FCGR and vibration of cracked structures were the concern of numerous investigations, limited number of investigations were reported on FCGR of structural systems at resonance.

Fatigue crack growth in resonating structures has been studied by Dentsoras (1987), and by Dentsoras and Dimargonas (1983a, 1989). They also have reported on resonance controlled fatigue crack propagation in a beam under longitudinal vibrations (1983b), and in cylindrical shafts under combined loading (1983c).

The effects of vibration frequency on fatigue crack propagation of a polymer at resonance was investigated by Dentsoras and Kouvaritakis (1995), and the effect of temperature on the fatigue crack propagation at resonance, by Dentsoras and Panteliou (1992).

2.7.2 Dentsoras and Dimargonas Investigations (1983a, b, c, 1987, 1989)

It is noticeable from the literature review that Dentsoras and Dimargonas have performed several investigations to study the response of a cracked system at resonance. Therefore, a brief review of their related work is presented.

They concluded the following:

1. the phenomenon of *dynamic crack arrest*, that is strongly affected by material damping, dominates the damping mechanism of the system,
2. very high fatigue propagation rate occurs at or very close to resonance,
3. fatigue life can be extended by several orders of magnitudes if the material damping is low; to some extent this influence is reduced by the external damping which is always present in a system,
4. in some loading conditions for a cantilever beam, the change of the dynamic behavior was undetectable for crack length to beam height ratios less than 0.2.

It should be observed that in most actual structures the contribution of the material damping to the total damping in the system is relatively small compared to other damping mechanisms. Consequently, the dynamic crack arrest is a remote possibility for most structures.

The conclusions of Dentsoras Ph.D. thesis are summarized in the following:

"Fatigue crack propagation in various resonating members is studied. The crack propagation rate is related to the stress intensity factor or the strain energy density factor depending on the kind of the load applied. For this purpose the well-known equations of Paris and Sih are used".

"The depth of the crack determines the local stiffness introduced by the crack, which in turn influences the dynamic response of the member under an external excitation of constant amplitude and frequency. As the crack propagates, it introduces additional flexibility to the system and guides it to a gradual shift away from resonance thus resulting to a smaller loading of the cracked section. This causes a drastic reduction of the crack propagation rate and, under certain circumstances, may lead to a propagation that takes place under a threshold level. This level is a characteristic of the material considered".

"The above phenomenon may be interpreted as dynamic crack arrest that, in case of combined load, is more drastic for torsion than for any other kind of external excitation. For structural members where the material damping mechanism dominates, the loss coefficient is considered to be constant during the whole crack propagation process. The value of this coefficient is proved to be the

main factor that determines decisively the crack propagation rate at the initial stages of the crack growth when, due to the resonance, the loading of the cracked section becomes maximum."

CHAPTER 3
FATIGUE CRACK GROWTH AT RESONANCE

3.1 INTRODUCTION

At resonance, the fluctuation range of the stress intensity factor and its maximum value increase substantially, and crack propagates at very high rate. This phenomenon should be considered in designing any structural element where the occurrence of resonance is a possibility. Predicting the crack propagation rate at resonance is a complex task and a limited number of investigations on the subject have been reported in the literature. In this chapter, the conditions that lead to resonance of an MDOF structural system and its dynamic response at resonance are reviewed; an estimation of the changes in the natural frequencies due to crack extension is given; finally, a procedure to predict the crack propagation rate at resonance is presented.

3.2 RESONANCE OF MDOF SYSTEMS

3.2.1 Introduction

In an SDOF system, resonance occurs when the excitation frequency matches the natural frequency of the system. However, for resonance to occur in an MDOF, two conditions should be met:

a. the excitation forces have the same time variation function, and their spatial distribution matches one of the natural mode shapes of the system Φ_n,
b. the frequency of the excitation forces ω, matches the natural frequency of the system ω_n, associated with the mode shape Φ_n.

A simple explanatory example is presented in the following sub-section.

3.2.2 Explanatory Example

Consider the idealized multi-story building shown in Figure (3-1a) together with its properties. The structure is excited by a lateral force P(t) = S. p(t), where "S" defines the relative distribution of force along the height of the structure, as shown in Figure (3-1b), and p(t) defines the time variation of the loading function. Predict the response of the system for the following load history:

$p(t) = 97.4 \sin 2\pi f.$

Where "t" is the time in seconds and "f" falls in the range 0 to 8 Hz. Consider K = 140.0 k/in, m = 0.252 k-sec^2/in, and a damping ratio of 5.0%.

Solution: A modal analysis and a frequency-domain harmonic analysis were performed using the finite element software package "ANSYS". The natural frequencies and mode shapes are as shown in Figure 3-1c. Notice how the spatial distribution of the lateral loads resembles the first mode shape of the system.

Figure 3-1d depicts the displacement response at the tip of the system versus the excitation frequency. Notice how resonance occurs at the fundamental frequency as expected.

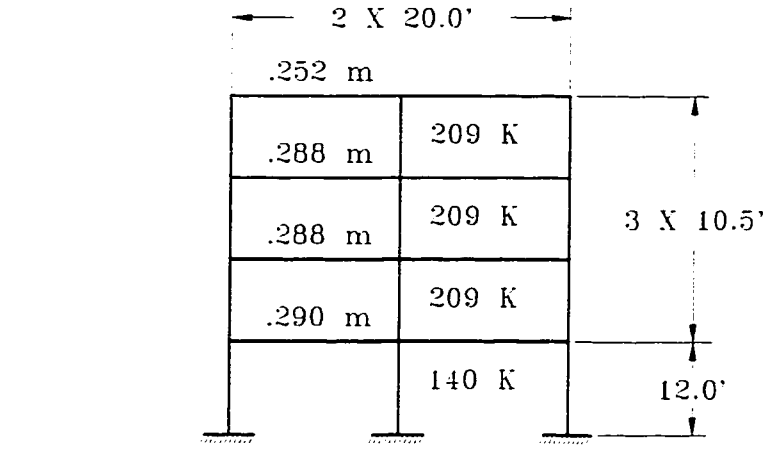

(a)

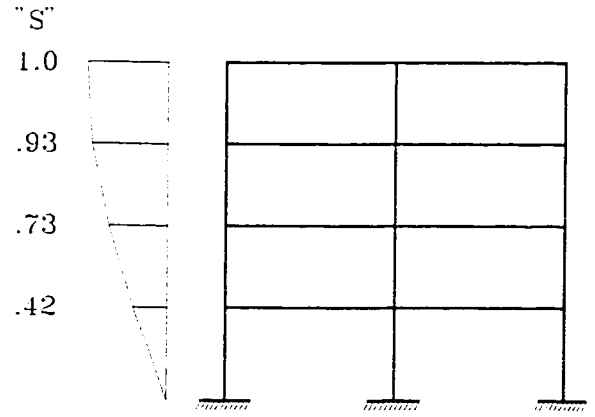

(b)

Figure 3.1a, b

Resonance in an MDOF system

(a) System; (b) Excitation vector.

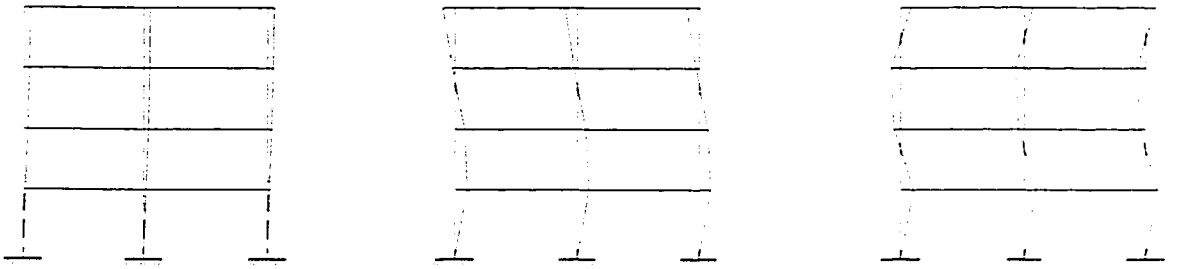

MODE 1
1.378 Hz

MODE 2
4.086 Hz

MODE 3
6.431 Hz

(c)

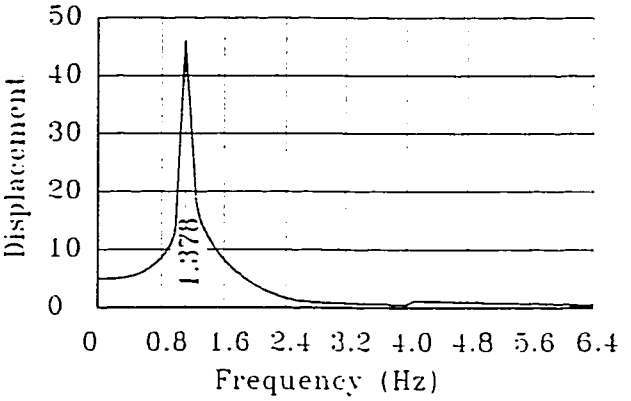

(d)

Figure 3.1c, d

(c) Natural modes; (d) Tip displacement.

3.3 DYNAMIC RESPONSE OF AN MDOF SYSTEM

Consider an elastic MDOF vibrating system with classical damping and N-DOF. Solving the characteristic eigenvalue problem gives the N natural frequencies (eigenvalues), and N natural mode shapes (eigenvectors). A single matrix equation can express the relations between the natural frequencies and mode shapes:

$$k\,\phi = m\,\phi\,\omega^2 \tag{3.1}$$

where k denotes the stiffness matrix; m, the mass matrix; and ϕ, the modal matrix:

$$\phi = \begin{bmatrix} \phi_{11} & \phi_{12} & \cdots & \phi_{1N} \\ \phi_{21} & \phi_{22} & \cdots & \phi_{2N} \\ \cdots & \cdots & \cdots & \cdots \\ \phi_{N1} & \phi_{N2} & \cdots & \phi_{NN} \end{bmatrix};$$

ω^2, the spectral matrix:

$$\omega^2 = \begin{bmatrix} \omega_1^2 & & & \cdots \\ & \omega_2^2 & & \\ & & \cdots & \\ \cdots & & & \omega_N^2 \end{bmatrix}.$$

Let M denote the generalized mass matrix:

$$M = \phi^T m \phi = \begin{bmatrix} M_1 & & & \cdots \\ & M_2 & & \\ & & \cdots & \\ \cdots & & & M_N \end{bmatrix}$$

where $M_n = \phi_n^T m \phi_n$; K, the generalized stiffness matrix:

$$K = \phi^T k \phi = \begin{bmatrix} K_1 & & & \cdots \\ & K_2 & & \\ & & \cdots & \\ \cdots & & & K_N \end{bmatrix}$$

where $K_n = \phi_n^T k \phi_n$.

Notice that both M and K are diagonal matrices due to the orthogonality of the natural modes. Since any vector proportional to the natural mode vector ϕ_n satisfies the characteristic equation, the natural mode can be normalized; Φ_n, so that M_n equals unity. In this case:

$$M_n = \Phi_n^T m \Phi_n = 1,$$

$$M = I \tag{3.2}$$

$$K_n = \Phi_n^T k \Phi_n = \omega_n^2 M_n = \omega_n^2,$$

$$K = \Phi_n^T k \Phi_n = \omega^2 \tag{3.3}$$

If the system under consideration is subjected to an excitation vector:

$P(t) = S\, p(t)$,

where the applied forces have the same time variation $p(t)$, and their spatial distribution is independent of time and defined by S, the equations of motion in matrix form are:

$$m\ddot{u} + c\dot{u} + k u = S\, p(t) \tag{3.4}$$

Since any set of N independent vectors can be used as a basis for representing any other vector of order N, both of the displacement vector u and the excitation vector S, can be expanded in terms of the natural modes:

$$u(t) = \sum_{n=1}^{N} \Phi_n q_n(t) = \Phi q(t) \tag{3.5}$$

$$S = \sum_{n=1}^{N} S_n = \sum \Gamma_n m \Phi_n \tag{3.6}$$

where the *modal coordinate* q_n is:

$$q_n = \frac{\Phi_n^T m u}{M_n},$$

and the modal participation factor Γ_n is:

$$\Gamma_n = \frac{\Phi_n^T S}{M_n}$$

The equations of motion (3.4) can be expressed in terms of q_n (t), the time variation of the modal coordinate, by substituting from (3.5) and (3.6) and pre-multiplying by Φ_n^T:

$$\sum_{n=1}^{N} \Phi_n^T m \Phi_n \ddot{q}_n(t) + \sum_{n=1}^{N} \Phi_n^T c \Phi_n \dot{q}_n(t) + \sum_{n=1}^{N} \Phi_n^T k \Phi q(t) = \sum_{n=1}^{N} \Phi_n^T \Gamma_n m \Phi_n p(t) \tag{3.7}$$

Let $P_n(t)$ denote the generalized force for the n^{th} mode:

$$P_n(t) = \Gamma_n M_n p(t),$$

and C_n, the generalized damping for the n^{th} mode:

$$C_n = \Phi_n^T c \Phi_n$$

Equation (3.7) can be rewritten as:

$$\sum_{n=1}^{N} M_n \ddot{q}_n(t) + \sum_{n=1}^{N} C_n \dot{q}_n(t) + \sum_{n=1}^{N} K_n q(t) = \sum_{n=1}^{N} P_n(t) \tag{3.8}$$

Equation (3.8) is the basis of the modal analysis for an elastic MDOF system with classical damping, where the coupled equations in nodal displacements u (t) were transformed to a set of uncoupled equations in modal coordinate q (t). Thus, any of the N equations can be solved independently. In other words, each equation in modal coordinates can be solved without even knowing the response due to other modes.

Moreover, each equation can be regarded as an equation governing the response, $q_n(t)$, of the SDOF system shown in Figure 3.2, where the mass M_n, is the generalized mass for the n^{th} mode; the stiffness K_n, is the generalized stiffness for the n^{th} mode; the damping C_n, is the generalized damping for the n^{th} mode; and the excitation force $P_n(t)$, is the generalized force for the n^{th} mode.

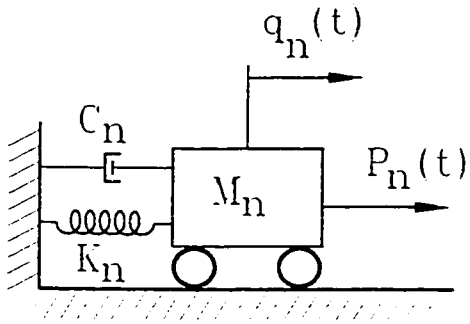

Figure 3.2

Generalized single degree of freedom system

3.4 DYNAMIC RESPONSE OF AN MDOF SYSTEM AT RESONANCE

If the system under consideration is subjected to a harmonic excitation vector:

$$P(t) = S\,p(t) = P_o \sin \omega t$$

the equations of motion of the system in modal coordinate and in matrix form:

$$M\ddot{q} + C\dot{q} + Kq = P_o \sin \omega t \tag{3.9}$$

Let ζ_n denote the *damping ratio* of the n^{th} mode, then:

$$\zeta_n = \frac{C_n}{2 M_n \omega_n}$$

and the solution of any of equations (3.9) is given by:

$$q_n(t) = \frac{P_{no}}{K_n}(\alpha_n \sin \omega t + \beta_n \cos \omega t) \tag{3.10}$$

where:

$$\alpha_n = \frac{1 - \left(\frac{\omega}{\omega_n}\right)^2}{\left[1 - \left(\frac{\omega}{\omega_n}\right)^2\right]^2 - \left(\frac{2\zeta_n \omega}{\omega_n}\right)^2},$$

$$\beta_n = \frac{-2\zeta_n \left(\frac{\omega}{\omega_n}\right)}{\left[1-\left(\frac{\omega}{\omega_n}\right)^2\right]^2 + \left(\frac{2\zeta_n \omega}{\omega_n}\right)^2},$$

and ω, the excitation frequency, which is the same for all modes.

Solving equation (3.10) for q_n and by substituting in equation (3.5), the response of the system is obtained:

$$u(t) = \sum_{n=1}^{N} \Phi_n q_n(t) = \sum_{n=1}^{N} \Phi_n \frac{P_{no}}{K_n} R_{nd} \sin(\omega t - \theta_n) \tag{3.11}$$

where R_{nd} denotes the *deformation response factor* for the n^{th} mode:

$$R_{nd} = \frac{1}{\sqrt{\left[1-\left(\frac{\omega}{\omega_n}\right)^2\right]^2 + \left[2\zeta_n\left(\frac{\omega}{\omega_n}\right)\right]^2}},$$

and θ_n, the *phase angle* for the n^{th} mode:

$$\theta_n = \tan^{-1} \frac{2\zeta_n \left(\frac{\omega}{\omega_n}\right)}{1-\left(\frac{\omega}{\omega_n}\right)}$$

Equation (3.11) can be rewritten as:

$$u(t) = \sum_{n=1}^{N} (u_{st})_{no} R_{nd} \sin(\omega t - \theta_n) \tag{3.12}$$

where $(u_{st})_{no}$ denotes the displacement response of the system under the static forces P_{no}:

$$(u_{st})_{no} = \frac{\phi_n P_{no}}{K_n}.$$

If the excitation force P (t) has the same time variation of one of the natural frequencies of the system, ω_{nr}, and its spatial distribution, P_o, is proportional to the natural vibration mode, Φ_{nr}, associated with the natural frequency ω_{nr}, a resonance condition occurs and the response of the system is entirely due to the contribution of the nr^{th} mode, and governed by the equation:

$$u_{nr}(t) = \Phi_{nr}\, q_{nr}(t) = \Phi_{nr} \frac{P_{nro}}{K_{nr}} R_{ndr} \sin\left(\omega_{nr} t - \frac{\pi}{2}\right) \tag{3.13}$$

the amplitude of the response is given by:

$$u_{nro} = (u_{nr})_{st}\, R_{ndr} \tag{3.14}$$

and the deformation response factor by:

$$R_{ndr} = \frac{1}{2\zeta_{nr}} \tag{3.15}$$

R_{ndr} is also a magnification factor for the system response due to resonance, which is a function of the damping of the resonant mode.

3.5 NATURAL FREQUENCY CHANGES DUE TO CRACKS

3.5.1 Estimation of the Frequency Change

As the crack propagates and increases in length, the stiffness of the system is reduced and so are the natural frequencies of the system. The change of natural frequencies due to crack extension can be determined by using finite element analysis or Gudmundson's perturbation method (1982). However, for small ratios of crack length to element depth, changes in natural frequency are undetectable.

Let Δk denote the change of the stiffness matrix due to crack extension Δa; $\bar{k}$, the corresponding shifted stiffness; $\Delta\omega_{nr}$, the change of the natural frequency for the generalized SDOF system of the resonant mode nr^{th}; then:

$$\omega_{nr}^2 = \frac{\Phi_{nr}^T\, k\, \Phi_{nr}}{\Phi_{nr}^T\, m\, \Phi_{nr}} = \frac{\Phi_{nr}^T\, k\, \Phi_{nr}}{M_{nr}} = \Phi_{nr}^T\, k\, \Phi_{nr} \tag{3.16}$$

for small ΔK_{nr} and $\Delta\omega_{nr}$, it can be assumed that the mode shape will not change, then:

$$(\bar{\omega}_{nr} + \Delta\omega_{nr})^2 = \Phi_{nr}^T \left(\bar{k} + \Delta k\right)\Phi_{nr}$$

$$\bar{\omega}_{nr}^2 + 2\,\bar{\omega}_{nr}\,\Delta\,\omega_{nr} + \Delta^2\omega_{nr} = \Phi_{nr}^T\,\bar{k}\,\Phi_{nr} + \Phi_{nr}^T\,\Delta k\,\Phi_{nr} \tag{3.17}$$

Equation (3.17) can be rewritten as:

$$\omega_{nr}^2 + 2\,\omega_{nr}\,\Delta\,\omega_{nr} = \omega_{nr}^2 + \Phi_{nr}^T\,\Delta k\,\Phi_{nr}$$

$$2\,\omega_{nr}\,\Delta\,\omega_{nr} = \Phi_{nr}^T\,\Delta k\,\Phi_{nr}$$

$$\Delta \omega_{nr} = \frac{\Phi_{nr}^T \Delta k \Phi_{nr}}{2 \omega_{nr}} \tag{3.18}$$

and the shifted frequency:

$$\overline{\omega}_{nr} = \omega_{nr} - \Delta\omega_{nr}$$

However, equation (3.18) is valid for small Δk only, and should be used up to a certain ratio of crack length to element depth, a/h, depending on the tolerated accuracy of the analysis. To set the limiting value of a/h, the value of $\Delta\omega_{nr}$ obtained from equation (3.18) should he examined against the exact value of $\Delta\omega_{nr}$ corresponding to a certain Δk. This exact value can be obtained by solving the eigenvalue problem for $\overline{k}$. The use of this equation is further explained in the following sub-section.

3.5.2 Explanatory Example

Consider a uniform simply supported beam of length L, with a rectangular cross-section, a mass m per unit length, and flexural rigidity EI.

The beam has been idealized as the lumped-mass system shown in Figure 3.3, and is subjected to the forces shown in the same figure.

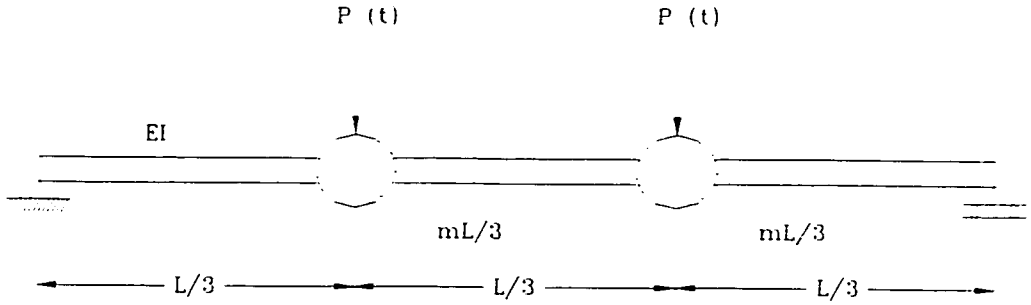

Figure 3.3

Idealization of a simply supported beam

The stiffness matrix is: $k = \frac{162\,EI}{5\,L^3}\begin{bmatrix} 8 & -7 \\ -7 & 8 \end{bmatrix}$,

the mass matrix: $m = \begin{bmatrix} \frac{mL}{3} & 0 \\ 0 & \frac{mL}{3} \end{bmatrix}$,

the natural frequencies:

$$\omega_1^2 = \frac{486\,EI}{5\,mL^4}, \quad \omega_2^2 = \frac{7290\,EI}{5\,mL^4},$$

the modal matrix: $\phi = \begin{bmatrix} 1 & 1 \\ 1 & -1 \end{bmatrix}$,

for $M = I$, the normalized modal matrix:

$$\Phi = \begin{bmatrix} \frac{1}{\sqrt{\frac{2\,mL}{3}}} & \frac{1}{\sqrt{\frac{2\,mL}{3}}} \\ \frac{1}{\sqrt{\frac{2\,mL}{3}}} & \frac{-1}{\sqrt{\frac{2\,mL}{3}}} \end{bmatrix},$$

the generalized stiffness matrix and the generalized spectral matrix:

$$K = \Omega^2 = \begin{bmatrix} \frac{486\,EI}{5\,mL^4} & 0 \\ 0 & \frac{7290\,EI}{5\,mL^4} \end{bmatrix}.$$

Now if a crack is introduced to this beam, the stiffness of the cracked beam is:

$$\bar{k} = \frac{k}{(1+\lambda)},$$

where λ is a function of the crack length, then:

$$\bar{k} = \frac{162\,EI}{5\,L^3(1+\lambda)} \begin{bmatrix} 8 & -7 \\ -7 & 8 \end{bmatrix}.$$

Solving the eigenvalue problem, the shifted natural frequencies:

$$\bar{\omega}_1^2 = \frac{486\,EI}{5\,mL^4(1+\lambda)}, \quad \bar{\omega}_2^2 = \frac{7290\,EI}{5\,mL^4(1+\lambda)},$$

and the change in the natural frequency

$$\Delta\omega_n = \omega_n\left(1 - \sqrt{\frac{1}{1+\lambda}}\right).$$

The change of the natural frequency can also be calculated from equation (3.18):

$$\Delta\omega_1 = \begin{bmatrix} \frac{1}{\sqrt{\frac{2\,mL}{3}}} & \frac{1}{\sqrt{\frac{2\,mL}{3}}} \end{bmatrix} \left(\frac{\lambda}{1+\lambda}\right)\left(\frac{162\,EI}{5\,L^3}\right) \begin{bmatrix} 8 & -7 \\ -7 & 8 \end{bmatrix} \begin{bmatrix} \frac{1}{\sqrt{\frac{2\,mL}{3}}} \\ \frac{1}{\sqrt{\frac{2\,mL}{3}}} \end{bmatrix} \left(\left(\frac{1}{2}\right)\sqrt{\frac{5\,mL^4}{486\,EI}}\right)$$

$$= \frac{\lambda}{2(1+\lambda)}\sqrt{\frac{486\,EI}{5\,mL^4}} = \frac{\lambda}{2(1+\lambda)}\omega_1 .$$

Let $\gamma = \frac{1}{(1+\lambda)}$, then the accuracy, μ, of equation (3.18) is:

$$\mu = \frac{1-\gamma}{2(1-\sqrt{\gamma})} .$$

3.6 PREDICTION OF FATIGUR CRACK GROWTH RATE AT RESONANCE

3.6.1 Introduction

This section presents a procedure to predict the FCGR at resonance. The first step is to obtain information on the stress intensity factor for the system under consideration, the material characteristic curve for FCGR versus the stress intensity factor range, estimation for the damping ratio of the system, and the fracture toughness of the material.

3.6.2 Assumptions

The following assumptions were made in predicting the fatigue crack growth rate at resonance:

a. the system is initially at resonance,
b. the loading mode is a pure opening loading mode (mode I),
c. the system is linear throughout the analysis, and the material is isotropic,
d. to validate the linearity of the system, the crack is open throughout the analysis (see sub-section 2.6.4), i.e.:

   $K_{\min} \geq K_{op}$

   and the stress intensity factor range is given by:

   $\Delta K_{eff} = \Delta K = K_{\max} - K_{\min}$,

where K_{min} denotes the minimum stress intensity factor; K_{max}, the maximum stress intensity factor; K_{op}, the partitioning stress intensity factor dividing ΔK_I in an effective part: K_{eff} and a non-effective part,

e. the applied loads consist of static forces and harmonic forces, where the harmonic forces have the same time variation and their relative distribution is defined by a vector S, independent of time,
f. the FCGR at resonance follows Paris law.
g. for the ring model considered in this investigation: the ring is thick enough to sustain plane strain fracture and the fracture criterion is the Plane Strain Fracture Toughness of the material; K_{Ic},
h. only the flexural vibration of the ring in the plane of the ring is considered; the effects of other vibration modes and coupling harmonics due to the crack propagation are neglected.

3.6.3 A Procedure to Predict the FCGR at Resonance

This procedure requires an expression for the change of the structure stiffness as a function of the crack length; also an expression for K_{op} as a function of ΔK. It can be implemented in the following steps:

a. performing a modal analysis to determine the natural frequencies and mode shapes of the system (see section 3.3),
b. determining the static response of the system under a static load vector S and other applied static forces,
c. determining the resonant mode shape; it is the mode shape that has the same configuration as the static response of the system obtained in step b, and the corresponding natural frequency,
d. determining the dynamic response of the system at resonance, the corresponding ΔK_I (see section 3.5),
e. using the appropriate formula for K_{op}, ΔK_{eff} is determined,
f. calculating the initial FCGR at resonance, using the appropriate formula (see sub-section 2.3.4),

g. calculating the change in stiffness corresponding to a certain crack extension Δa_0 using the appropriate formula (from literature),

h. calculating $\Delta\omega_{nr}$, the corresponding change in natural frequency due to Δa_0 (see section 3.5),

i. calculating the dynamic response of the system corresponding to the shifted frequency $\overline{\omega_{nr}}$, for the crack extension Δa_0, and the corresponding ΔK_I,

j. calculating ΔK_{eff} and the FCGR corresponding to crack extension Δa_0,

k. repeating steps g, h, i, and j for different values of crack extension Δa_1, Δa_2, etc., till the required range of a/h is covered, where h is the member width.

In performing this procedure, the following points should be observed:

1. the stress intensity factor range should be within stage II of the characterizing fatigue crack growth curve of the material (see Figure 2.2),
2. as the crack propagates, a gradual shift from resonance occurs, and the dynamic response of the system is no longer the response of the resonant mode, the contribution of other modes should be considered (see section 3.3),
3. step h can be performed using equation (3.18) (see section 3.5), or using the results of Yao and Dimargonas, in case of a ring (see sub-section 2.6.8),
4. the static forces that keep the crack open do not contribute to ΔK_{eff}, however, they raise the value of K_{max}.

The procedure is further explained in the following sub-section.

3.6.4 Prediction of FCGR for a Simply Supported Beam

Consider a uniform simply supported beam of length L, with a rectangular cross-section, a mass m per unit length, and flexural rigidity EI.

The beam is approximated by a generalized SDOF system with the following properties, the mode shape function:

$$\Psi(x) = \sin\frac{\pi x}{L} \tag{3.19}$$

the modal mass:

$$\tilde{m} = \int_0^L m(x)[\Psi(x)]^2\,dx = \frac{mL}{2} \tag{3.20}$$

the modal stiffens:

$$\tilde{k} = \int_o^L EI(x)[\Psi''(x)]^2\,dx = \frac{\pi^4 EI}{2L^3} = \frac{\pi^4 \bar{k}}{4L^2} \tag{3.21}$$

where $\bar{k}$ is the stiffness of the cracked beam, and $\Psi'' = \frac{d^2\Psi}{dx^2}$,

the modal frequency:

$$\tilde{\omega} = \sqrt{\frac{\tilde{k}}{\tilde{m}}} = \frac{\pi^2}{L^2}\sqrt{\frac{EI}{m}} \tag{3.22}$$

and the modal damping:

$$\tilde{c} = 2\tilde{\zeta}\,\tilde{m}\,\tilde{\omega} \tag{3.23}$$

where $\tilde{\zeta}$ is the modal damping ratio.

If the beam is subjected to a harmonic excitation by a moment couple acting at the two supports in opposite directions, as shown in Figure 3.4, then the equation of motion is:

$$\tilde{m}\,\ddot{z} + \tilde{c}\dot{z} + \tilde{k}z = \tilde{P}(t)$$

where $\tilde{P}(t)$ is the modal excitation,

and the solution is given by:

$$z(t) = \tilde{z}_{st}\,\tilde{R}_d \sin\left(\omega t - \tilde{\theta}\right)$$

where:

$\tilde{z}_{st}$ is the static response,

$$\tilde{R}_d = \frac{1}{\sqrt{\left[1-\left(\frac{\omega}{\tilde{\omega}}\right)^2\right]^2 + \left[2\tilde{\zeta}\left(\frac{\omega}{\tilde{\omega}}\right)^2\right]^2}},$$

and

$$\tilde{\theta} = \tan^{-1}\frac{2\zeta\left(\frac{\omega}{\tilde{\omega}}\right)}{1-\left(\frac{\omega}{\tilde{\omega}}\right)}.$$

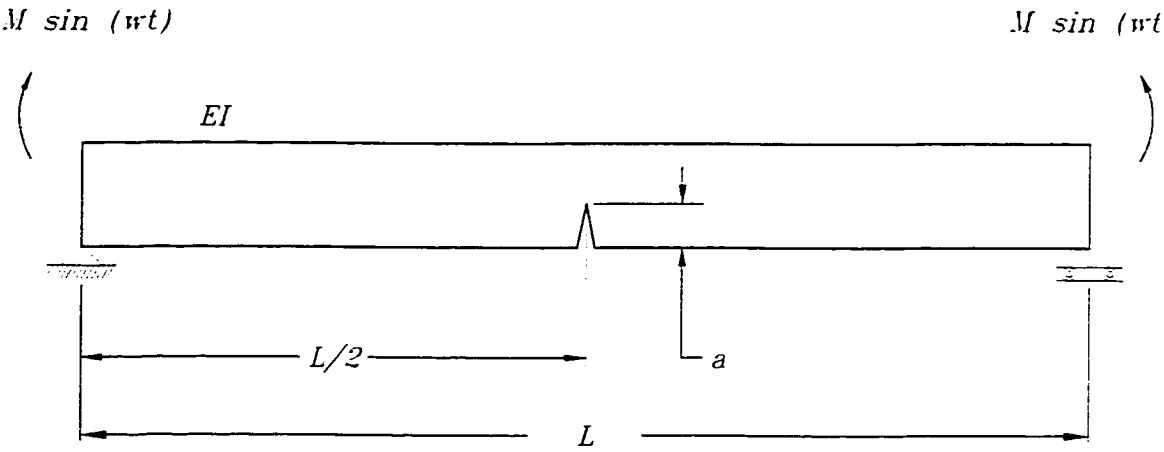

Figure 3.4

Harmonic excitation for a cracked simply supported beam

The stiffness of the cracked beam is:

$$\bar{k} = \frac{1}{C_O + C_S} = \frac{K_O K_S}{K_O + K_S} = \frac{K_O}{1+\lambda} \tag{3.24}$$

where C_O is the compliance of the uncracked beam and C_S is the additional compliance introduced by the crack. For a simply supported beam under pure bending moment:

$$C_O = \frac{1}{K_O} = \frac{L}{2EI}$$

$$C_S = \frac{1}{K_S} = \frac{E b h^2 F(s)}{36(1-\nu)^2} \tag{3.25}$$

where h is the height; b, the width of the rectangular cross-section; $s = \frac{a}{h}$; a, the crack length; and

$$F(s) = 1.98 s^2 - 3.277 s^3 + 14.43 s^4 - 31.26 s^5 + 63.56 s^6 - 103.36 s^7 + 147.52 s^8 - 127.69 s^9 + 61.50 s^{10} \tag{3.26}$$

Equations (3.25, 3.26) were derived analytically (Okamura *et al.* 1969) from the stress intensity factor given by Gross and Srawley (1965) and was verified experimentally (Brown and Srawley 1966).

Now if the beam has the following characteristics:

$b = 0.125\,m$, $h = 0.25\,m$, $L = 1.00\,m$,

$E = 200 x 10^9 \ Pa,$

$m = 7850 \ kg/m^3,$

Solving for the aforementioned properties and for $\tilde{\zeta} = 0.05$:

$\tilde{m} = 122.65625,$

$\tilde{k} = 1585.4344 \ X \ 10^6,$

$\tilde{\omega} = 3595.2517,$

The stress intensity factor is given by Gross and Srawley (1965):

$$K_I = \frac{6 M a^{\frac{1}{2}}}{b h^2} f(s) \tag{3.27}$$

where M is the bending moment, and

$$f(s) = 1.99 - 2.47 s + 12.97 s^2 - 23.17 s^3 + 24.80 s^4 \tag{3.28}$$

Using equation (3.27), K_{max} corresponding to each value of "s" is calculated.

For an open crack with a small positive K_{min} value that approaches zero,

$\Delta K = K_{max}$

If the beam is made of ferritic-pearlitic steel, using equation (2.10), the propagation rate corresponding to each value of "*s*" can be estimated. Table 3.1 shows the values of the deformation response factor for each value of "*s*". The effect of resonance is demonstrated by comparing the dynamic and static stress intensity factors corresponding to each value of "*s*" as shown in Table 3.2.

Figure 3.5 shows the change of the deformation response factor with the crack propagation. Figure 3.6 shows the change of the stress intensity factor of the beam with the crack growth under static bending moment. The change of the cracked beam stiffness with the crack growth is shown in Figure 3.7. It's obvious from Table 3.2 that the propagation rate decreases gradually as the crack tip moves further ahead and the natural frequency changes and shifts away from the excitation frequency. Also, it should be noticed that at each value of "s", an initial stationary condition was assumed, and the effect of the inertial forces due to the initial velocity was ignored.

Table 3.1

Deformation Response Factor for different crack lengths

s	$F(s)$	$\bar{k}$	$\tilde{k}$	$\tilde{\omega}$	$\tilde{R}_d$
0.00	0.0000000000	65104166.667	1585434424.48	3595.25170166	10.00000083
0.05	0.0046217116	64696022.982	1575495198.13	3583.96451089	10.01171526
0.10	0.0177079777	63567648.280	1548016709.63	3552.57275422	9.84326333
0.15	0.0390021477	61813351.678	1505295600.27	3503.20905510	9.10992573
0.20	0.0691322035	59490334.058	1448724841.57	3436.75135191	7.76780423
0.25	0.1094182320	56644045.090	1379411236.26	3353.52878353	6.25159904
0.30	0.1619012243	53320576.695	1298477227.39	3253.66119214	4.94168507
0.35	0.2295967006	49569203.314	1207122759.61	3137.11816749	3.93591054
0.40	0.3170286182	45440192.919	1106571972.22	3003.62002869	3.19101417
0.45	0.4311585554	40983870.708	998050398.24	2852.53771222	2.63930006
0.50	0.5829140625	36256042.405	882917033.84	2682.96561285	2.22545015
0.55	0.7896601335	31331922.969	763003534.25	2494.12625120	1.91073105
0.60	1.0791707674	26325262.428	641079971.12	2286.18443153	1.66936911
0.65	1.4959653543	21401815.488	521182848.33	2061.34277840	1.48431310
0.70	2.1112989307	16771112.149	408414697.55	1824.76036795	1.34385357
0.75	3.0386579933	12647066.580	307984814.96	1584.60058088	1.23924082
0.80	4.4573363405	9189968.881	223796628.84	1350.77162406	1.16324585
0.85	6.6475701119	6462636.326	157379882.57	1132.73877473	1.10952722
0.90	10.0418196209	4426721.682	107800733.84	937.48864731	1.07253527
0.95	15.2981195093	2975247.492	72454038.45	768.57536014	1.04762545

Table 3.2

Number of cycles for static loading and for resonance conditions

s	$f(s)$	(K_I) Static	$\widetilde{R}_d$	(K_I) Dynamic	(da/dN) Static	(da/dN) Dyn.	(N) St.	(N) Dy.
0.00	1.99000000	0.0000	10.00000083	0.000000	0	0.00000000	0	0
0.05	1.89618375	5.1826	10.01171526	51.886606	0.00000096	0.00096386	13014294	12969
0.10	1.85201000	7.1585	9.843263333	70.463430	0.00000253	0.00241402	17952701	18147
0.15	1.84568125	8.7374	9.109925726	79.597333	0.0000046	0.00347972	20668576	21739
0.20	1.86912000	10.2172	7.767804227	79.365509	0.00000736	0.00344941	22367056	25363
0.25	1.91796875	11.7218	6.251599039	73.279753	0.00001111	0.00271520	23491874	29967
0.30	1.99159000	13.3334	4.941685074	65.889617	0.00001636	0.00197379	24256123	36300
0.35	2.09306625	15.1356	3.935910545	59.572190	0.00002392	0.00145875	24778599	44869
0.40	2.22920000	17.2330	3.191014167	54.990683	0.00003531	0.00114740	25132580	55763
0.45	2.41051375	19.7650	2.639300061	52.165814	0.00005328	0.00097951	25367202	68524
0.50	2.65125000	22.9149	2.225450149	50.995858	0.00008302	0.00091507	25517762	82184
0.55	2.96937125	26.9170	1.910731051	51.431212	0.00013456	0.00093871	25610654	95501
0.60	3.38656000	32.0639	1.669369111	53.526411	0.00022746	0.00105817	25665610	107314
0.65	3.92821875	38.7109	1.484313096	57.459152	0.00040027	0.00130896	25696839	116863
0.70	4.62347000	47.2823	1.343853575	63.540462	0.00072936	0.00177011	25713977	123925
0.75	5.50515625	58.2749	1.239240824	72.216651	0.00136551	0.00259873	25723132	128735
0.80	6.60984000	72.2632	1.163245851	84.059887	0.00260376	0.00409841	25727932	131785
0.85	7.97780375	89.9030	1.10952722	99.749821	0.00501385	0.00684834	25730425	133610
0.90	9.65305000	111.9353	1.072535271	120.054583	0.00967722	0.01193948	25731717	134657
0.95	11.68330125	139.1902	1.047625454	145.819220	0.01860695	0.02139407	25732389	135241

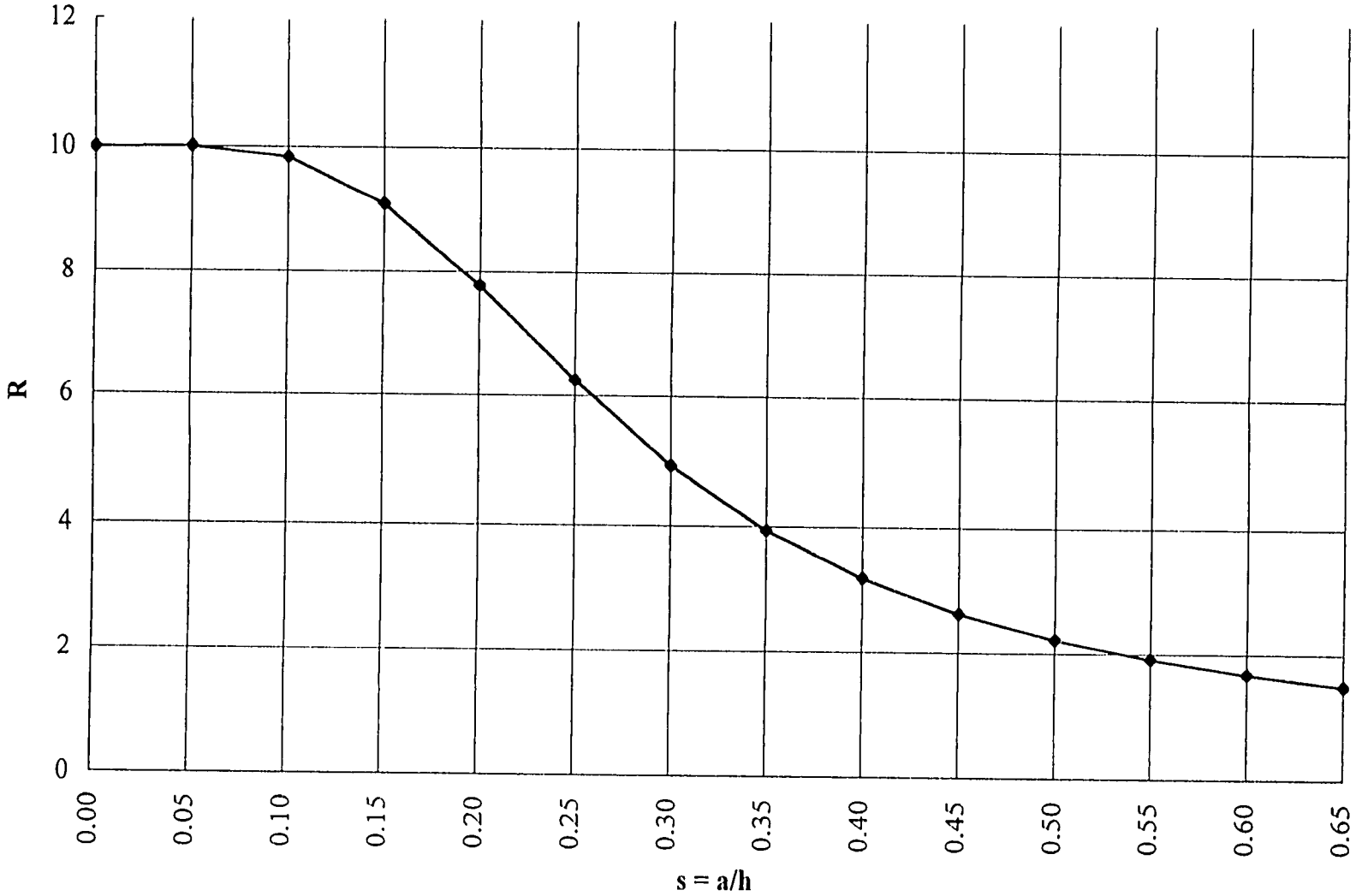

Figure 3.5

Change of the deformation response factor with crack propagation

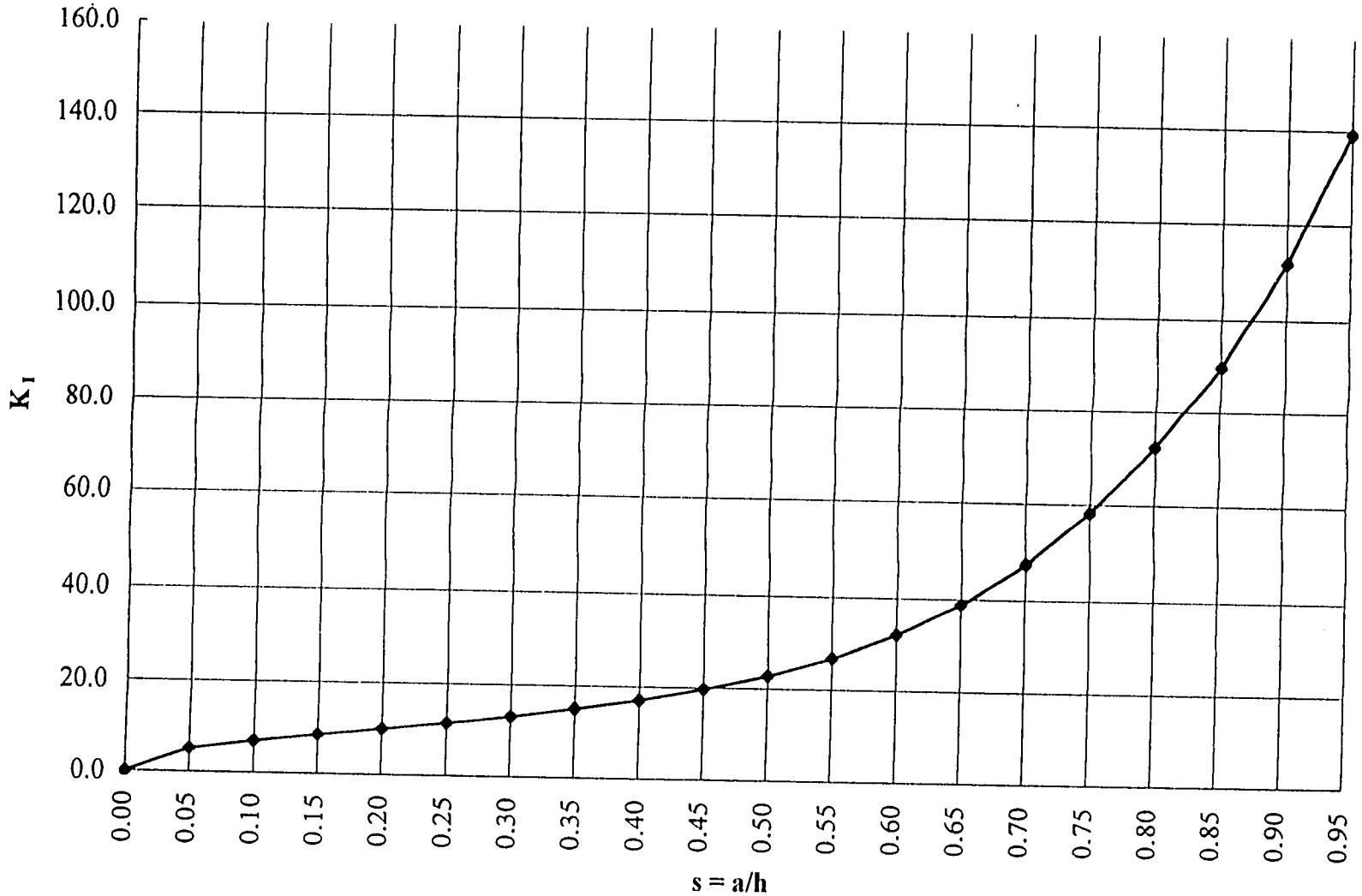

Figure 3.6

Change of the stress intensity factor with crack propagation in a simply supported beam

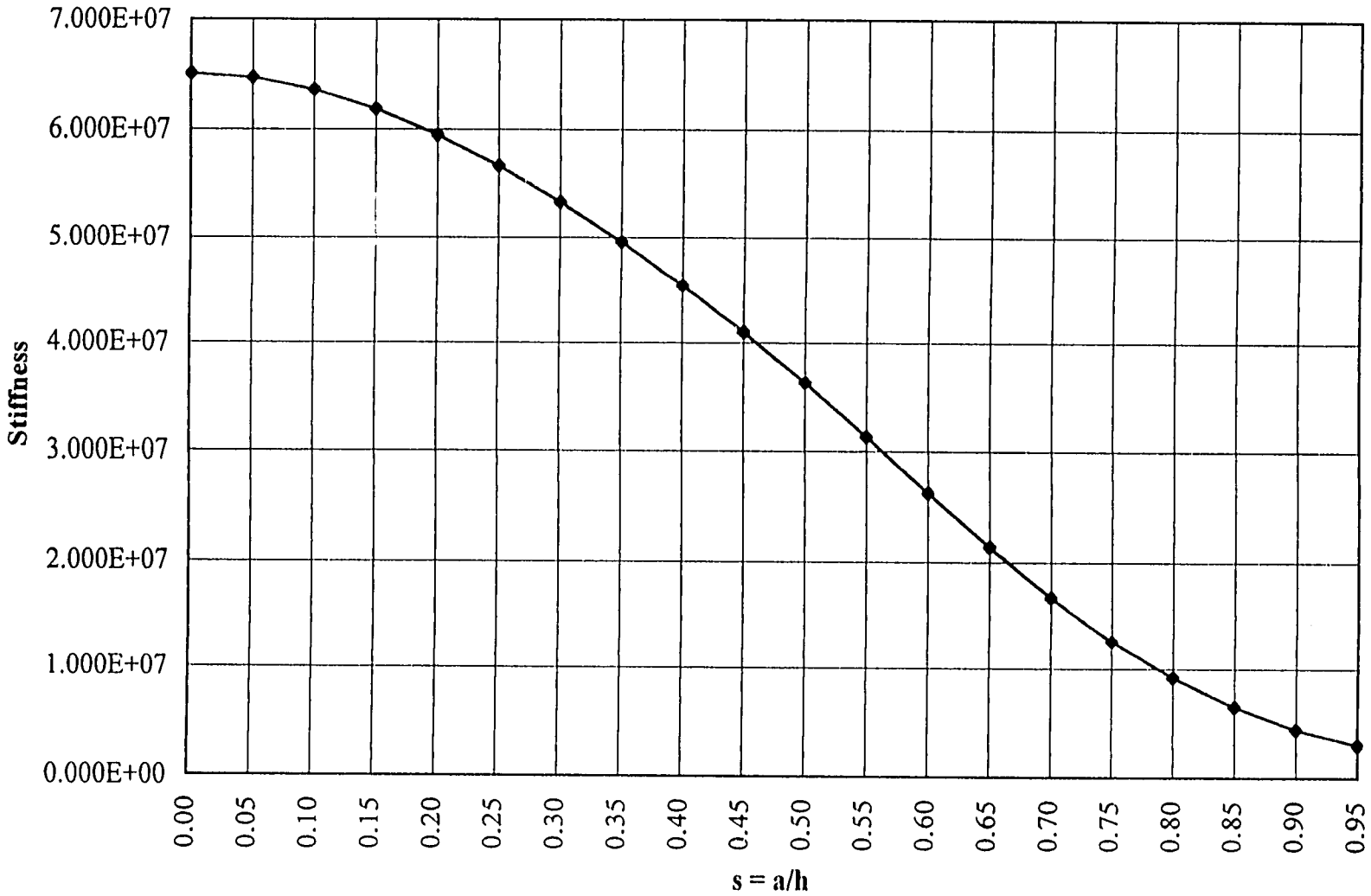

Figure 3.7

Change of the stiffness of a simply supported beam with crack propagation

CHAPTER 4
FINITE ELEMENT ANALYSES

4.1 INTRODUCTION

In predicting the FCGR it was assumed that an expression for the stress intensity factor is obtained from the literature. However, if the expression is not available, it can be obtained using one of the methods referred to in sub-section 2.4.1.

Finite element analysis can be used to simulate the compliance calibration method to obtain an expression for the stress intensity factor, and then the analysis can proceed as was explained in Section 3.6. This procedure will be discussed further in the following sections.

4.2 THE COMPLIANCE CALIBRATION SIMULATION METHOD

The compliance of the ring was obtained for two different boundary conditions: unconstrained and constrained side movement, see Figure 4.1. Because of symmetry, only one quarter of the ring with half of the thickness was considered.

The software package ABAQUS was used in the analyses, samples of the input files for different analyses are appended (Appendix A).

The ring material is assumed to be SAE 1045 with the following properties (Trucker *et al.* 1974):

1. Modulus of Elasticity E = 200 GPa,
2. Poisson's ratio = 0.3,
3. Yield strength = 634 MPa,
4. Density = 7850 kg/m^3,
5. Ferritic-Pearlitic microstructure,

The value of K_{Ic} was not available and it was assumed to be 44.0 MPa. m$^{1/2}$, the same as SAE 1018, a low carbon steel with a similar micro structure (Ripling 1974).

The mesh was mainly composed of three-dimensional solid elements (element type C3D20R in ABAQUS); these hexahedral brick elements have twenty nodes and use a reduced integration scheme, see Figure 4.2. Second order wedge elements (element type C3D15) were also used to refine the mesh at the crack tip as shown in Figure 4.3.

The total number of elements was 3640, with 4 layers of elements through the thickness of the model, the average dimensions of a brick element are 1 x 1 x 3mm.

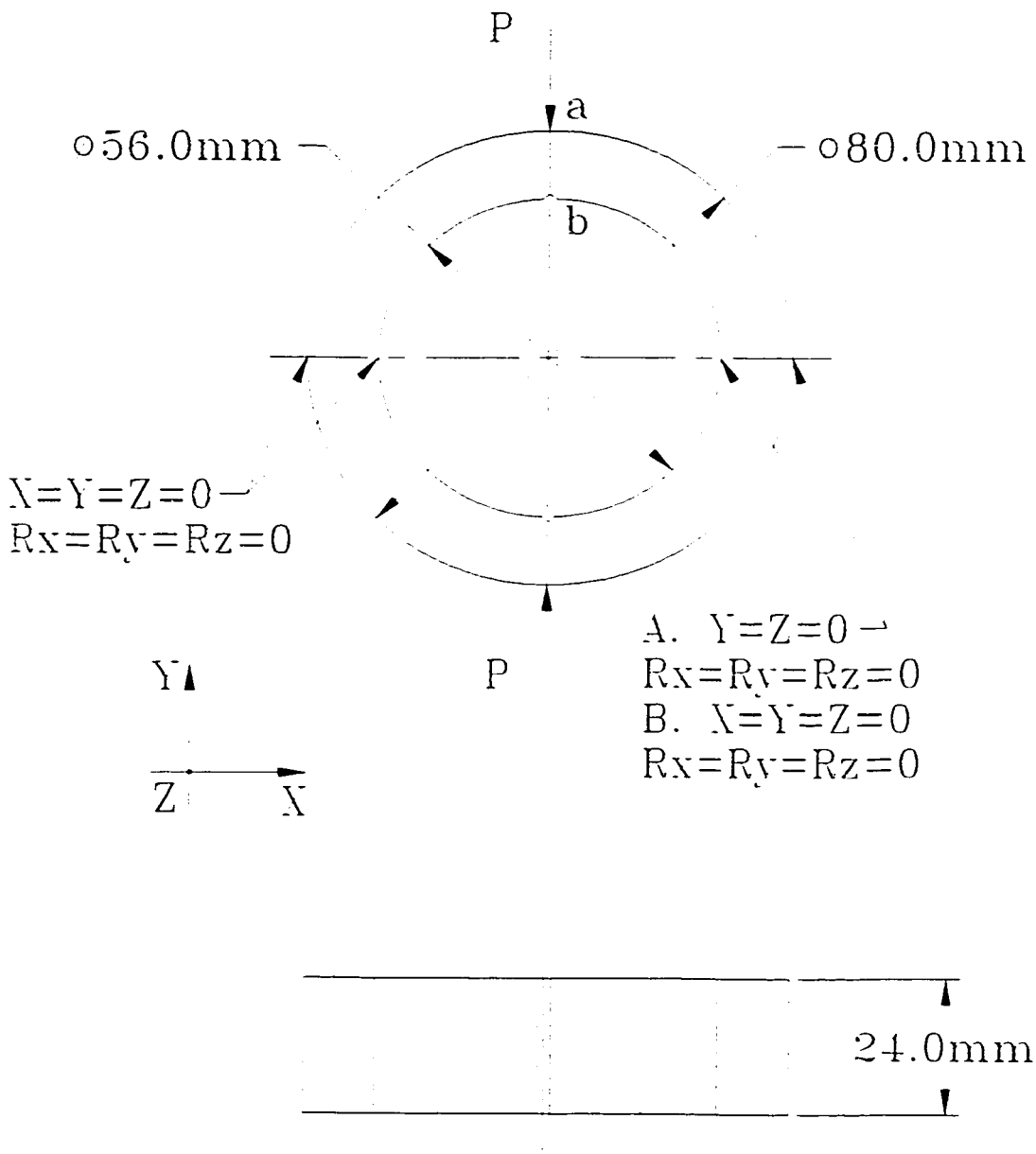

Figure 4.1

Ring dimensions and boundary conditions

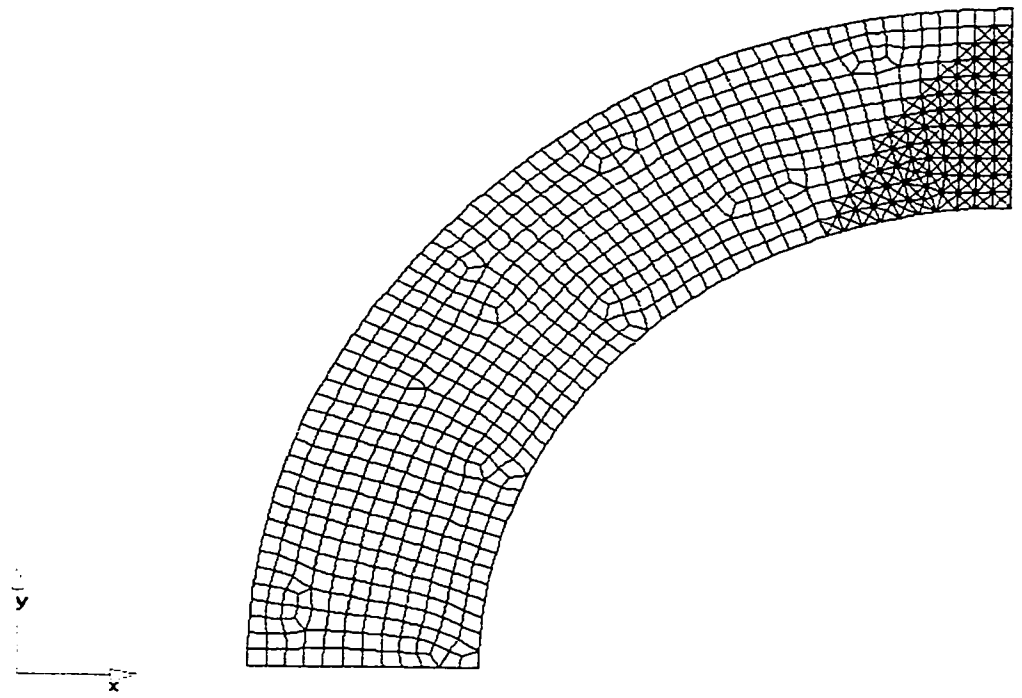

Figure 4.2

Meshed ring

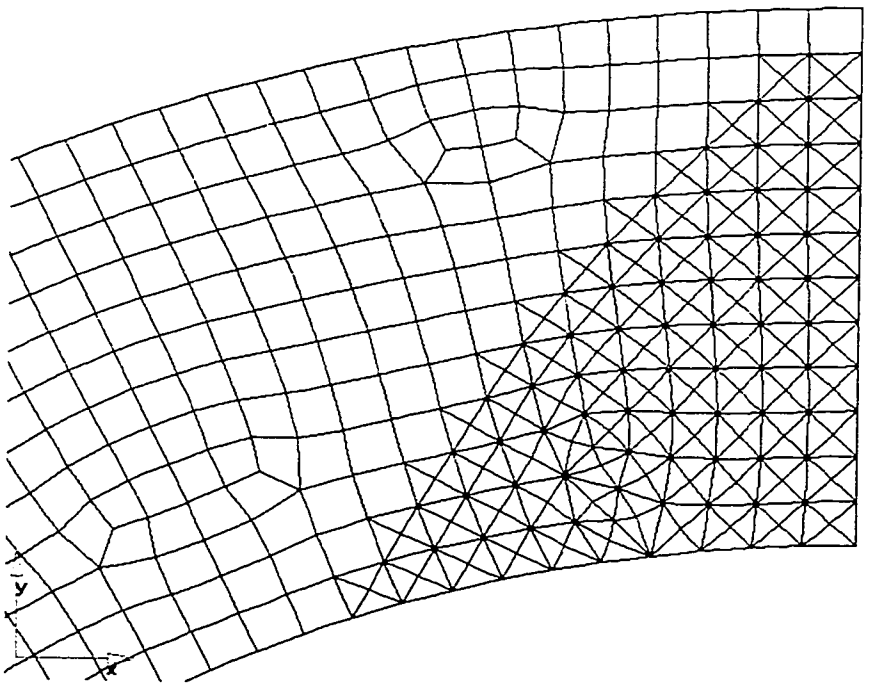

Figure 4.3

Mesh refinement at the crack tip

Symmetry boundary conditions were applied to all nodes located in the uncracked ligament and in the plane of symmetry (along line ab, Figure 4.1), starting from the node at the crack tip, obviously, that number was different for each crack length. The symmetry boundary conditions were also applied to all nodes in the XY plane that bisect the thickness of the ring. The deflection of the ring corresponding to each crack length was obtained by averaging the deflection values of all nodes to which the symmetry boundary conditions were applied. In order to check the validity of the linear assumption; the displacements of the nodes located on the crack surface were checked and the crack was found open in all analyses.

In order to avoid singularity, the concentrated load P (100 kN) was simulated by a pressure applying on the outer surface of the ring, on the faces of the elements that are located along the symmetry plane ab.

The validity of the plane strain assumption was checked using an empirical rule: predominantly plane strain behavior may be expected when the calculated size of the plane stress plastic zone, i.e. the diameter $2r_y$ in Irwin's analysis, is no larger than one tenth of the specimen thickness (Ewalds and Wanhill 1985). According to Irwin:

$$r_y = \frac{1}{2\pi}\left(\frac{K_I}{\sigma_{ys}}\right)^2 \tag{4.1}$$

For $K_I = K_{Ic}$, the minimum thickness for plane strain condition for the case under consideration is $7.7mm \ll 24.0mm$.

The incremental deflections due to crack extension were obtained from the analyses and the compliance values corresponding to different crack lengths, where calculated from the relation:

$$C = \frac{\partial\delta}{P} \tag{4.2}$$

where C is the compliance; $\partial\delta$, the incremental deflection; P, the applied load.

The compliance values were used to obtain the stress intensity factors corresponding to different crack lengths using the following formula, which is applicable to plane strain condition:

$$K_I^2 = \frac{P^2 E}{2b(1-\upsilon^2)}\left(\frac{dC}{da}\right) \tag{4.3}$$

where b is the ring thickness.

The results of the analyses are tabulated in Table 4.1 for unconstrained side movement boundary condition, and in Table 4.2 for the constrained side movement.

The deflection of the uncracked ring under the same loading conditions for the unconstrained side movement case compared very well to the theoretical values obtained from (Roark 1954; Durelli and Lin 1986) The deflection of the ring from the FEA analysis is 0.492mm; from (Roark 1954) is 0.512mm; and from (Durelli and Lin 1986) is 0.47mm.

Values of the stress intensity factor were used to calculate the dimensionless shape factor f (s) from the relation:

$$\frac{K_I\, b\, h^2}{P\, R\, a^{1/2}} = f(s) \tag{4.4}$$

a fourth degree polynomial was fitted to the results of the shape factor, and the stress intensity factor for the unconstrained lateral movement is given by:

$$K_I = \frac{P\, R\, a^{1/2}}{b\, h^2}\left(0.223 + 32.481\, s - 118.447\, s^2 + 172.906\, s^3 - 85.628\, s^4\right) \tag{4.5}$$

and for the constrained side movement by:

$$K_I = \frac{P\, R\, a^{1/2}}{b\, h^2}\left(0.142 + 14.103\, s - 54.974\, s^2 + 75.575\, s^3 - 35.163\, s^4\right) \tag{4.6}$$

The variation of the stress intensity factor with the crack length for the unconstrained and the constrained boundary conditions are shown in Figure 4.4 and Figure 4.5 respectively.

It should be noticed that at small values of "s", a small crack extension results in a substantial increase of K_I. This can be observed by investigating the values of the first derivative of the function S (s) at small values of "s", where S (s) is defined by:

$$S(s) = \frac{K_I\, b h^{3/2}}{PR}$$

For the unconstrained side movement condition:

$$S(s) = 0.112\, s^{-1/2} + 48.722\, s^{1/2} - 296.118\, s^{3/2} + 605.171\, s^{5/2} - 385.326\, s^{7/2} \tag{4.7}$$

for a = 0.50mm, and a = 1.0mm:

$$\left.\frac{\partial S(s)}{\partial s}\right|_{s=.0417} = 8.18, \text{ and } \left.\frac{\partial S(s)}{\partial s}\right|_{s=.0833} = 8.48.$$

For the constrained side movement condition:

$$S(s) = 0.071s^{-1/2} + 21.155s^{1/2} - 137.435s^{3/2} + 264.513s^{5/2} - 158.234s^{7/2} \quad (4.8)$$

for a = 0.50mm, and a = 1.0mm,

$$\left.\frac{\partial S(s)}{\partial s}\right|_{s=.0417} = 3.59, \text{ and } \left.\frac{\partial S(s)}{\partial s}\right|_{s=.0833} = 3.55$$

TABLE 4.1

Stress Intensity Factor for a ring (unconstrained side movement)

D (mm)	a (mm)	a/h	D/P (mm/N)	dC/da	K_I	F (s)
0.492770621	0	0.00000000	0.000004927706	0	0	0
0.508069939	1	0.08333333	0.000005080699	0.000000152993	83.69696448	2.690323616730
0.547073826	2	0.16666667	0.000005470738	0.000000390039	133.6372798	3.037438168406
0.605784444	3	0.25000000	0.000006057844	0.000000587106	163.9577737	3.042749515302
0.685575207	4	0.33333333	0.000006855752	0.000000797908	191.1392994	3.071954726738
0.79034486	5	0.41666667	0.000007903449	0.000001047697	219.0238639	3.148482261707
0.92588172	6	0.50000000	0.000009258817	0.000001355369	249.1164429	3.269050169634
1.099088608	7	0.58333333	0.000010990886	0.000001732069	281.61531	3.421385875972
1.315892308	8	0.66666667	0.000013158923	0.000002168037	315.0699819	3.580608607048
1.57554902	9	0.75000000	0.000015755490	0.000002596567	344.8049244	3.694426423361
1.859081081	10	0.83333333	0.000018590811	0.000002835321	360.3087184	3.662432149089
2.111782609	11	0.91666667	0.000021117826	0.000002527015	340.1555934	3.296674667803

TABLE 4.2

Stress Intensity Factor for a ring (constrained side movement)

D (mm)	a (mm)	a/h	D/P (mm/N)	dC/da	K_I	F (s)
0.166569491525	0	0.00000000	0.000001665695	0.000000000000	0.000000000000	0.000000000000
0.170066871166	1	0.08333333	0.000001700669	0.000000034974	40.017050176103	1.286292947832
0.176720134228	2	0.16666667	0.000001767201	0.000000066533	55.193893433934	1.254500531572
0.184651111111	3	0.25000000	0.000001846511	0.000000079310	60.261095851137	1.118333190969
0.193057024793	4	0.33333333	0.000001930570	0.000000084059	62.039193883678	0.997082209091
0.201427102804	5	0.41666667	0.000002014271	0.000000083701	61.906811442990	0.889914433294
0.209320430108	6	0.50000000	0.000002093204	0.000000078933	60.117891304402	0.788901770001
0.216356962025	7	0.58333333	0.000002163570	0.000000070365	56.761388945782	0.689602473924
0.222229230769	8	0.66666667	0.000002222292	0.000000058723	51.853329121738	0.589286467215
0.226735294118	9	0.75000000	0.000002267353	0.000000045061	45.422635543645	0.486682680796
0.229913513514	10	0.83333333	0.000002299135	0.000000031782	38.147459439878	0.387757705381
0.232521739130	11	0.91666667	0.000002325217	0.000000026082	34.557813864413	0.334922816962

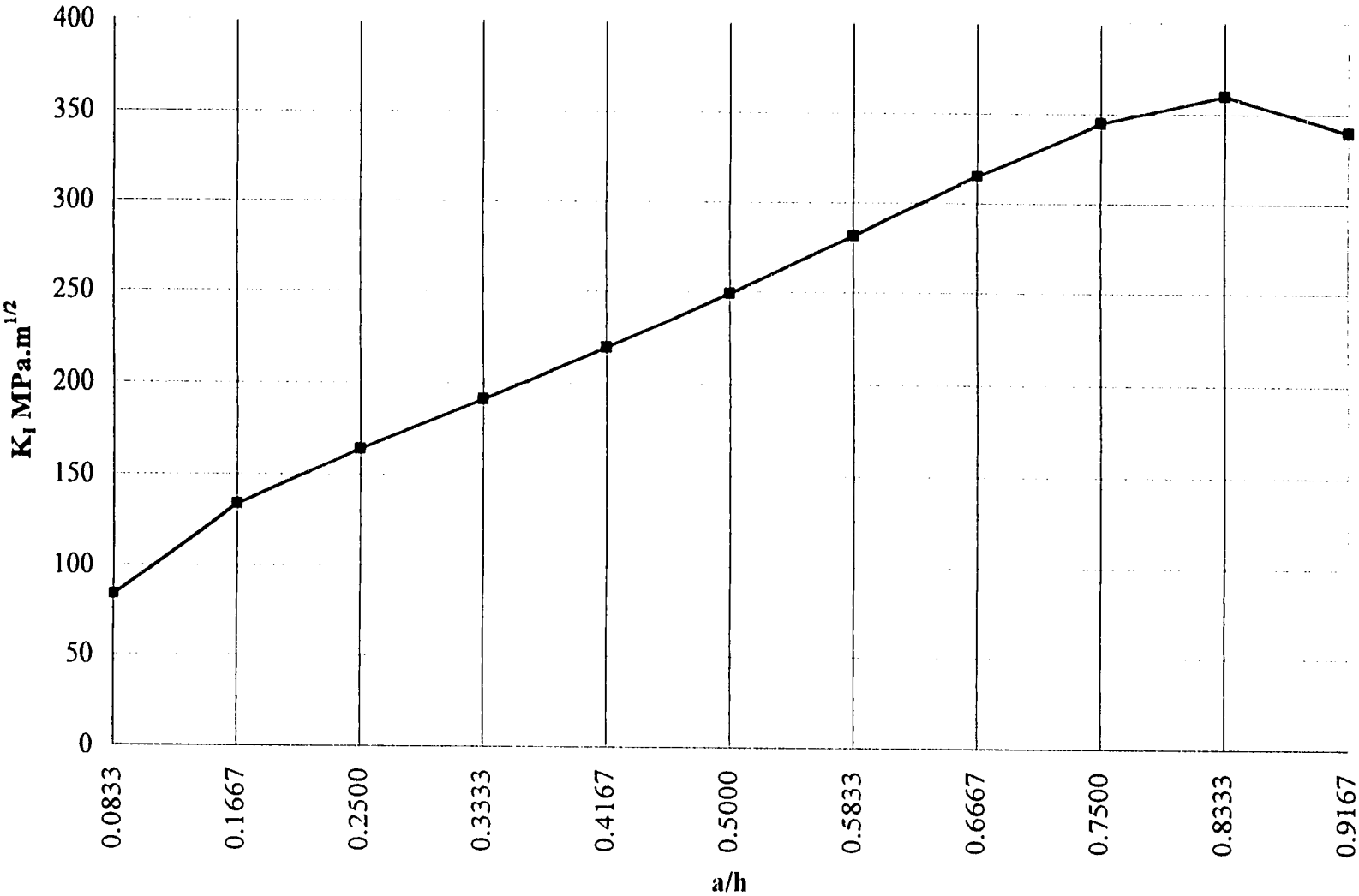

Figure 4.4
Stress Intensity Factor for a ring (unconstrained side movement)

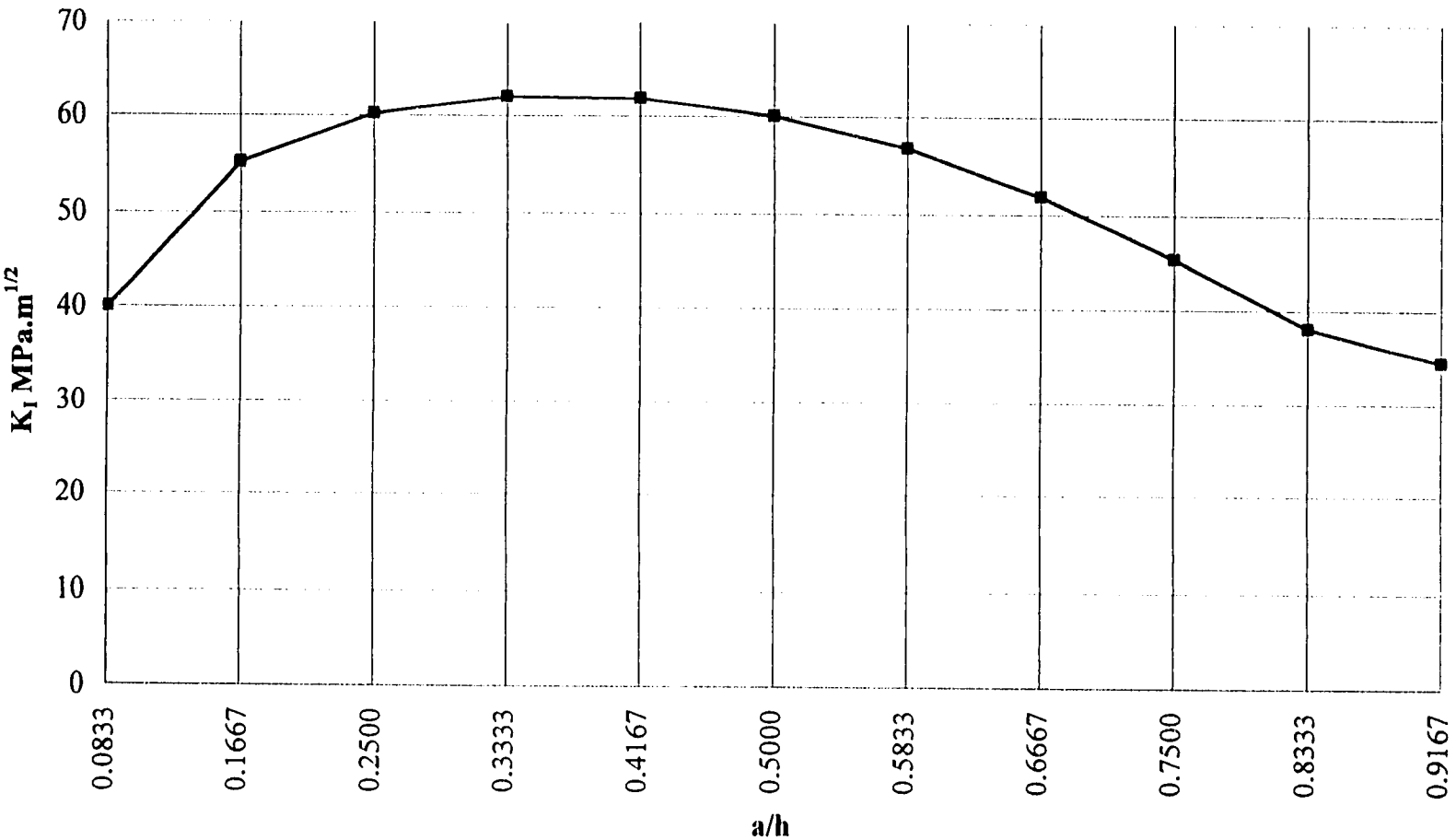

Figure 4.5
Stress Intensity Factor for a ring (constrained side movement)

4.3 MODAL ANALYSIS

As was mentioned in Section 3.6, a modal analysis is required in order to determine the resonant frequency. The deformed shape of the system under a static load vector "S" is compared to the natural mode shapes to determine the critical frequency of "S" at which resonance occurs. Modal analysis was performed for the ring model shown in Figure 4.1, for boundary conditions that simulated the constraints imposed by the fixture used in the test performed in Chapter 5.

The software package "LSDYNA" was used to carryout the analysis; the meshed ring was composed of 9684 elements, with several transitional zones, as shown in Figure 4.6. The average element size at the crack tip was 0.20 x 0.15mm and 4.0 x 4.0mm at the coarsest zone. The refined mesh at the crack tip is shown in Figure 4.7. Appendix B is the input deck of the modal analysis.

The first five modes were extracted and the natural frequencies are listed in Table 4.3. Figures 4.8a, b, and c show the first, second and third mode shapes of the ring, respectively. The deformed shape of the ring for the loading condition under consideration is readily known, however, for more complex loading conditions, a static analysis should be performed to determine the exact deformed shape. It is obvious that the first mode shape is the closest to the deformed shape of the diametrically loaded ring with two equal and opposite concentrated loads. Consequently, a resonance condition occurs if the frequency of the applied loads is 4677 Hz.

Table 4.3
Natural frequencies of the ring

Mode	Frequency (hertz)
1	4677.00
2	11994.0
3	14779.0
4	17568.0
5	23162.0

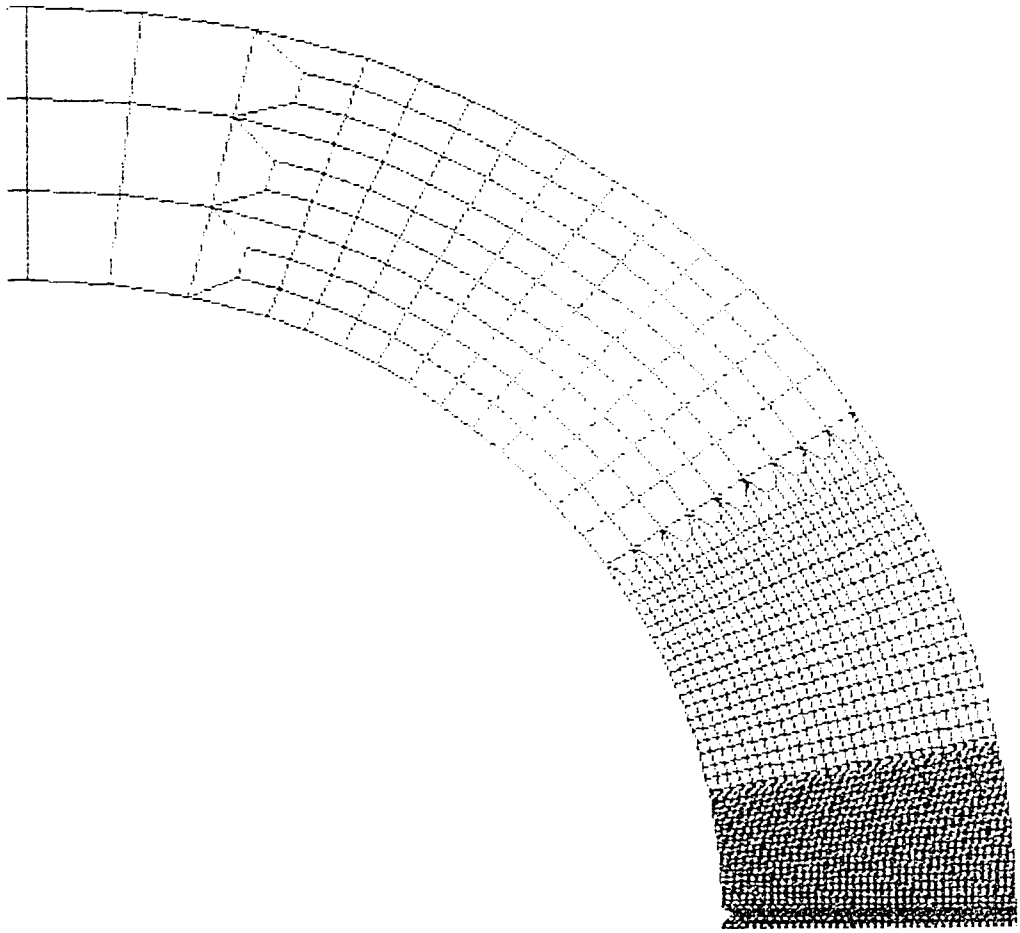

Figure 4.6

Transitional zones of the mesh

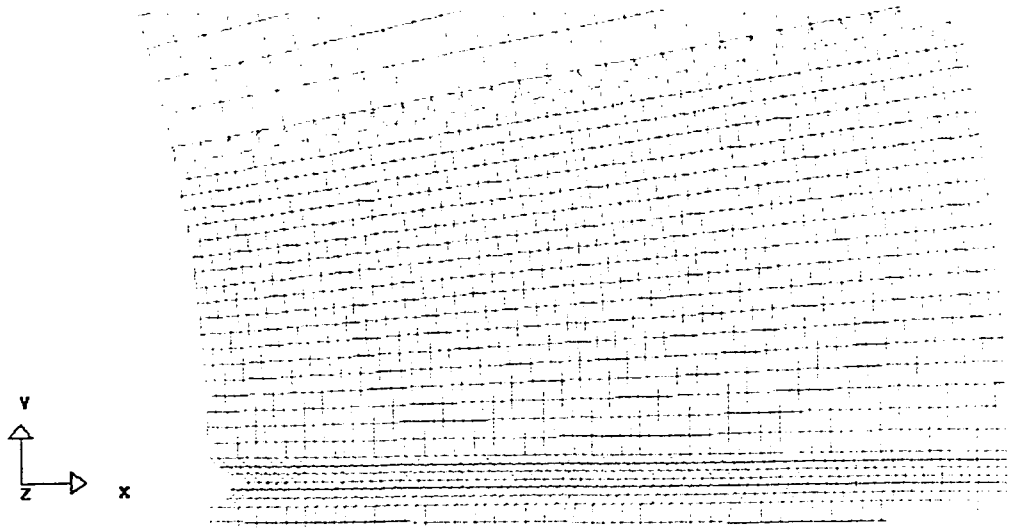

Figure 4.7

Mesh refinement at the crack tip

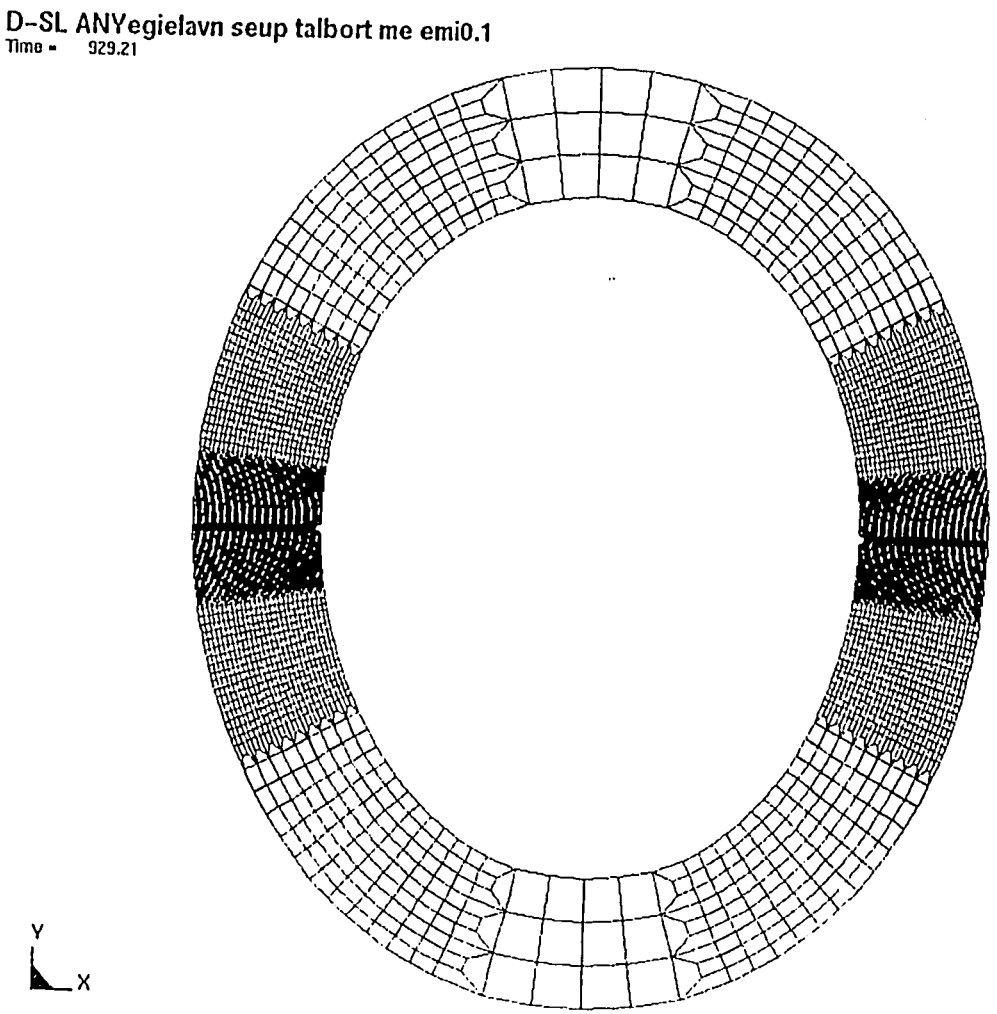

Figure 4.8a
First mode shape

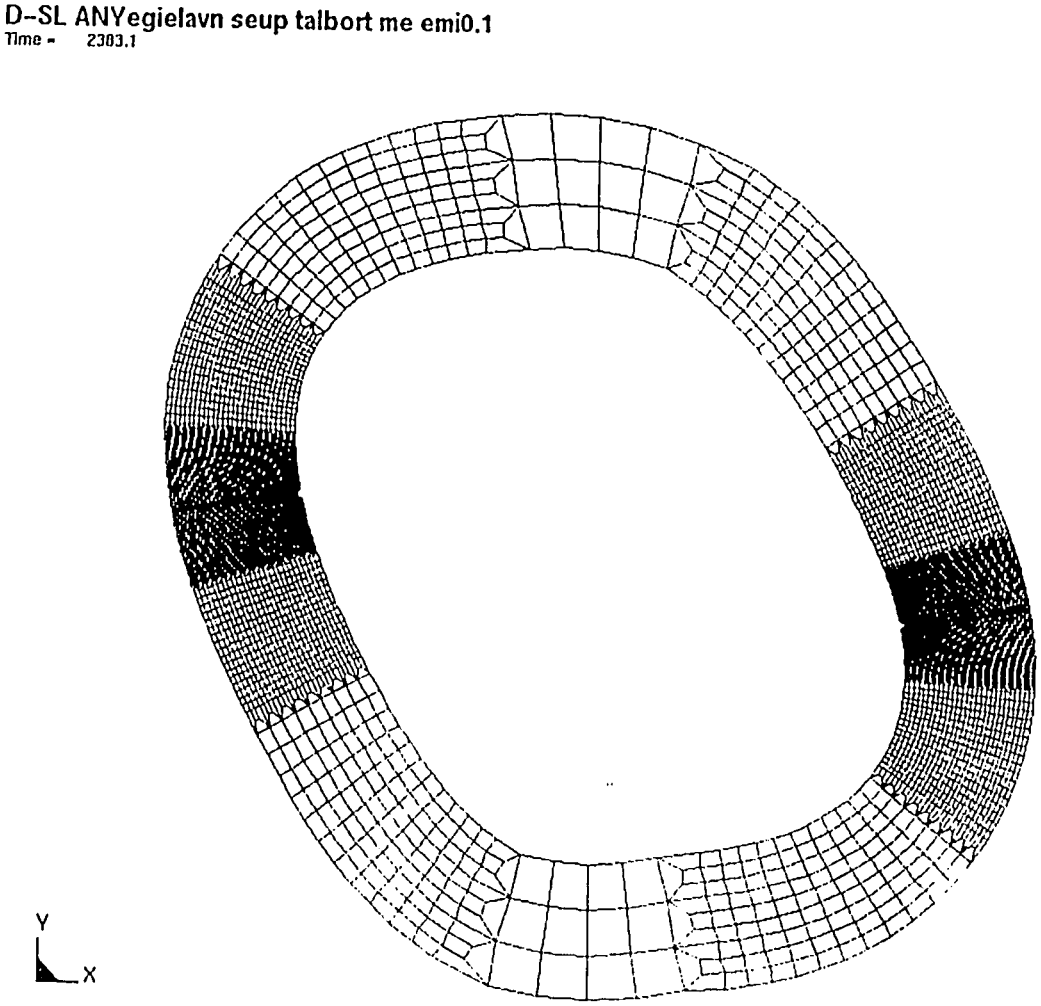

Figure 4.8b
Second mode shape

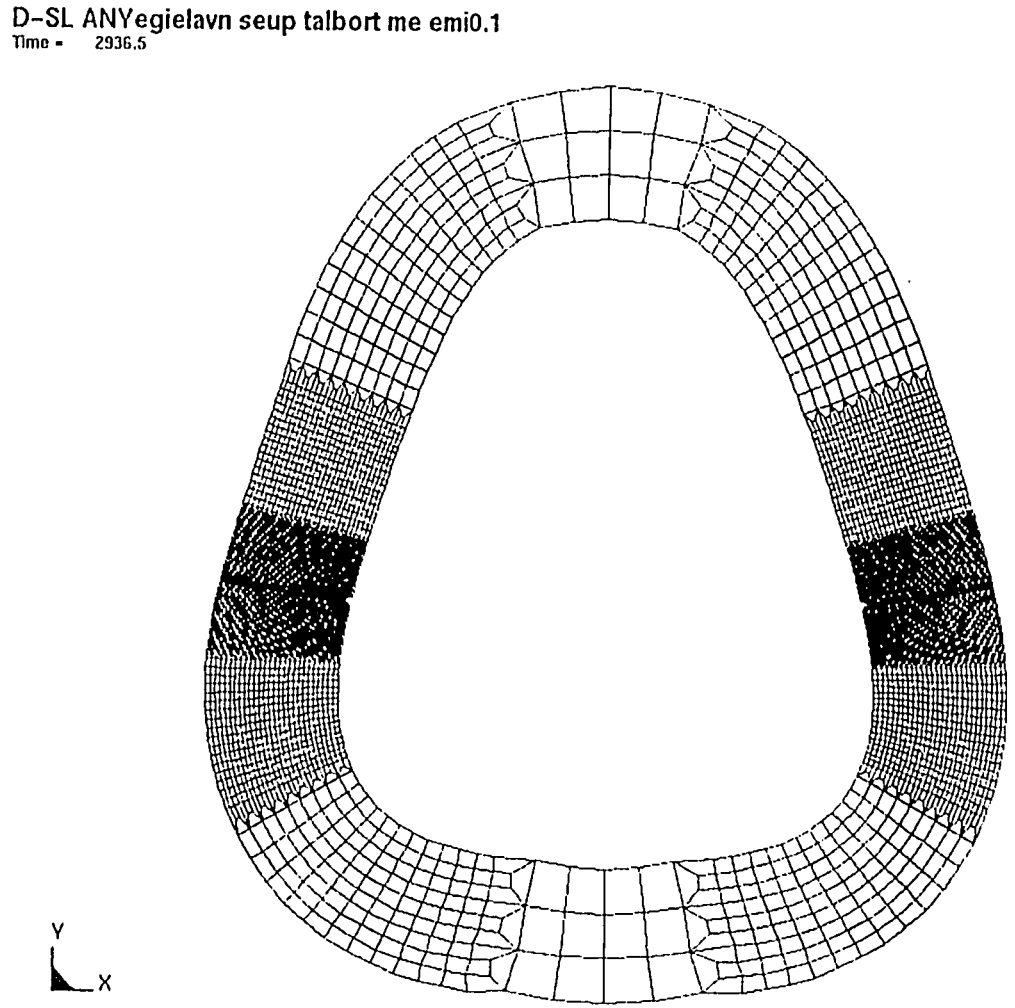

Figure 4.8c
Third mode shape

4.4 FATIGUE CRACK GROWTH IN A CRACKED RING

4.4.1 The Stiffness of a Cracked Ring

The additional compliance caused by the crack can be calculated by substituting for K_I from equation (4.4) in equation (4.3), and integrating:

$$\int_{C_o}^{\bar{C}} dC = \int_0^a \frac{2\,K_I^2\,b\left(1-\upsilon^2\right)}{P^2\,E}\,da$$

$$\bar{C} - C_o = C_S = \frac{2\,R^2\,(1-\upsilon^2)}{E\,b\,h^2}\int_0^s s\,[f\,(s)]^2\,ds$$

$$C_S = \frac{2\,R^2\,(1-\upsilon^2)}{E\,b\,h^2}\,F\,(s) \tag{4.9}$$

using the expression for K_I given by equation (4.5); F(s) for the unconstrained side movement is given by:

$$\begin{aligned} F\,(s) = {} & 0.025\,s^2 + 4.838\,s^3 + 250.527\,s^4 - 1523.473\,s^5 + 4203.976\,s^6 \\ & - 6646.148\,s^7 + 6272.667\,s^8 - 3290.148\,s^9 + 733.222\,s^{10} \end{aligned} \tag{4.10}$$

Similarly, using the expression for K_I given by equation (4.6); F(s) for the constrained side movement is given by:

$$\begin{aligned} F\,(s) = {} & 0.01\,s^2 + 1.333\,s^3 + 45.829\,s^4 - 305.837\,s^5 + 857.307\,s^6 \\ & - 1328.726\,s^7 + 1197.199\,s^8 - 590.535\,s^9 + 123.641\,s^{10} \end{aligned} \tag{4.11}$$

The vertical deflection along the line of force application of the uncracked ring is given by:

$$\delta = \rho\,\frac{P\,R^3}{E\,I} \tag{4.12}$$

where ρ is a factor that can be obtained by considering the ring as an undetermined structural system and solving the problem using the standard structural analysis methods. Then the compliance of the uncracked ring is obtained by:

$$C_o = \frac{\rho\,R^3}{E\,I} \tag{4.13}$$

and the stiffness of the cracked ring is given by:

$$\bar{k} = \frac{1}{C_O + C_S} = \frac{K_O\,K_S}{K_O + K_S} \tag{4.14}$$

For the model considered in this problem, $\rho = 0.09$, for unconstrained side movement condition.

Having obtained the stiffness of the cracked ring; the analysis to predict FCGR at resonance can proceed in a similar manner to sub-section 3.6.4 as further explained in the following sub-section.

4.4.2 Explanatory Example

Consider a diametrically loaded circular ring, where two opposite and equal concentrated loads apply vertically. The ring dimensions and boundary conditions are shown in Figure 4.9. From symmetry, only one half of the ring is considered.

The ring is approximated by a generalized SDOF system; the deformation values at different angles θ under the applied loads were obtained from Durelli and Lin (1986), see Figure 4.10.

A fourth degree polynomial was fitted to the R values corresponding to different values of θ, is given by:

$$R(\theta) = 34.3687 + 0.3261\,\theta - 1.7817\,\theta^2 + 1.0682\,\theta^3 - 0.1700\,\theta^4 \qquad (4.15)$$

and the arc length is given by:

$$d\,s = R\,d\theta,$$

$$s = \int_0^s R\,d\theta = 34.3687\,\theta + 0.1631\,\theta^2 - 0.5939\,\theta^3 + 0.2670\,\theta^4 - .0340\,\theta^5 \qquad (4.16)$$

the mode shape function is given by:

$$\Psi(\theta) = R_o - R = -0.3687 - 0.3261\,\theta + 1.7817\,\theta^2 - 1.0682\,\theta^3 + 0.1700\,\theta^4 \qquad (4.17)$$

and as a function of s by:

$$\Psi(s) = (367833.0 + 10190.2\,s - 1566.34\,s^2 + 27.5515\,s^3 - 0.129017\,s^4)\,10^{-6} \qquad (4.18)$$

This formula was obtained by fitting a fourth order polynomial to the values of Ψ corresponding to different values of s.

Assuming that the ring is made of the same material used in the compliance simulation analyses (see Section 4.2), then the modal mass:

$$\tilde{m} = \int_o^s m(s)\,[\Psi(s)]^2\,ds$$

$$\tilde{m} = 8.8261\,m'$$

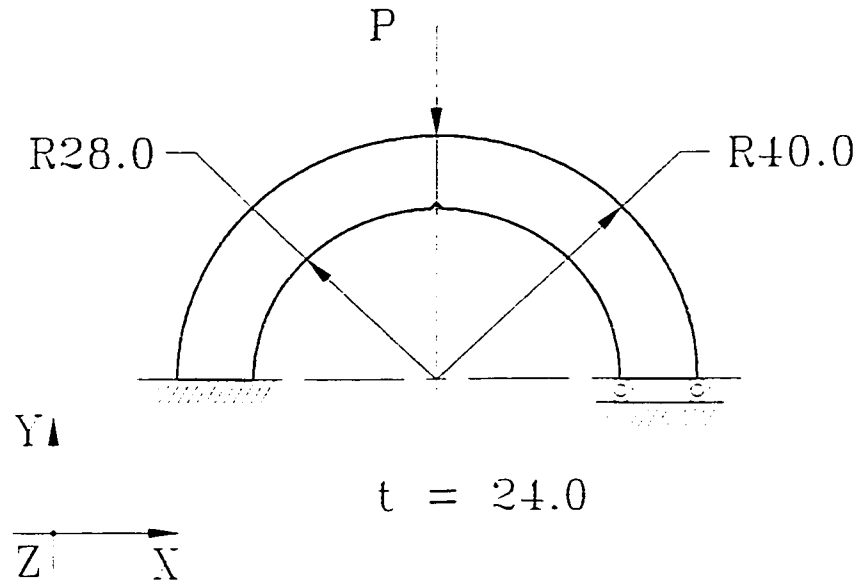

Figure 4.9

Geometry and boundary conditions for the ring

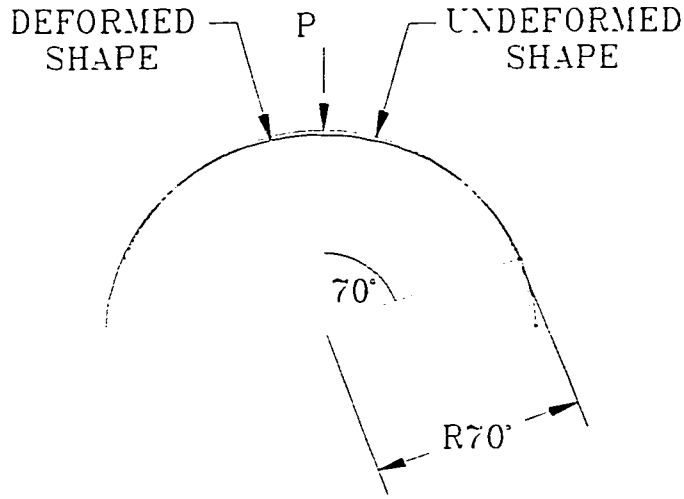

ANGLE	R mm
0°	34.47
10°	34.40
20°	34.33
30°	34.20
40°	34.07
45°	0
50°	33.93
60°	33.80
70°	33.73
80°	33.66
90°	34.60

Figure 4.10

The deformed shape of the ring

the modal stiffness:

$$\tilde{k} = \int_{o}^{s} EI(s)[\Psi''(s)]^2 \, ds$$

$$\tilde{k} = 0.0204\, EI = 72.0968\, \bar{k}$$

where $\Psi'' = \frac{d^2\Psi}{ds^2}$, and $\bar{k}$ is the stiffness of the cracked ring,

the modal frequency:

$$\tilde{\omega} = \sqrt{\frac{\tilde{k}}{\tilde{m}}} = 2.8581 \sqrt{\frac{\bar{k}}{m'}},$$

and the modal damping:

$$\tilde{c} = 2\tilde{\zeta}\, \tilde{m}\, \tilde{\omega} ,$$

where $\tilde{\zeta}$ is the modal damping ratio and it was assumed to be 0.05 in this problem.

If the ring is subjected to a harmonic excitation by a couple of vertical diametrical loads acting in opposite directions, 10 kN each, then using a procedure similar to that used in Sub-section 3.6.4, the propagation rate corresponding to each "s" value can be predicted. Table 4.4 shows the values of the deformation response factor for different values of "s". The effect of resonance is demonstrated by comparing the stress intensity factor values for the dynamic and static loading conditions, see Table 4.5. Figure 4.11 shows the change of the deformation response factor with the crack propagation. The change of the stress intensity factor of the ring with the crack growth is shown in Figure 4.12 and the change of the stiffness of the cracked ring with crack growth is shown in Figure 4.13.

Table 4.4

Deformation Response Factor for Different crack lengths

s	$F(s)$	$\bar{k}$	$\tilde{k}$	$\tilde{\omega}$	$\tilde{R}_d$
0.00	0.0000000000	195399.959	14087703.86	225612.36002669	10.00000000
0.05	0.0018175737	195188.952	14072490.93	225490.51075404	10.00481979
0.10	0.0185043323	193272.829	13934344.63	224380.98767448	9.99518078
0.15	0.0660458175	188014.351	13555225.42	221307.51100546	9.51274201
0.20	0.1514659580	179251.612	12923460.38	216088.76608190	7.90486361
0.25	0.2725815164	168140.421	12122379.49	209284.33348622	5.96900981
0.30	0.4224054342	156165.725	11259042.72	201694.24895123	4.54975834
0.35	0.5937669623	144403.180	10411001.34	193949.66454394	3.63927235
0.40	0.7824336439	133345.222	9613758.43	186375.74143311	3.04742067
0.45	0.9885747656	123049.705	8871485.00	179036.23774092	2.64078153
0.50	1.2170576426	113349.533	8172133.99	171834.56231555	2.34322882
0.55	1.4770768980	104017.877	7499351.83	164609.40540350	2.11271771
0.60	1.7812425620	94880.517	6840577.83	157213.26091474	1.92631000
0.65	2.1437551932	85888.433	6192277.71	149578.09372981	1.77193163
0.70	2.5769351517	77151.249	5562355.04	141766.01600508	1.64361251
0.75	3.0854084576	68921.420	4969011.02	133991.65814484	1.53846344
0.80	3.6579431933	61530.903	4436178.68	126603.96192118	1.45476315
0.85	4.2585379882	55309.348	3987624.79	120032.79668834	1.39098651
0.90	4.8211475878	50523.846	3642605.54	114722.56637528	1.34557748
0.95	5.2566497051	47352.421	3413956.13	111063.60074165	1.31706900

Table 4.5

Number of cycles for static loading and for resonance conditions

s	$f(s)$	(K_I) Static	$\widetilde{R}_d$	(K_I) Dynamic	(da/dN) Static	(da/dN) Dyn.	(N) St.	(N) Dy.
0.00	1.99000000	0.0000	10.00000083	0.000000	0.00000000	0	0	0
0.05	1.89618375	5.1826	10.01171526	51.886606	0.00096386	0.00000096	12969	13014294
0.10	1.85201000	7.1585	9.843263333	70.463430	0.00241402	0.00000253	18147	17952701
0.15	1.84568125	8.7374	9.109925726	79.597333	0.00347972	0.0000046	21739	20668576
0.20	1.86912000	10.2172	7.767804227	79.365509	0.00344941	0.00000736	25363	22367056
0.25	1.91796875	11.7218	6.251599039	73.279753	0.00271520	0.00001111	29967	23491874
0.30	1.99159000	13.3334	4.941685074	65.889617	0.00197379	0.00001636	36300	24256123
0.35	2.09306625	15.1356	3.935910545	59.572190	0.00145875	0.00002392	44869	24778599
0.40	2.22920000	17.2330	3.191014167	54.990683	0.00114740	0.00003531	55763	25132580
0.45	2.41051375	19.7650	2.639300061	52.165814	0.00097951	0.00005328	68524	25367202
0.50	2.65125000	22.9149	2.225450149	50.995858	0.00091507	0.00008302	82184	25517762
0.55	2.96937125	26.9170	1.910731051	51.431212	0.00093871	0.00013456	95501	25610654
0.60	3.38656000	32.0639	1.669369111	53.526411	0.00105817	0.00022746	107314	25665610
0.65	3.92821875	38.7109	1.484313096	57.459152	0.00130896	0.00040027	116863	25696839
0.70	4.62347000	47.2823	1.343853575	63.540462	0.00177011	0.00072936	123925	25713977
0.75	5.50515625	58.2749	1.239240824	72.216651	0.00259873	0.00136551	128735	25723132
0.80	6.60984000	72.2632	1.163245851	84.059887	0.00409841	0.00260376	131785	25727932
0.85	7.97780375	89.9030	1.10952722	99.749821	0.00684834	0.00501385	133610	25730425
0.90	9.65305000	111.9353	1.072535271	120.054583	0.01193948	0.00967722	134657	25731717
0.95	11.68330000	139.1902	1.047625454	145.819220	0.02139407	0.01860695	135241	25732389

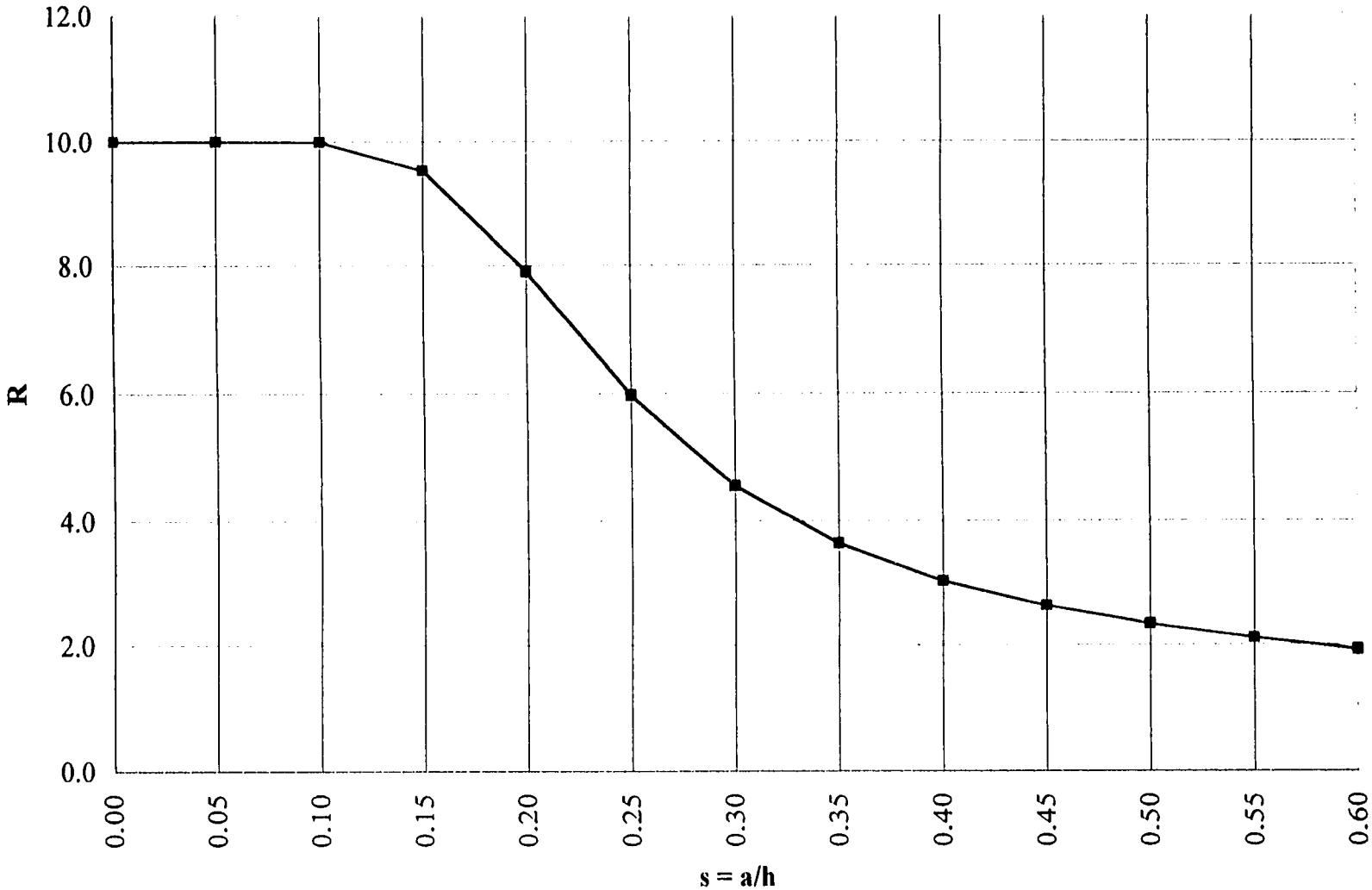

Figure 4.11
Change of the deformation response factor with crack propagation

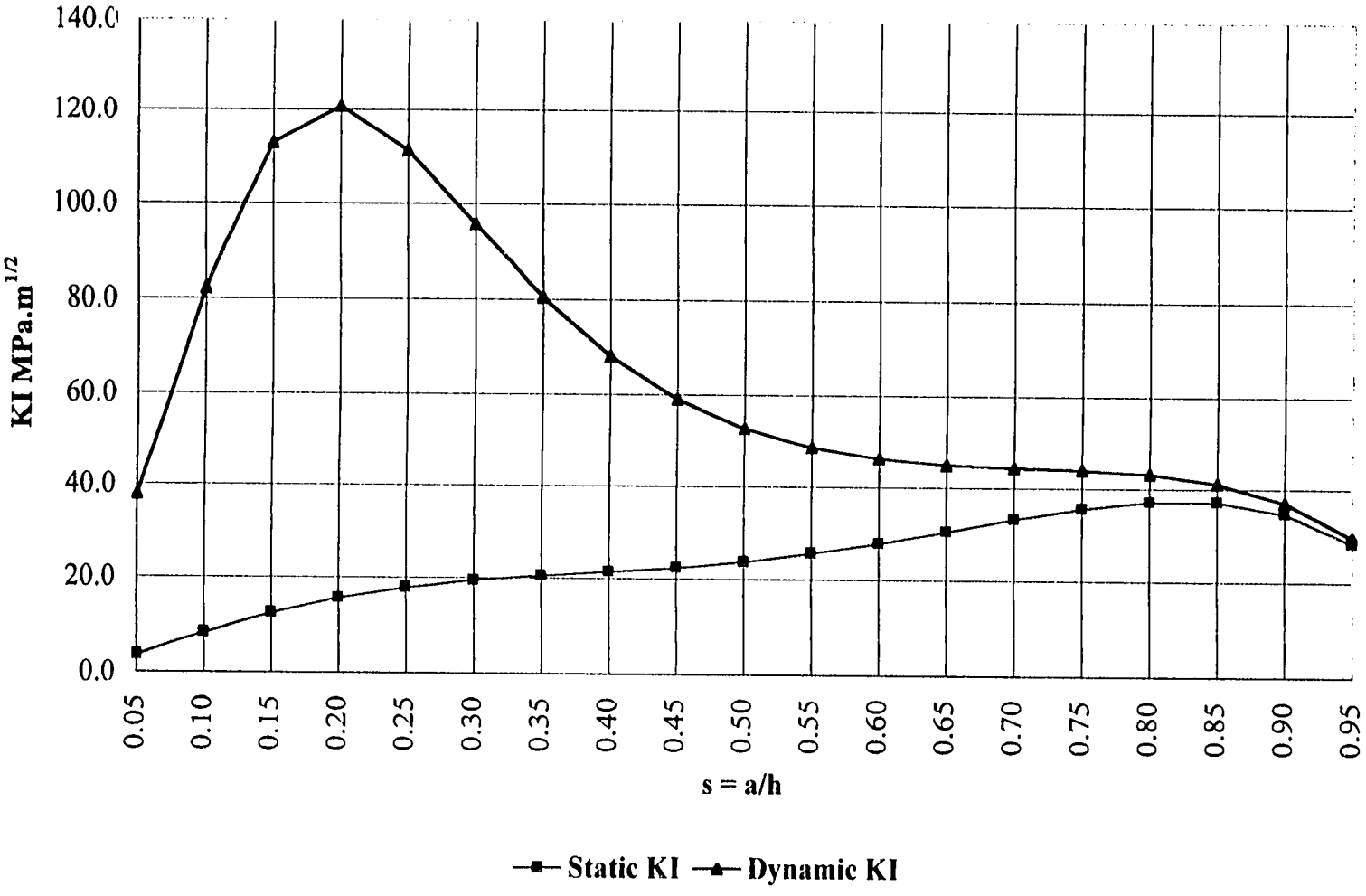

Figure 4.12
Change of the stress intensity factor with crack propagation in the ring

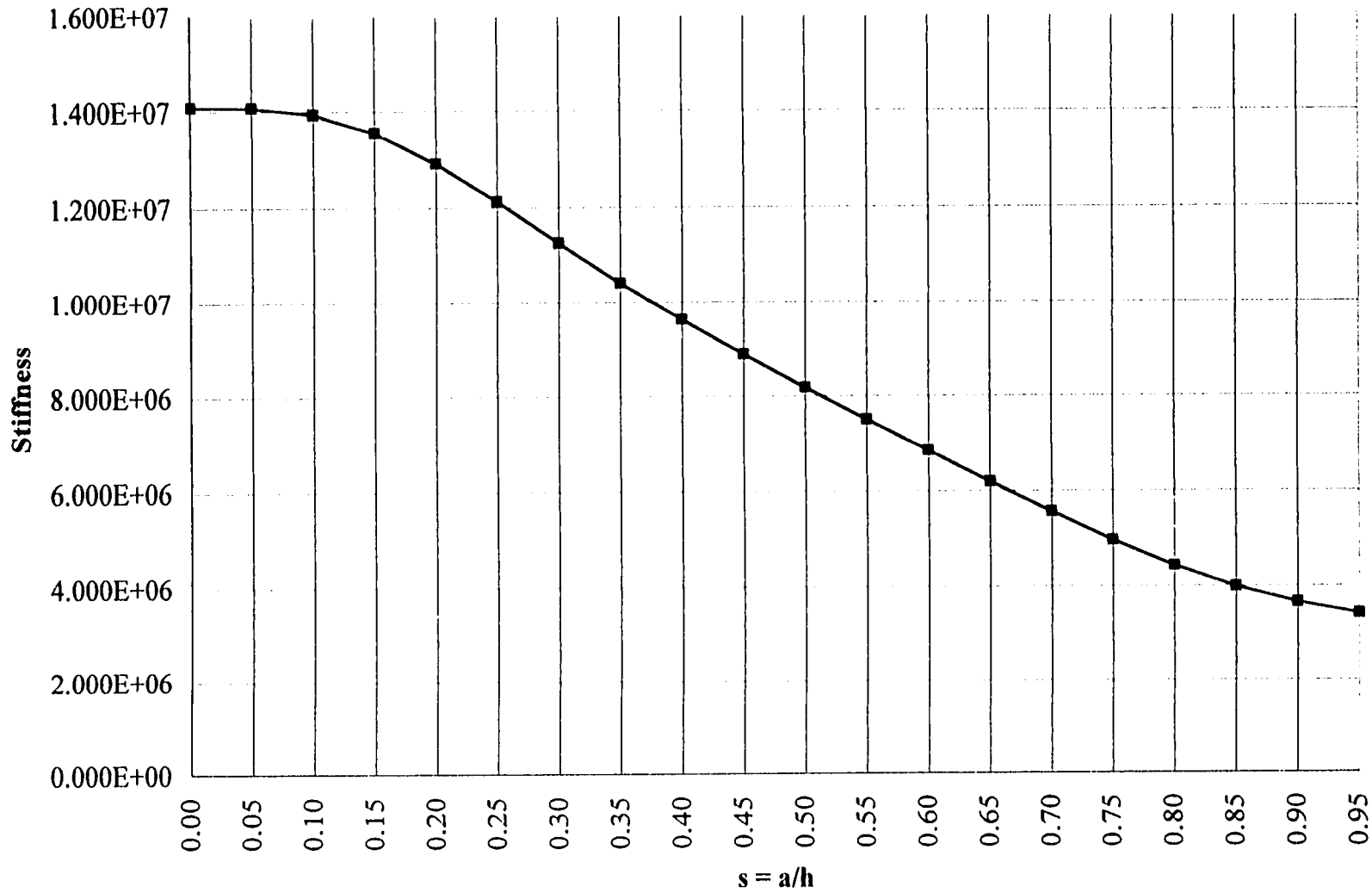

Figure 4.13
Change of the stiffness of the ring with crack propagation

4.5 SUMMARY

The key elements of the procedure, outlined in Section 3.6 to predict the FCGR at resonance and was implemented in this Chapter, can be stated in the following:

1. determining the deformation response factor of the system at resonance, which depends heavily on the damping of the system,
2. obtaining the stress intensity factor for the system as a function of the crack length,
3. determining the reduced stiffness of the system due to crack extension and the corresponding change in natural frequencies.

It should be noticed in performing the aforementioned steps that several alternatives are available for each one. For instance, the stress intensity factor can be obtained from the literature, analytically using one of the methods mentioned in sub-section 2.4.1, experimentally, or using the finite element analysis. Also, the reduced stiffness due to crack extension can be determined experimentally or using finite element analysis, if it is not already available in the literature. The method used in the analysis should depend on the tolerated accuracy of the results and the allocated costs and resources.

CHAPTER 5
EXPERIMENTAL ANALYSIS

5.1 INTRODUCTION

While most of this investigation is dedicated to present the analytical treatment, it is important to emphasize that theoretical analysis gives an estimation only. In the previous analyses, it was assumed that Paris law is valid at resonance, and the effect of resonance is to magnify the stress intensity factor range. However, experimentation is necessary to get an accurate description of the fatigue crack propagation rate at resonance for a specific material, and the results may not follow Paris law.

5.2 TEST OBJECTIVES

To investigate FCGR at resonance, a resonance condition should be achieved at the test, and the required modal analysis described earlier should be performed prior to the test to determine the frequency at which the test should be performed.

As was mentioned earlier in the modal analysis (Section 4.3), the boundary conditions used in the analysis simulated the constraints imposed by the fixture used to mount the specimen to the testing machine. Also, the first mode shape is the closest mode to the deformed shape of the ring under the applied loads during the test. However, the natural frequency of the first mode is well above the testing machine limit. Therefore, the objective of this test was limited to investigate the sensitivity of K_I to the crack length.

5.3 TEST DESCRIPTION

The geometry of the test specimens is shown in Figure 5.1, and the geometry of the fixture used to hold the specimen to the machine is shown in Figure 5.2. Dimensions in both figures are in millimeters. Figure 5.3 shows the fixture mounted to the testing machine. Figures 5.4 and 5.5 show the specimen mounted to the machine during the test. The specimens were made of SAE 1045, a medium carbon steel that is used in the industry to manufacture forgings such as steering arms, truck front axles, axle shafts, connecting rods, and tractor wheels. The fixture was made of steel SAE 1020.

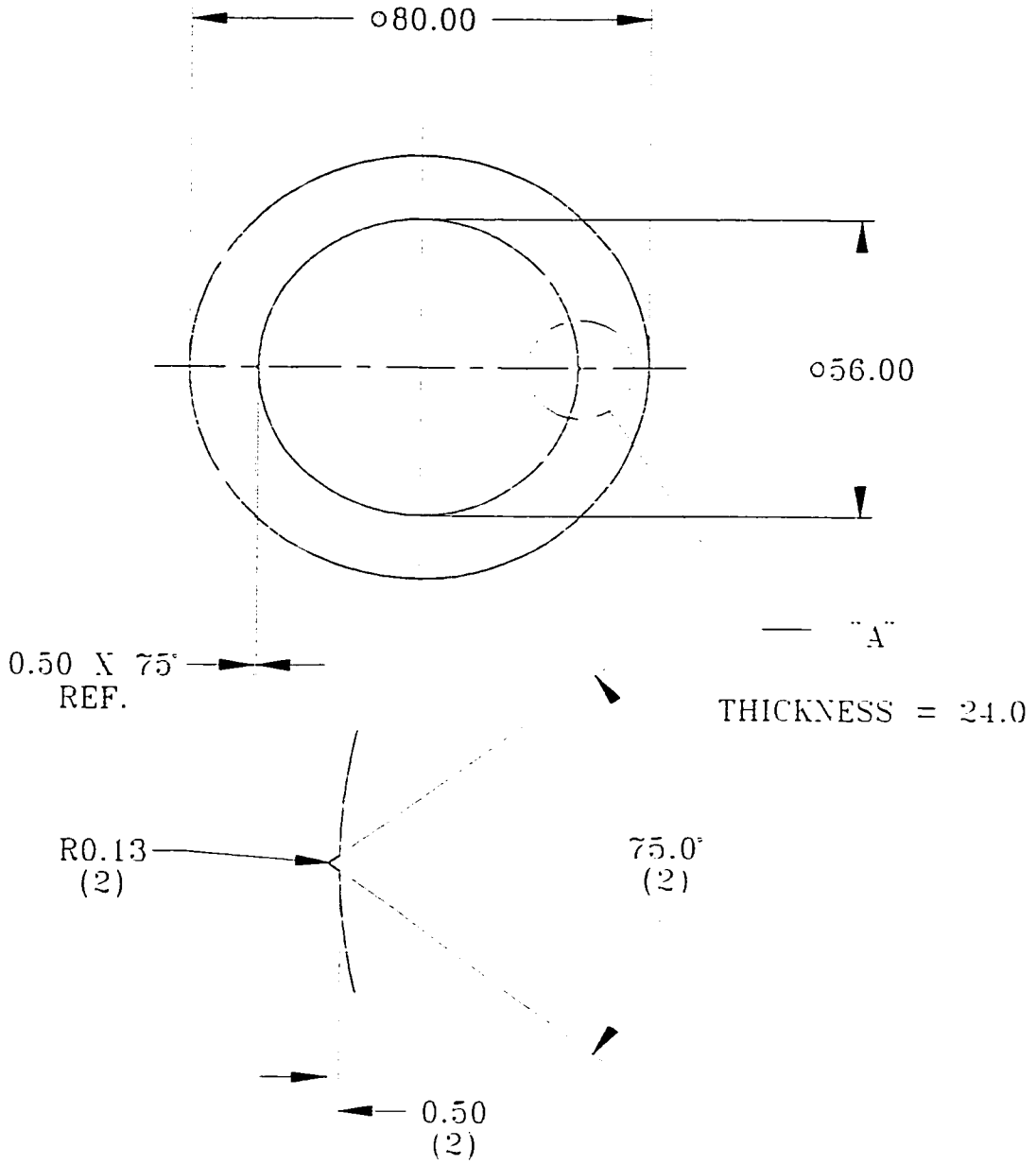

Figure 5.1

Geomtry of the test specimen

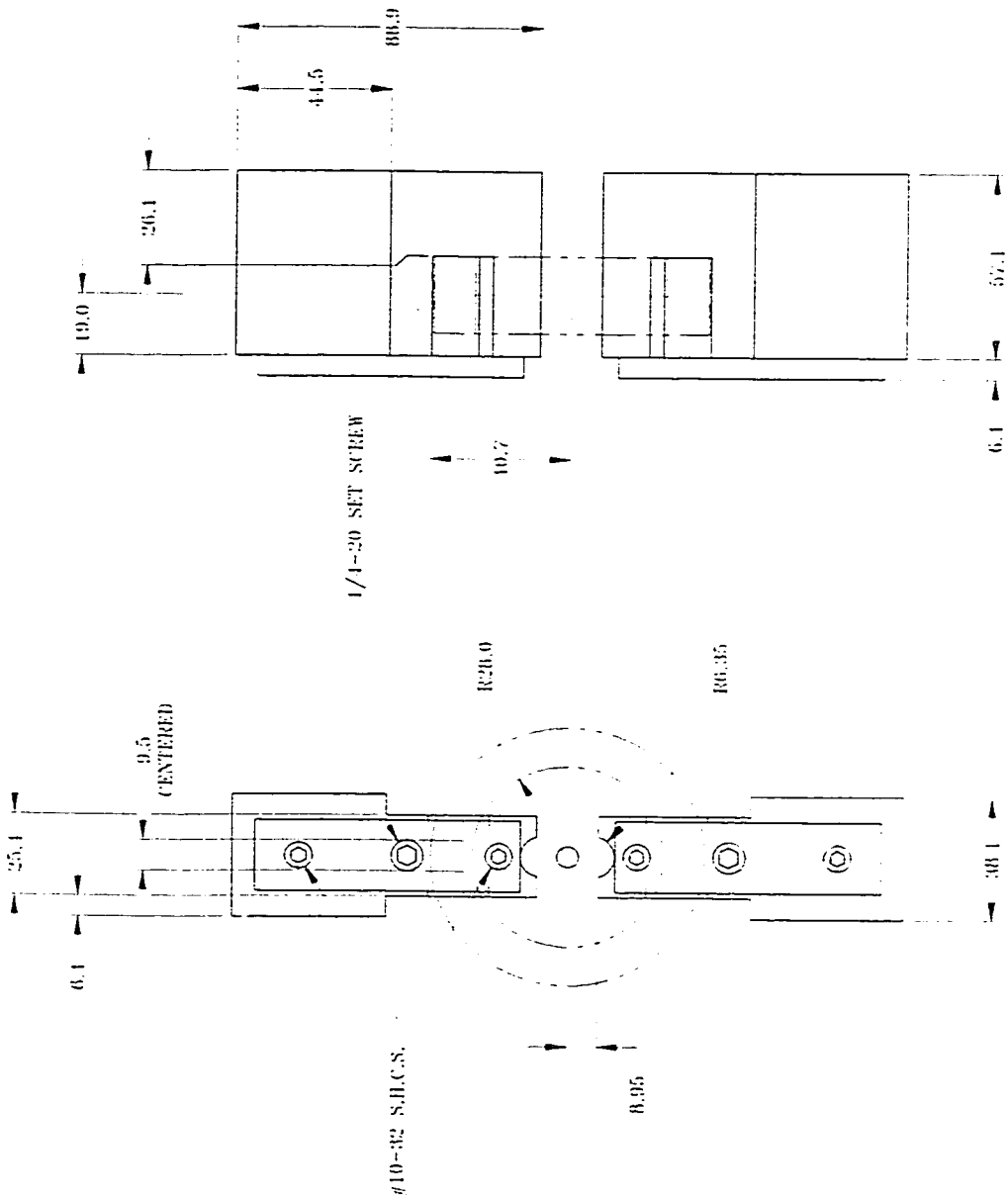

Figure 5.2
Test fixture

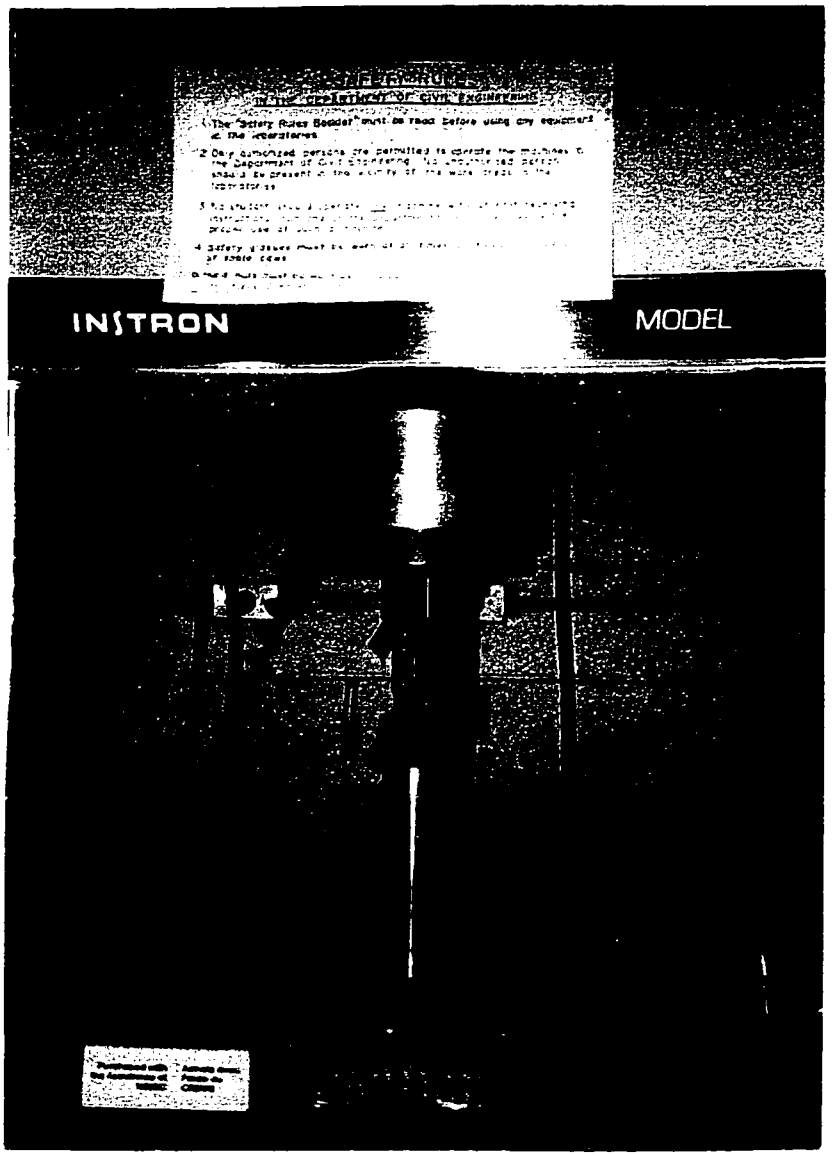

Figure 5.3

The fixture mounted to the testing machine

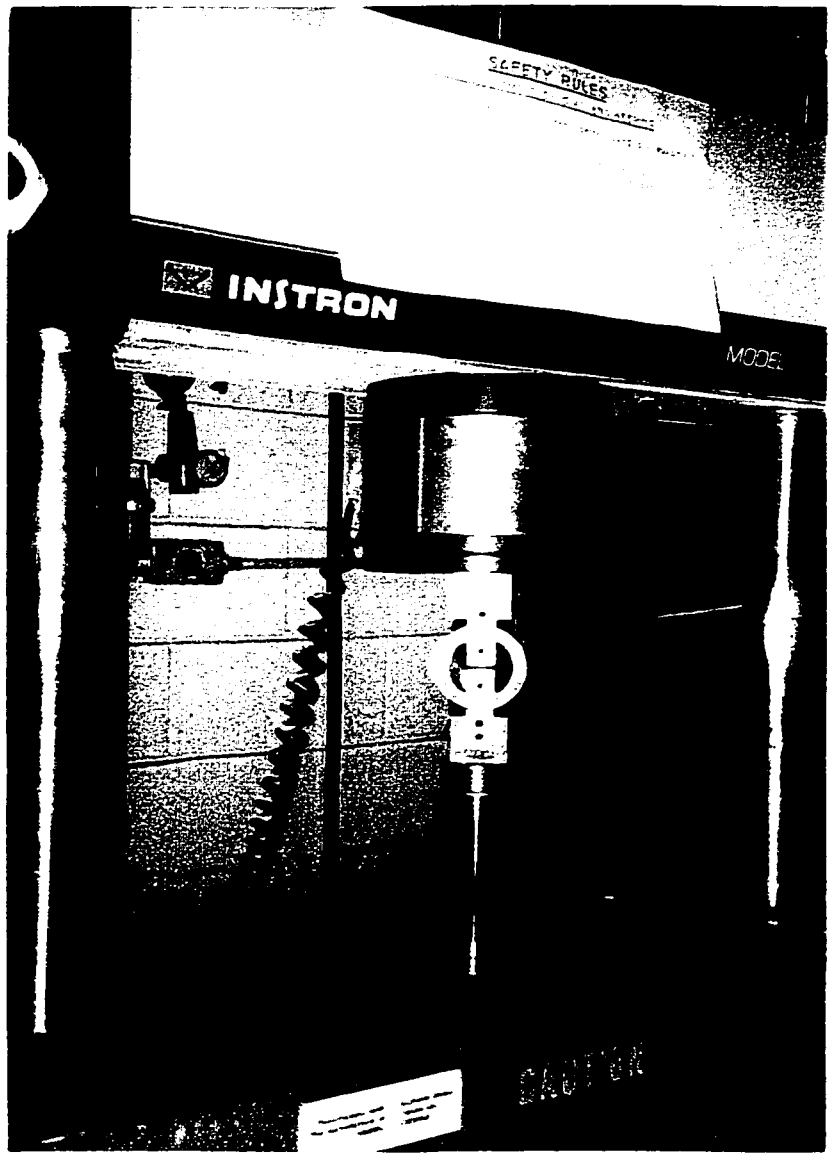

Figure 5.4

A front view of the specimen mounted to the testing machine

Figure 5.5

A side view of the specimen mounted to the testing machine

5.4 TEST RESULTS

Six specimens were tested at room temperature on the fatigue-testing machine INSTRON model No. 1332, a servohydraulic machine. The waveform of the alternating load was sinusoidal. The results are tabulated in Table 5.1, and a sample of the test results is appended (Appendix C)

It should be noticed that specimen No. 2 was subjected to 50-60 kN alternating force for 129960 cycles and did not fail, then it was subjected to 40 to 70 kN and failure occurred after 13036 cycles.

From the test results, the static load required to crack the ring is 101.129 kN; the corresponding stress intensity factor is the assumed fracture toughness value of 44.0 $MPa.m^{1/2}$ and the fatigue crack growth can be estimated using equation (2.10) as follows:

$$a = 6.9 \times 10^{-9} \times Number\ of\ cycles \left(\frac{altenation\ range}{101.129} \times 44.0 \right)^3 \qquad (5.1)$$

One can make the following observations from the test results:

1. As it is expected, the stress intensity range is the main factor that determines the FCGR, this can be concluded by comparing the number of cycles to failure for samples 2, 3, and 6.
2. Failure occurs when the crack length reaches a critical length that brings the stress intensity factor up to the fracture toughness value of the material. For example, if the alternating range is 40-70 kN, the crack propagates till the stress intensity factor caused by 70 kN reaches K_{Ic} (44.0 $MPa.m^{1/2}$), then failure occurs. A comparison between the upper bound of the alternating forces, the static load to failure, and the estimated crack growth values shows that the stress intensity factor of the ring is sensitive to the crack length. A small extension of the crack causes a significant increase in the stress intensity factor of the ring. For instance, consider specimen No. 6; the crack extended from 0.50mm to 0.80mm and that reduced the load required to reach K_{Ic} from 101.129 kN to 50.0 kN. This observation is the same as that was made in Section 4.2.

Table 5.1

Test results

Specimen Number	Load Range kN	Frequency hertz	Number of Cycles to failure	Time seconds	Estimated Crack extension mm
1	101.129	static	-	-	-
2	50 TO 60	36.1	129960	3600	0.070
2	40 TO 70	36.1	13036	361	0.200
3	40 TO 70	36.1	14701	407	0.226
4	40 TO 66	60.0	28783	480	0.287
5	40 TO 70	10.0	15166	1517	0.233
6	10 TO 50	36.1	8265	229	0.301

CHAPTER 6
OBSERVATIONS AND CONCLUSIONS

6.1 OBSERVATIONS

The following observations can be noted in this investigation:

1. The effect of resonance was considered to be the magnification of K_I by a factor equal to the dynamic displacement response factor of the system and the FCGR at resonance follows Paris law, however the validity of this assumption should be examined experimentally.
2. The presented method to predict the FCGR gives more accurate prediction for smaller crack length to element depth ratios "s". For larger "s" values, the mode shapes may be different from the mode shapes of the uncracked structural element, and the shape function used to describe the vibration of the generalized system is less accurate.
3. Damping has a substantial effect on the dynamic response of a structural system and, thus, on the magnification of K_I and the predicted FCGR at resonance. However, it should be noticed that the contribution of the material damping to the total damping of the system is usually very small except for some materials such as polymers. The phenomenon of the dynamic crack arrest referred to by Dentsoras should not be expected in steel structures, since steels in general have small damping coefficients.
4. The plastic zone at the crack tip introduces an additional damping to the cracked structural system, in a ductile material this contribution could be significant and may change the FCGR.

6.2 CONCLUSIONS

At resonance, the fatigue crack propagation rate is higher than the rate at other frequencies. The magnification of the fatigue crack propagation rate due to resonance depends primarily on the damping of the system. For steel structures, the external damping is the main source of damping and the material damping is small. As the crack propagates, the stiffness of the element decreases and the natural frequencies and mode shapes of the system change. Consequently, a gradual shift from the resonance condition occurs.

For the ring model considered in this investigation, it is observed that the increase of the stress intensity factor with the crack length has a high rate at small values of crack length to ring width. Since a high rate of fatigue crack propagation at resonance is expected, it should be expected that the fracture of a steel ring due to fatigue at resonance is very likely to occur at a relatively small loads and in a much shorter time than at other frequencies. This possibility is greater for steels of higher strength with low fracture resistance.

6.3 RECOMMENDED FURTHER STUDIES

The following topics could be the subjects of further research work:

1. Performing extensive experimental investigations to determine the FCGR at resonance for the ring and for different structural elements that made of materials with known characteristic properties especially the fracture toughness and the constants of Paris law.
2. Using finite element analysis to simulate the compliance calibration method, as was followed in this investigation, to determine the stress intensity factor for rings with different sizes and different loading and boundary conditions. The analysis can extend to other structural elements as well.
3. Extending the investigations to cover the areas of structural systems with combined loading modes, different vibration modes, and different material models.
4. Studying the FCGR at resonance for a closing crack condition.

References

ASTM (1983). "Standard Test Method for Constant-Load-Amplitude Fatigue Crack Growth Rates above 10m/cycle." E647-83.

ASTM (1984). "Standard Test Method for Plane-Strain Fracture Toughness of Metallic Materials." E399-83.

Barsom, J. M. (1973). "Fatigue Crack Propagation in Steels of Various Yield Strength." Trans. ASME, Journal of Engineering for Industry, Series B, **93**.

Bowie, O. L. and Freese, C. E. (1970). "Elastic Analysis for Radial Crack in a Circular Ring." U.S. AMMRC monograph MS-70-3, Watertown, MA.

Broek, D. (1988). "The Practical Use of Fracture Mechanics." FractuREsearch Inc., Galena, OH, USA, Kluwer Academic Publishers.

Brown, F. W. and Srawley, J. E. (1966). "Plane Strain Crack Toughness Testing of High Strength Metallic Materials." ASTM STP 410.

Buchalet, C. B. and Bamford, W. H. (1976). "Stress Intensity Factor Solutions for Continuous Surface Flaws in Reactor Pressure Vessels." ASTM STP 590.

Bueckner, H. F. (1958). "The Propagation of Cracks and the Energy of Elastic Deformation." Trans. ASME, **80**, pp.1225-1229.

Bueckner H. F. and. Giaever, I. (1966). "Zeitschrift fur angewandte Mathematik und Mechanik." pp. 265-273.

Carwright, D.J. and Rooke, D.P. (1974). "Approximate Stress Intensity Factors Compounded from Known Solutions." Engineering Fracture Mechanics, **6**, pp. 563-571.

Chona, R. (1993). "Fracture Mechanics." (from the 23rd symposium), ASTM STP 1189.

Chondros, T. G. and Dimargonas, A. D. (1980). "Identification of Cracks in Complex Structures by Vibration Analysis." Journal of Sound and Vibration, **69**, pp 531-538.

Chondros, T. G. (1981). "Dynamics of Cracked Structures." Dr. Engineering Thesis, University of Patras, Greece.

Chopra, A. K. (1995). "Dynamics of Structures." Prentice Hall, Upper Saddle River, New Jersey, USA.

Christides, S. and Barr, A. D. S. (1984). "One-dimensional Theory of Cracked Bernoulli-Euler Beams." International Journal of Mechanical Science, **26**, pp. 639-648.

Christides, S. and Barr, A. D. S. (1986). "Torsional Vibration of Cracked Beams of Non-Circular Cross-section." International Journal of Mechanical Science, **28**, pp. 473-490.

Delale, F. and Erdogan, F. (1982). "Stress Intensity Factors in A Hollow Cylinder Containing a Radial Crack." International Journal of Fracture, **20**, pp. 251-265.

Dentsoras, A. and Dimargonas, A. (1983a). "Resonance Controlled Fatigue Crack Propagation." Engineering Fracture Mechanics, **17**, pp. 381-386.

Dentsoras, A. and Dimargonas, A. (1983b). "Resonance Controlled Fatigue Crack Propagation in a Beam under Longitudinal Vibrations." International Journal of Fracture, **23**, pp. 15-22.

Dentsoras, A. and Dimargonas, A. (1983c). "Resonance Controlled Fatigue Crack Propagation in Cylindrical Shafts under Combined Loading." ASME Winter Annual Meeting, Boston, USA.

Dentsoras, A. (1987). "Resonance Controlled Fatigue Crack Propagation." Ph.D. Thesis, Patras University, Greece [in Greek].

Dentsoras, A. and Dimargonas, A. (1989). "Fatigue Crack Propagation in Resonating Structures." Engineering Fracture Mechanics, **34**, pp. 721-728.

Dentsoras, A. and Panteliou, S. (1992). "Fatigue Crack Propagation in Resonating Machine Members at Elevated Room Temperature." Proc. of the 9th biennial Eur. Conf. on Fracture, pp. 471-476, Varna, Bulgaria.

Dentsoras, A. and Kouvaritakis, E. (1995). "Effects of Vibration Frequency on Fatigue Crack Propagation of a Polymer at Resonance." Engineering Fracture Mechanics, **50**, pp. 467-473.

Dimargonas, A. D. (1976). "Vibration Engineering." West Publishers, St Paul.

Dimargonas, A. D. (1996). "Vibration of Cracked Structures: A State of the Art Review." Engineering Fracture Mechanics, **55**, pp. 831-857.

Durelli, A. J. and Lin, Y. H. (1986). "Stresses and Displacements on the Boundaries of Circular Rings Diametrically Loaded." Journal of Applied Mechanics, **53**, pp. 213-219.

Elber, W. (1971). "The Significance of Fatigue Crack Closure." Damage Tolerance in Aircraft Structures, ASTM STP 486.

Emery, A. F. and Segedin, C. M. (1972). "The Evaluation of the Stress Intensity Factors for Cracks Subjected to Tension, Torsion, and Flexure by an Efficient Numerical Technique." Journal of Basic Engineering, Transactions of ASME 94, pp. 387-393.

Entwistle, R. D. and Stone, B. J. (1990). "Survey of the Use of Vibration Methods in the Assessment of Component Geometry." Vibration and Noise-Meas. Pred. and Cont., Inst. of Engineering, **90**, pp. 210-217.

Erik Oberg et al. (1996). "Machinery's Handbook." 25th Edition, Industrial Press Inc., New York, USA.

Ewalds, H. L. and Wanhill, R. J. H. (1985). "Fracture Mechanics." Edward Arnold Publishers, Baltimore, USA.

Fox, C. H. J. (1992). "The location of Defects in Structures: a Comparison of the Use of Natural Frequency and Mode Shape Data." Proc. 10th International Modal Analysis Conf., San Diego, USA, **1**, pp. 522-528.

Frocht, M. (1941). "Photoelasticity." Vol. I, John Wiley & Sons, New York, USA.

Frost, N.E. and Dixon, J.R. (1967). International Journal of Fracture Mechanics, **3**, pp. 301.

Frost, N.E. and Dugdale, D.S. (1958). "The Propagation of Fatigue Cracks in Sheet Specimens." Journal of the Mechanics and Physics of Solids, **6**, pp. 92.

Frost, N. E., Pook, L. P. and Denton, K., A (1971). "Fracture Mechanics Analysis of Fatigue Crack Growth Data for Various Materials." Engineering Fracture Mechanics, **3**, pp. 109-126.

Gomez, A. J. M.A. and Montalvao e Silva, J. M. (1990). "Experimental Determination of the Influence of the Cross-section Size in the Dynamic Behavior of Cracked Beams." Proc. IMMDC2, Los Angles, USA, pp. 124-130.

Gomez, A. J. M. A. and Montalvao e Silva, J. M. (1991). "Theoretical and Experimental Data on Crack Depth Effects in the Dynamic Behavior of Free-free Beams." International Modal Analysis Conference, IMAC, Union Coll., Schenectady, NY, USA, **9**, pp. 274-283.

Griffith, A. A. (1921). "The Phenomena of Rupture and Flow in Solids." Philosophical Transactions, Royal Society of London, Series A221, pp. 163-198.

Gross B. and Srawley, J. E. (1965). "Stress-intensity Factors for Single-edge-notch Specimens on Bending or Combined Bending and Tension by Boundary Collocation of a Stress Function." NASA Tech. Note No. D-2603.

Gudmundson, P. (1982). "Eigenfrequency Changes of Structures Due to Cracks, Notches or Other Geometrical Changes." Journal of the Mechanics and Physics of Solids, **30**, pp. 339-353.

Gudmundson, P. (1983). "The Dynamic Behavior of Slender Structures with Cross-Sectional Cracks." Journal of the Mechanics and Physics of Solids, **31**, pp. 329-345.

Head, A. K. (1953). Philosophical Magazine, **44**, pp.925.

Head, A. K. (1956). Journal of Applied Mechanics, **78**, pp.407.

Irwin, G. R. (1957a). "Analysis of Stresses and Strains Near the End of a Crack Transversing a Plate." Journal of Applied Mechanics, **24**, pp. 361-364.

Irwin, G. R. (1957b). "Relation of Stresses Near a Crack to the Crack Extension Force." 9th Cong. Applied Mechanics, Brussels.

Irwin, G. R. (1960). "Fracture Mechanics." Structural Mechanics, Pergamon Press, New York, USA, pp. 557-592.

Isibasi, T. (1958). "Proc. 1ST Japanese Congress on Testing Materials, pp.37.

Jerina and Paris (2000). "Fatigue and Fracture Mechanics." **30**, ASTM STP 1360.

Jones, A. T. (1973). "A Radially Cracked, Cylindrical Fracture Toughness Specimen." SLL-73-5009, Sandia Laboratories, Livermore, Calif., Nov.

Jones, A. T. (1973). "Fracture Toughness Testing with Sections of Cylindrical Shells." SLL-73-0050, Sandia Laboratories, Livermore, Calif., Nov.

Kapp, J. A. (1977). "The Effect of Autofrettate on Fatigue Crack Propagation in Externally Flawed Thick-walled Disks." U.S. ARADCOM Tech. Rep. ARCLB-TR-77025, Watervliet, N.Y.

Kirmsher, P. G. (1944). "The Effect of Discontinuities on the Natural Frequency of Beams." Proc. ASTM, **44**, pp. 987-904.

Kobayashi, A. S., Maiden, D. E. and Simon, B. J. (1969). "Application of Finite Element Analysis Method to Two-dimensional Problems in Fracture Mechanics."

ASME Paper No. 69-WA/PVP-12.

Labbens, R., Pellissier-Tanon, A. and Heliot, J. (1976). "Practical Method for Calculating Stress-Intensity Factors Through Weight Functions." ASTM STP 590.

Liebowitz, H., Vanderveldt, H. and Harris, D. W. (1967). "Carrying Capacity of Notched Column." International Journal of Solids and Structures, **3**, pp. 489-500.

Liebowitz, H. and Claus, W. D. (1968). "Failure of Notched Columns." Engineering Fracture Mechanics, **1**, pp. 379-383.

Love, A. E. H. (1927). "A Treatise on the Mathematical Theory of Elasticity."

Murakami, Y. (1987). "Stress Intensity Factors Handbook." Pergamon Press, New York.

Naval Publications and Forms Center (1981). "Metallic Materials and Elements for Aerospace Vehicle Structures." MIL-HDBK-5.

Nelson, C. W. (1939). "Stresses and Displacements in a hollow Circular Cylinder." Ph.D. Thesis, University of Michigan, USA.

Okamura, H., Liu, H. W., Chu, Chorng-Shin and Liebowitz, H. (1969). "A Cracked Column under Compression." Engineering Fracture Mechanics, **1**, pp. 547-564.

Ostachowicz, W. M. and Krawczuk, M. (1992). "Coupled Torsional and Bending Vibrations of a Rotor with an Open Crack." Arch. Appl. Mech., **62**, pp. 191-201.

Pandey, A. K., Biswas, M. and Samman, M. M. (1991). "Damage Detection from Changes in Curvature Mode Shapes." Journal of Sound and Vibration, **145**, pp. 321-332.

Paris, P. C., Gomez, M. P., and Anderson, W. E. (1961). "The Trend in Engineering." University of Washington, **13**, pp. 9.

Paris, P. C. Bucci, R. J., and Loushin, L. L. (1974). "Dynamic Compact Tension Testing for Fracture Toughness." ASTM STP 559.

Paris, P.C., McMeeking, R.M. and Tada, H. (1976). "The Weight Function Method for Determining Stress Intensity Factors." ASTM STP 601.

Paris, P. C. (1977). "Fracture Mechanics in the Elastic-Plastic Regime." ASTM STP 631.

Pelloux, R.M. (1970). "Review of Theories and Laws of Fatigue Crack Propagation." Proc. of Air Force Conference on Fracture and Fatigue of Aircraft Structures, pp.409.

Pook, L.P. and Frost, N.E. (1973). "A Fatigue Crack Growth Theory." International Journal of Fracture, **9**, pp. 53-61.

Provan, J. W. (1989). "An Introduction to Fatigue." Journal of Materials Education, Material Education Council, Pennsylvania State University.

Rice, J.R. (1967). "Fatigue Crack Propagation." ASTM STP 415.

Rice, J. R. (1968). "A Path Independent Integral and the Approximate Analysis of Strain Concentration by Notches and Cracks." Journal of Applied Mechanics, **35**, pp. 379-386

Rice, J. R. and Levy, N. (1972). "The Part-through Surface Crack in an Elastic Plate." Journal of Applied Mechanics, **39**, pp.185-194.

Ripling, E. J. (1974). "Fracture Properties of a Cold-Worked Mild Steel." ASTM STP 559.

Roark, R. (1954). "Formulas for Stress and Strain." 3rd edition, McGraw Hill.

Rolfe, S.T., and Barsom, J.M. (1977). "Fracture and Fatigue Control in Structures." Prentice-Hall Inc.

Rooke, D. P. and Cartwright, D. J. (1976)."A Compendium of Stress Intensity Factors." Her Majesty's Stationery Office, London, England.

SAE (1997). "Fatigue Design Handbook." Society of Automotive Engineers, Fatigue Design and Evaluation Committee, Warrendale, PA.

Sih, G. C. (1973). "Handbook of Stress Intensity Factors." Institute of Fracture and Solid Mechanics, Lehigh University, USA.

Sih, G.C. (1973). "Methods of Analysis and Solutions of Crack Problems." Noodhoff International Publishing, Leyden.

Silva, J. M.M. and Gomez, A. J. M. A. (1990). "Experimental Dynamic Analysis of Cracked Free-free Beams." Exp. Mech., **30**, pp. 20-25.

Tada, H., Paris, P., and Irwin, G. R. (1985). "The Stress Analysis of Cracks Handbook." Del Research Corporation, Hellertown, Pennsylvania, USA.

Timoshenko, S. and Young, D. H. (1955). "Vibration Problems in Engineering." D. Van Nostrand Company Ltd., London, England.

Timoshenko, S. (1922). "On the Distribution of Stress in a Circular Ring Compressed by Two Forces Along a Diameter." Philosophical Magazine, **44**, pp. 1014.

Toth, L. and Krasovsky, A. J. (1997). "Material Characterization Required for Reliability Assessment of Cyclically Loaded Engineering Structures." Part 2: Fatigue

Application, Klu wen Academic Publishers, Netherlands, pp. 225-272.

Tracy, P.G. (1975). "Analysis of a Radial Crack in a Circular Ring Segment." Journal of Engineering Fracture Mechanics, **7**, pp. 253-260.

Tracy, P.G (1979). "Elastic Analysis of Radial Cracks Emanating from the Outer and Inner Surfaces of a Circular Ring." Journal of Engineering Fracture Mechanics, **11**, pp. 291-300.

Trucker L., Landgraf, R. and Brose, W. (1986). "Proposed Technical Report on Fatigue Properties for the SAE Handbook." SAE technical paper No. 740279.

University of Dayton (1983). "Damage Tolerance Design Handbook." MCIC-HB-01R, published and distributed by Battelle Columbus Division, Columbus, OH, USA.

Wauer, J. (1990). "Cracked Rotor Dynamics: a State of the Art Survey." Applied Mechanics Reviews, **43**, pp. 13-17.

Weertman, J. J. (1965). Conf. Fracture, Sendai, Japan, **1**, pp. 154.

Weibull, W. (1961). Crack Propagation Symposium, Cranfield, England, pp271.

Wells, A. A. (1962). "Unstable Crack Propagation in Metals: Damage and Fast Fracture." Proceedings of the Crack Propagation Symposium Cranfield, The College of Aeronautics, **1**, pp. 210-230, Cranfield, England.

Westmann, R. A. and Yang, W.H. (1967). "Stress Analysis of Cracked Rectangular Beams." Journal of Applied Mechanics, **32**, pp. 693-701.

Yao, J. Y. and Dimargonas, A. D. (1988). "Vibration of a Circular Ring with a Transverse Crack." ASME Paper No. 88-Wa/DSC-42.

Zacek, 1938. "Radial and Torsional Vibration of Rings." Philosophical Magazine, **25**, pp.168.

Appendix A

ABAQUS INPUT FILES

For the compliance calibration simulation method

A. Side Movement Unconstrained

```
*HEADING
*PREPRINT,ECHO=NO,MODEL=NO,HISTORY=NO
*SOLID SECTION, ELSET=RING, MATERIAL=STEEL
*MATERIAL, NAME=STEEL
*ELASTIC
200000, 0.3
*STEP, PERTURBATION
*STATIC
*BOUNDARY
UNCRACK,XSYMM
LONG,YSYMM      (*)
HALF,ZSYMM
*DLOAD
LOAD,P6,2089.60214
*RESTART,WRITE
*NODE PRINT,NSET=UNCRACK
U2
*END STEP
```

B. Side Movement constrained

The file is identical to case A, except that the line marked (*) has been replaced by:

```
LONG,PINNED
```

Appendix B

LS-DYNA input file for modal analysis

```
*KEYWORD
$---+----1----+----2----+----3----+----4----+----5----+----6----+----7----+----8
$
$ DYNA3D(936) DECK WAS WRITTEN BY: ETA/FEMB VERSION 26
$ DATE  : Nov 15, 2000 at 15:04:28
$
$---+----1----+----2----+----3----+----4----+----5----+----6----+----7----+----8
$                    (1) TITLE CARD.
$---+----1----+----2----+----3----+----4----+----5----+----6----+----7----+----8
*TITLE
MODAL ANALYSIS
$---+----1----+----2----+----3----+----4----+----5----+----6----+----7----+----8
$                    (2) CONTROL CARDS.
$---+----1----+----2----+----3----+----4----+----5----+----6----+----7----+----8
*CONTROL TERMINATION
$   ENDTIM    ENDCYC     DTMIN    ENDNEG    ENDMAS
       1.0         0      .000      .000      .000
*CONTROL IMPLICIT GENERAL
$   IMFLAG        DT0    IMFORM       NSBS        IGS
         1        1.0
*CONTROL IMPLICIT EIGENVALUE
         5
$*CONTROL TIMESTEP
$   DTINIT       SCFT       ISDO    TSLIMT       DTMS       LCTM      ERODE      MS1ST
$      .000       .900          0
$---+----1----+----2----+----3----+----4----+----5----+----6----+----7----+----8
$                    (3) DATABASE CONTROL CARDS - ASCII HISTORY FILE
$---+----1----+----2----+----3----+----4----+----5----+----6----+----7----+----8
$*DATABASE HISTORY OPTION
$      ID1        ID2        ID3        ID4        ID5        ID6        ID7        ID8
$
$OPTION : BEAM    BEAM SET   NODE   NODE SET
$         SHELL   SHELL SET  SOLID  SOLID SET
$         TSHELL  TSHELL SET
$---+----1----+----2----+----3----+----4----+----5----+----6----+----7----+----8
$                    (4) DATABASE CONTROL CARDS FOR ASCII FILE
$---+----1----+----2----+----3----+----4----+----5----+----6----+----7----+----8
$---+----1----+----2----+----3----+----4----+----5----+----6----+----7----+----8
$*DATABASE OPTION
$       DT
$
$OPTION : SECFORC RWFORC NODOUT ELOUT  GLSTAT
$         DEFORC  MATSUM NCFORC RCFORC DEFGEO
$         SPCFORC SWFORC ABSTAT NODFOR BNDOUT
$         RBDOUT  GCEOUT SLEOUT MPGS   SBTOUT
$         JNTFORC AVSFLT MOVIE
$---+----1----+----2----+----3----+----4----+----5----+----6----+----7----+----8
$                    (5) DATABASE CONTROL CARDS FOR BINARY FILE
$---+----1----+----2----+----3----+----4----+----5----+----6----+----7----+----8
*DATABASE BINARY D3PLOT
$  DT/CYCL      LCDT    NOBEAM
  .500E-01
*DATABASE BINARY D3THDT
$  DT/CYCL      LCDT    NOBEAM
  .500E-01
$*DATABASE BINARY OPTION
$  DT/CYCL      LCDT    NOBEAM
$
$OPTION : D3DRFL D3DUMP RUNRSF INTFOR
$---+----1----+----2----+----3----+----4----+----5----+----6----+----7----+----8
*DATABASE EXTENT BINARY
```

```
         0          0          3          0          1          1          1          1
         0          0          0          0          0          0
$---+----1----+----2----+----3----+----4----+----5----+----6----+----7----+----8
$                    (6) DEFINE PARTS CARDS
$---+----1----+----2----+----3----+----4----+----5----+----6----+----7----+----8
*PART
$HEADING
 PART PID =          7 PART NAME :RING
$      PID        SID        MID      EOSID       HGID       GRAV     ADPOPT       TMID
         7          8          1
$---+----1----+----2----+----3----+----4----+----5----+----6----+----7----+----8
$                    (7) MATERIAL CARDS
$---+----1----+----2----+----3----+----4----+----5----+----6----+----7----+----8
*MAT ELASTIC
$MATERIAL NAME:STEEL
$      MID         RO          E         PR         DA         DB          K
         1 7.850E-09 2.000E+05 3.000E-01
$---+----1----+----2----+----3----+----4----+----5----+----6----+----7----+----8
$                    (7.1) SECTION CARDS
$---+----1----+----2----+----3----+----4----+----5----+----6----+----7----+----8
*SECTION SHELL
$PROPERTY NAME:RING
$      SID     ELFORM       SHRF        NIP      PROPT    QR/IRID      ICOMP
         8         13  .100E+01        2.0        1.0         .0
$       T1         T2         T3         T4       NLOC
 2.400E+01 2.400E+01 2.400E+01 2.400E+01
$---+----1----+----2----+----3----+----4----+----5----+----6----+----7----+----8
$                    (8) NODAL POINT CARDS
$---+----1----+----2----+----3----+----4----+----5----+----6----+----7----+----8
*NODE
$   NODE                X                   Y                   Z       TC       RC
       2  .278649800E+03  .331779700E+03  .120000000E+02
    .....................................................
   10493  .258002600E+03  .268489500E+03  .120000000E+02
$---+----1----+----2----+----3----+----4----+----5----+----6----+----7----+----8
$                    (9) SOLID ELEMENT CARDS
$---+----1----+----2----+----3----+----4----+----5----+----6----+----7----+----8
*ELEMENT SOLID
$    EID     PID      N1      N2      N3      N4      N5      N6      N7      N8
$---+----1----+----2----+----3----+----4----+----5----+----6----+----7----+----8
$                    (10) BEAM ELEMENT CARDS
$---+----1----+----2----+----3----+----4----+----5----+----6----+----7----+----8
*ELEMENT BEAM
$    EID     PID      N1      N2      N3
$---+----1----+----2----+----3----+----4----+----5----+----6----+----7----+----8
$                    (11) SHELL ELEMENT CARDS
$---+----1----+----2----+----3----+----4----+----5----+----6----+----7----+----8
*ELEMENT SHELL
$    EID     PID      N1      N2      N3      N4
     507       7       3      10      11       4
    ...............................................
   10351       7   10493    7912    5317    5316
$---+----1----+----2----+----3----+----4----+----5----+----6----+----7----+----8
$                    (16) BOUNDARY CONDITION CARDS
$---+----1----+----2----+----3----+----4----+----5----+----6----+----7----+----8
*BOUNDARY SPC NODE
$ NID/NSID       CID      DOFX      DOFY      DOFZ     DOFRX     DOFRY     DOFRZ
         3         0         1         0         0         0         0         0
        ..........................................................................
      5316         0         1         1         1         1         1         1
$---+----1----+----2----+----3----+----4----+----5----+----6----+----7----+----8
*END
```

Appendix C

Sample of test results

```
 "Standardized Data File  V1.17 Data File"
""
"Data generated on : ""10-23-2000"  "05:23p"
"Data exported  on : " "10-23-2000"  "05:35p"
""
"System Configuration :"
"Number Of Movers  "          1
"Number Of Channels"          5
""
"Mover List :"
"Axial"
""
"Channel List :"
"LoadMet"     "DispMet"     "StrnMet"     "Axial Cmd"   "Axial Err"
"kN"   "mm"   "mm"   "kN"   "%"
""
"Peak/Valley Data File for {System}"
""
"Nov.8 40 to 70 kn at 36.1 hz"
"[Axial] Counts : "     1
"Point""LoadMet"     "DispMet"
"Point""kN"   "mm"
1          0.760          0.0000
2          0.652          0.0000
""
"[Axial] Counts : "     101
"Point""LoadMet"     "DispMet"
"Point""kN"   "mm"
1          70.374         -59.0866
2          40.346         -59.6447
.....
""
"[Axial] Counts : "     1501
"Point""LoadMet"     "DispMet"
"Point""kN"   "mm"
1          70.103         -59.0122
2          40.128         -59.5703
.....
""
"[Axial] Counts : "     2901
"Point""LoadMet"     "DispMet"
"Point""kN"   "mm"
```

```
1          70.157          -59.0494
2          40.074          -59.5703
.....
""
"[Axial] Counts : "     4301
"Point""LoadMet"     "DispMet"
"Point""kN"    "mm"
1          70.103          -59.0494
2          40.183          -59.5703
.....
""
"[Axial] Counts : "     5701
"Point""LoadMet"     "DispMet"
"Point""kN"    "mm"
1          70.265          -59.0122
2          40.346          -59.5703
.....
""
"[Axial] Counts : "     8101
"Point""LoadMet"     "DispMet"
"Point""kN"    "mm"
1          70.103          -59.0122
2          39.911          -59.5703
""
"[Axial] Counts : "     9501
"Point""LoadMet"     "DispMet"
"Point""kN"    "mm"
1          70.374          -58.9749
2          40.020          -59.5331
.....
""
"[Axial] Counts : "     10901
"Point""LoadMet"     "DispMet"
"Point""kN"    "mm"
1          70.265          -58.9005
2          40.020          -59.4587
.....
""
"[Axial] Counts : "     12301
"Point""LoadMet"     "DispMet"
"Point""kN"    "mm"
1          70.103          -58.8261
2          40.183          -59.3842
.....
""
"[Axial] Counts : "     13701
```

"Point""LoadMet" "DispMet"
"Point""kN" "mm"
1 69.994 -58.7145
2 39.966 -59.2726
.....
""
"[Axial] Counts : " 14701
"Point""LoadMet" "DispMet"
"Point""kN" "mm"
1 70.211 -58.4168
2 40.237 -58.9749
" "

VITA AUCTORIS

Sameh Guirgis was born in Cairo, Egypt. He obtained a B.Sc. in Structural Engineering from the Faculty of Engineering, Ain-Shams University, Cairo, Egypt, in 1988. He worked as a project engineer under the supervision of the U.S. Army Corps of Engineers for four years in Egypt. In 1994 he immigrated to Canada, and in 1997 he obtained a license as a Professional Engineer in the province of Ontario. He is currently a candidate for the Master's degree in Civil Engineering at the University of Windsor and hopes to graduate in Fall 2000.